

Ionic basis of resting and action potentials

BERTIL HILLE | *Department of Physiology and Biophysics, University of Washington
School of Medicine, Seattle, Washington*

CHAPTER CONTENTS

Development of Membrane Theory
 Before intracellular recording
 Origins
 Stimulation
 Conduction
 Cable
 Impedance
 First intracellular recordings from squid giant axons
 Resting potential
 Action potential
 Afterpotential
 Direct Measurement of Ionic Currents in Axon Membranes
 Voltage-clamp method
 Electrochemical separation of ionic currents
 Ion substitution experiments
 Reversal of current at Nernst potential
 Tracer flux measurement
 Potassium current
 Pharmacological separation of ionic currents
 Selective block
 Separate channels
 Hodgkin-Huxley Model
 Quantitative analysis of I_{Na} and I_K
 Ionic conductances
 Hodgkin-Huxley equations
 Calculations with Hodgkin-Huxley model
 Variety of Excitable Cells
 Myelinated nerve
 Saltatory conduction
 Ionic basis
 Other axons
 Cell bodies
 Gastropod ganglia
 Vertebrate cell bodies
 Muscle
 Ionic Channels
 Sodium channels
 Number of channels
 Ionic selectivity
 Gating
 Potassium channels
 Long pore
 Ionic selectivity
 Gating
 Calcium channels
 Equations of Ionic Hypothesis
 Solving Hodgkin-Huxley model
 Empirical constants
 Solutions

Diffusion of charged particles in electric field
 Nernst-Planck equations
 Goldman-Hodgkin-Katz equation
 Ussing flux ratio
 Independence relation
 Eyring rate theory
 Practical calculations

EXCITABLE CELLS like other cells are completely surrounded by a thin unit membrane. Excitation of excitable cells is always accompanied by changes in the membrane potential. These changes may be abrupt or slow, brief or long lasting, depending on the cell and the stimulus, but the mechanisms of potential change are fundamentally the same. They always involve a change in the permeability of the membrane to ions. The guiding principles, called the membrane theory or ionic hypothesis, may be stated as follows: potentials *a)* develop across unit membranes, *b)* depend on ionic concentration differences, and *c)* arise because the membrane is selectively permeable to some ions. A corollary of these principles is that electric current flowing across membranes is carried by the movement of ions. This chapter describes the electric phenomena of excitability, particularly as seen in axons, and shows how the potentials and currents at rest and during activity may be analyzed and explained by the ionic hypothesis. The approach is first historical, tracing the early development and first tests of the ionic hypothesis on squid giant axons, then broadens to deal with the modern consolidation of facts in many tissues, and concludes with derivations of some of the fundamental equations used to describe membrane potentials and ion fluxes. Some familiarity with classic properties of excitable cells and the cable properties of axons is assumed (see the chapter by Rall in this *Handbook*). Specific applications of the ionic hypothesis to muscles, synapses, and sensory receptors are found in other chapters in this *Handbook*.

Significant features of membrane excitation can be seen by recording electric potential variations with an intracellular electrode. By convention the membrane potential is defined as inside minus outside

The author's original work was supported by grant NS 08174 from the National Institutes of Health.

potential. The recorded potential suddenly becomes more negative as the recording electrode is moved from outside to inside, so excitable cells are said to have a negative *resting potential*. Again by convention any potential change in the positive direction from rest is called a depolarization, whereas a change in the negative direction is called a hyperpolarization. Intracellular records from several types of nerve fiber and a motoneuron are shown in Figure 1. In each example in Figure 1 excitation is initiated by a depolarizing electric shock, and the nerve cell responds with a depolarizing electric response, the *action potential*, also called a *spike* or *impulse*. Action potentials are generally similar in all cells but differ in details of shape and time course from one cell type to another. The simple observation that both the stimulus and response are electric is intimately tied in with the mechanism of propagation of activity or conduction of action potentials. The response is said to be *regenerative* because electric currents generated by the action potential in one part of an axon are sufficient to excite the next part of the axon, and so forth. Thus the impulse travels as a wave down the length of an axon at fairly steady speed and amplitude. This voltage pulse is the unit of information in nerve fibers and, as will be shown, is generated and shaped by ionic permeability changes in each patch of axon membrane. Sodium and potassium ions are by far the most important ions.

DEVELOPMENT OF MEMBRANE THEORY

Before Intracellular Recording

ORIGINS. The membrane theory dates from the beginning of this century and has roots in previous centuries. At the end of the eighteenth century Galvani concluded that nerves and muscles use a flow of "animal electricity" to communicate with the brain. He supposed that the body stores positive and negative electricity separated by insulators. In the nineteenth century the electric currents of nerve and muscle were found to produce brief, externally negative voltage pulses traveling at high velocity along nerves and muscles. Nerves were correctly likened to electrical cables with a surface insulation—the core conductor theory. There were arguments whether the electricity is there all the time or is generated only at the time of the impulse. Near the end of the century there was an essential advance in physical chemistry. Arrhenius (17) showed that salts dissociate into ions. Then Nernst (180, 181) and Planck (191, 192) gave theories for equilibrium and diffusion potentials in ionic solutions, and Nernst and W. V. Ostwald remarked that biological potentials might also be explainable by the same theories.

The membrane theory is usually attributed to the physiologist Bernstein (26, 27) who suggested in 1902 that nerve and muscle cell membranes are selectively

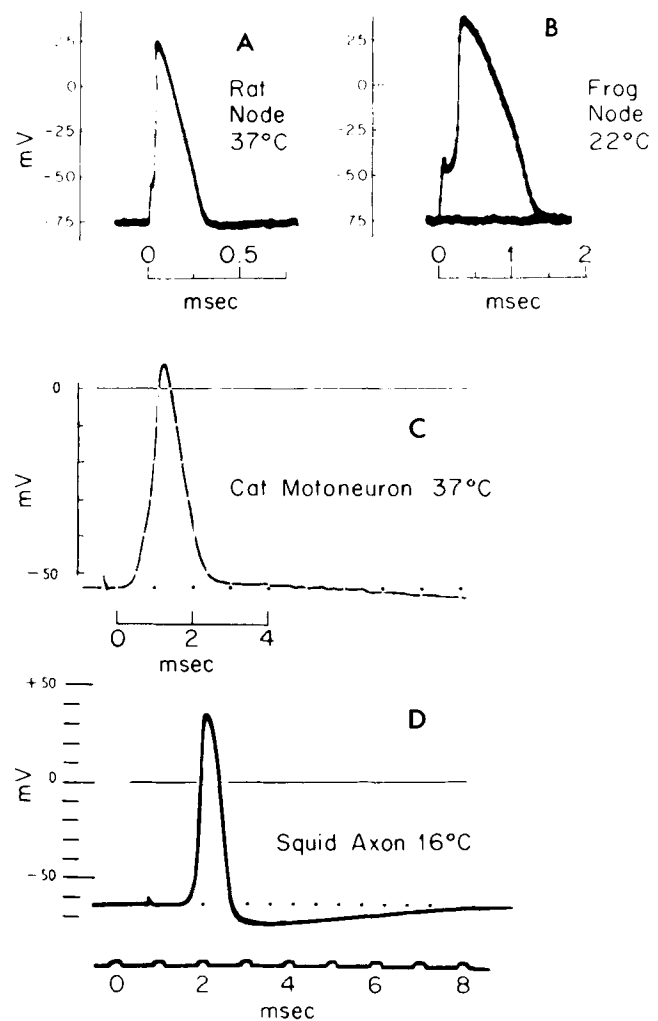


FIG. 1. Intracellularly recorded resting and action potentials from several nerve cells. A: single node of Ranvier of rat myelinated nerve fiber at 37°C. Brief stimulus applied at same node. (W. Nonner, M. Horáková, and R. Stämpfli, unpublished data.) B: same type of recording from frog myelinated fiber as in A, but at 22°C. [From Dodge (56).] C: cat lumbar spinal motoneuron at 37°C, excited antidromically by stimulation of motor axon. (W. E. Crill, unpublished data.) D: propagating action potential in squid giant axon at 16°C. Stimulus applied about 2 cm from recording site. [From Baker et al. (22).]

permeable to potassium ions at rest. Bernstein knew that K^+ is at higher concentration inside cells than outside. Thus K^+ would tend to diffuse out, removing positive charge from the cell interior and setting up a negative internal potential. The potential continues to develop until it is so large as to oppose the further net efflux of K^+ (i.e., until diffusion forces and electric forces exactly cancel). For a membrane exclusively permeable to K^+ , the potential can be calculated from the Nernst equation for equilibrium potentials

$$E_K = \frac{RT}{zF} \ln \frac{[K]_o}{[K]_i} \quad (1)$$

where $[K]_o$ and $[K]_i$ are the outside and inside potassium ion concentrations, z the valence (+1), R the gas constant, T the absolute temperature, and F the Faraday. At 20°C the value of RT/F is 25.3 mV (see Table 4 in section EQUATIONS OF IONIC HYPOTHESIS). E_K is called the potassium equilibrium potential. For no concentration difference, E_K is 0 mV, and for a 10-fold higher internal K^+ concentration than outside, E_K is -58.2 mV. Bernstein's theory was suggested by the depolarizing effect of salts of potassium applied to the surface of nerves. Bernstein (26) further suggested that the propagated impulse involves "an increase of membrane permeability for the retained ion due to a chemical change of the plasma [membrane]." In his view this wave of permeability change overcomes the potassium potential by allowing all ions to diffuse across the membrane simultaneously. In the English-language literature the permeability increase was dubbed a membrane "breakdown." Unfortunately intracellular recording was unknown in 1902, so most quantitative features of Bernstein's proposal were temporarily untestable.

STIMULATION. Bernstein's ideas were generally accepted for 40 years with little proof, as axonologists worked on questions approachable with extracellular recording. When a nerve is artificially stimulated by an externally applied electric shock, the impulse normally arises at the electrode producing depolarization, the cathode or negative (external) electrode. Large shocks stimulate more of the fibers in a nerve than small shocks, and none of the fibers is excited if the shock is too weak. Each individual fiber either does or does not give a propagated response, depending on if the shock is greater or less than a critical *threshold* value for that fiber. For single rectangular current pulses, threshold depends both on the pulse amplitude and duration, and physiologists first thought that study of this strength-duration relation might explain action potentials. As shown in Figure 2A, the required current amplitude is smallest if the shock is long and larger for short shocks. L. Lapicque introduced the terms *rheobase* for the threshold current with long shocks and *chronaxie* for the minimum shock duration required when applying a current of twice the rheobase. While these terms may be used in a descriptive sense, it is now understood that little can be deduced from strength-duration curves on how axons actually are excited. The shape of the curve at long times reflects a complicated interaction between applied depolarizations and the sodium and potassium permeability mechanisms. The hyperbolic shape for short shocks reflects a requirement for a constant amount of charge (current \times time) to depolarize the membrane capacity to a critical starting potential. Once the short shock is over, the membrane immediately begins to repolarize as the charge spreads down the cable and leaks through the membrane (182a). At the same time, the permeability changes of excitation begin to develop. There ensues

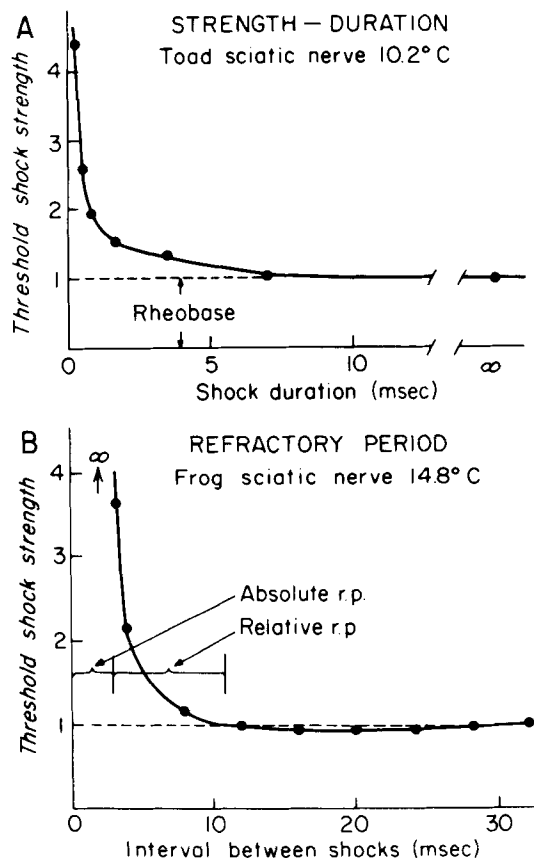


FIG. 2. Strength-duration curve and refractory period in large myelinated fibers of cooled amphibian sciatic nerve. Threshold shock measured as the smallest amplitude shock to the nerve that makes a just-detectable twitch in an attached whole muscle. A: threshold shock amplitude vs. shock duration for a single rectangular shock. [Data from Lucas (162).] B: threshold shock amplitude for a second shock vs. time after a first suprathreshold stimulus. For the first 3 ms the nerve cannot be reexcited [absolute refractory period (*r.p.*)]. For the next 7 ms only a supranormal stimulus will excite (relative refractory period). [Data from Adrian & Lucas (4).]

a race between repolarization and the development of excitation that finally determines if an action potential will develop. With a just-threshold shock, the repolarization is halted at the threshold firing potential where the membrane potential may linger for some time before the action potential finally arises. This *latency* for firing is much shorter with suprathreshold shocks. Because permeability changes develop more slowly at low temperatures, larger short shocks are needed to fire cooled axons. In some axons steady, applied depolarizing currents cause *repetitive firing*. The frequency of the repetitive discharge increases with increasing current strength until at high currents only one impulse is initiated again (116, 218, 206b).

Axons in low external calcium or those partly depolarized by treatments such as elevated external potassium often fire poorly, if at all, at the turnoff (make) of a cathodal current and respond better to the turnoff (break) of an anodal current. This is called

anode-break excitation. As shown later, prolonged depolarization and low calcium depress or inactivate the sodium permeability system. The inactivation may be removed by an applied hyperpolarization, and the axon then fires when the hyperpolarization is turned off (break of anodal current). In some cases with low calcium an axon may fire repetitively with no further stimulus as the hyperpolarizing afterpotential (see subsection *AFTERPOTENTIAL*) from each impulse plays the same role as an anode-break stimulus.

Studies of threshold have revealed several important membrane properties. One is a refractoriness to stimulation following an action potential. For a short period following an adequate stimulus, a second shock cannot elicit an action potential. This is the *absolute refractory period*, which lasts slightly longer than the action potential. Then follows the *relative refractory period*, when a second shock can stimulate but the threshold is elevated (Fig. 2B). As described later, the relative refractory period coincides with the recovery time of ionic permeability mechanisms to their resting state. A second membrane property discovered through studies of threshold is the subthreshold response (115, 146). This is a local extra depolarization elicited by depolarizing stimuli too small to reach threshold. The local response does not propagate as a wave but dies out in the vicinity of the stimulus site. The subthreshold response is now known to be a weak local activation of the membrane permeability changes of excitation.

CONDUCTION. Action potentials in single fibers are all-or-nothing waves propagating without decrement. Figure 3 is a modern recording with two intracellular microelectrodes showing the nearly identical shape of a propagated action potential recorded at two points 16 mm apart in the squid giant axon. The action potential arrives at electrode B 0.75 ms after reaching electrode A. This time delay over a 16-mm conduction distance indicates a conduction velocity of 21.3 m/s in this axon at room temperature.

Conduction velocity depends on axon diameter and temperature. Table 1 gives measured velocities for several different fiber types. Myelinated axons conduct impulses faster than unmyelinated axons of the same diameter. According to a theory of Hodgkin (118) conduction velocity in unmyelinated nerve fibers should vary as the one-half power of axon diameter if axoplasmic resistivity and membrane properties per unit area are constant. Experiments show that these relations apply only approximately. Unmyelinated fibers (2–520 μm) of cephalopod molluscs have a velocity proportional to the 0.57 power of diameter (33a, 194); small fibers (1.6–20 μm) of locust and cockroach obey powers between 0.7 and 0.8 (189), whereas from less direct evidence Gasser (82) concluded that unmyelinated C fibers (0.4–1.2 μm) of the cat saphenous nerve fit the first power with a mean velocity of 1.7 m/s for a 1- μm diameter at 38°C. The

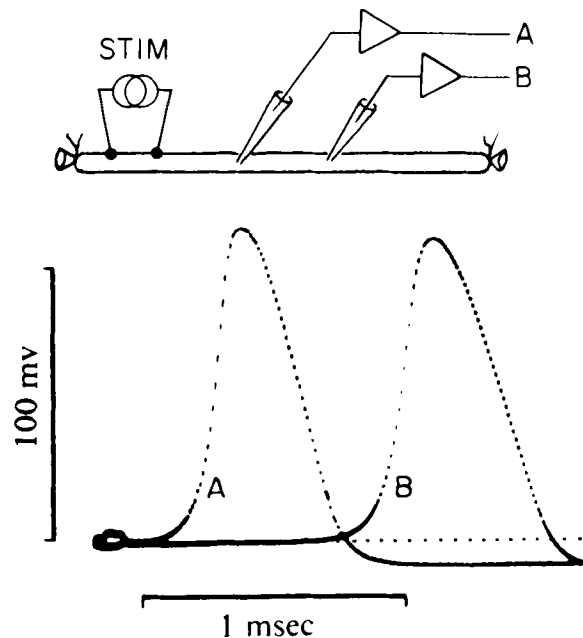


FIG. 3. Propagated action potential recorded intracellularly from 2 points in a squid giant axon. Recording micropipette electrodes A and B separated by 16 mm. Two traces below are the intracellular potentials recorded simultaneously from the microelectrodes showing a 0.75-ms delay or propagation time between points A and B, corresponding to a condition velocity of 21.3 m/s. Temperature, 20°C; axon diameter, about 500 μm . STIM, stimulator. [Adapted from del Castillo & Moore (53).]

TABLE 1. *Conduction Velocities in Nerve and Muscle*

Tissue	Temperature, °C	Fiber Diameter, μm	Velocity, m/s
Cat myelinated nerve fibers	38	2–20	10–100
Cat unmyelinated nerve fibers	38	0.3–1.3	0.7–2.3
Frog myelinated nerve fibers	24	3–16	6–32
Crab large nerve fibers (unmyelinated)	20	30	5
Squid giant axon (unmyelinated)	20	500	25
Frog muscle fibers (unmyelinated)	20	60	1.6

Data from Hodgkin (120).

deviations from Hodgkin's simple theory mean that axoplasmic resistivity or membrane properties are not perfectly invariant as assumed. For myelinated fibers Rushton (203) has shown theoretically that velocity should vary as the first power of diameter, again with provisions of constant properties and certain geometric scaling between fiber sizes. The first power relationship is well established for large myelinated fibers (4–25 μm) (138, 139a, 210). For example, cat nerve fibers at 38°C gain about 6 m/s in velocity per micrometer of outside diameter [(138), but see (49a)]. In the theories mentioned for mye-

linated and unmyelinated fibers the action potential duration does not depend on fiber diameter. However, experiments show a tendency toward longer action potentials (and refractory periods) in the smaller nerve fibers of a related class (64, 139, 187-189).

The temperature coefficient of an experimentally observable quantity can be described by the Q_{10} , the ratio of the measured value at one temperature to the value at a temperature 10° lower. Table 2 gives the effect of 10° temperature changes on conduction velocity in mammalian vagus nerve fibers. Raising the temperature 10° increases velocity by a factor of 1.6-4.8. Myelinated and unmyelinated fibers are similarly affected, with Q_{10} 's rising as the temperature decreases. In the modern theory the high Q_{10} at low temperatures reflects the temperature coefficient of the rate of activation of membrane permeability changes. The Q_{10} is lower at high temperatures because permeability changes become so fast that discharging of the membrane capacitance by fully activated permeability mechanisms begins to be rate limiting (140). Table 2 is for axons of warm-blooded animals. Conduction velocity in cold-blooded animals such as frogs, lobsters, and earthworms is less temperature sensitive than in mammals. For example, in large single myelinated fibers of spring toad nerve the Q_{10} is constant at 1.8 in the range $5-20^\circ\text{C}$ and then falls off at higher temperatures (213). Conduction velocity and its Q_{10} also change with temperature acclimation and seasons.

CABLE. In the 1930's the passive cable properties of axons were worked out in mathematical detail (see the chapter by Rall in this *Handbook*). Cole, Curtis, Hodgkin, and Rushton (39, 41, 133a) found that the surface membrane in squid giant axons and crab nerves is a slightly leaky insulator with the high electrical capacitance of $1 \mu\text{F}/\text{cm}^2$. By contrast, the axoplasm of these fibers is almost as good a conductor as the bathing seawater. These properties demonstrate that the membrane is thin but only poorly permeable to ions, whereas axoplasm contains ions moving almost as freely as in water. The $1 \mu\text{F}/\text{cm}^2$ capacitance is now thought to be a property of surface membranes in all kinds of cells, both excitable and inexcitable. The insulating part of this membrane is probably only 30-40-Å thick.

TABLE 2. *Temperature Dependence of Conduction Velocity in Vagus Nerve*

Unmyelinated Fibers, Desheathed Rabbit Vagus*		Myelinated Fibers, Intact Cat Vagus†	
Temperature, $^\circ\text{C}$	Q_{10}	Temperature, $^\circ\text{C}$	Q_{10}
0-10	3.5	8-18	4.8
10-20	2.1	18-28	2.5
20-30	1.7	27-37	1.6

* Data from Howarth et al. (136). † Data from Paintal (187).

The cable equation for a propagating wave, like the action potential (see Eq. 9), was derived in this same period. The equation requires that impulse propagation involve more than electrotonic spread in a passive cable. Each patch of membrane must become activated to generate a special inward current supporting the disturbance as it passes by. External recording reveals the inward current as a small wave of negative potential sweeping along the outside of the axon. Hodgkin (113, 114) proved that this current is also the stimulus triggering activation in the next patch of membrane. This idea is called the local circuit theory of propagation. Hodgkin demonstrated a temporal parallelism between the action potential in frog sciatic nerve and the threshold decrease beyond a point blocked by cooling to 0°C or by compressing the nerve. Tasaki & Takeuchi (215, 216) extended and expanded these observations with single myelinated nerve fibers.

IMPEDANCE. The last important biophysical accomplishment of this era of extracellular recording returned to the question of membrane changes during activity. Cole & Curtis (41) placed an active squid giant axon between two electrodes in an alternating current impedance bridge to look for changes of membrane resistance and capacitance associated with action potentials. They found a tremendous reduction of membrane impedance developing soon after the first sign of depolarization and lasting some milliseconds after the repolarization (Fig. 4). The membrane resistance drops from $1,000 \Omega\cdot\text{cm}^2$ to $25 \Omega\cdot\text{cm}^2$ during the action potential. Further, although resistance drops 40-fold, membrane capacitance measured at high frequencies changes less than 2%. Their result shows that a vast increase in membrane ionic perme-

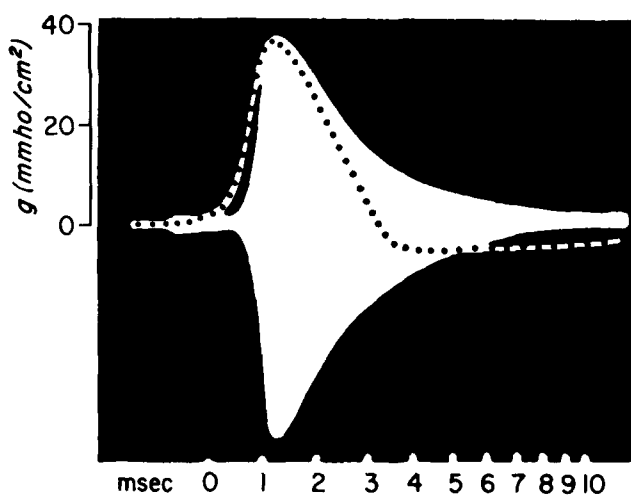


FIG. 4. Membrane conductance increase during propagated action potential. Squid giant axon at about 6°C . Impedance is measured with the bridge circuit and a very high-frequency alternating current applied to extracellular electrodes. Conductance increase shows as a widening of the white band of unresolved high-frequency waves. Time course of action potential is given as a dotted line for comparison. [From Cole & Curtis (41).]

ability does occur in agreement with Bernstein's suggestion. Still this by no means constitutes a total breakdown of the membrane, since the high-frequency capacitance is unaltered, and even in the most permeable state the membrane resistance is a million times higher than that of a corresponding thickness of salt water. Cole and Curtis called the change during activity delicate. Cole & Baker (40) went on to find a resistance change associated with long-applied electric currents as well. The resistance increased under an externally applied anode and decreased under the cathode, or in more modern terminology hyperpolarization increased and depolarization decreased the resistance to current flow. As shown later, this rectifying property of the membrane reflects an important voltage-dependent and time-dependent potassium permeability system in the membrane sometimes called *delayed rectification*. This same potassium permeability system is activated in the late part of the action potential and contributes to the measured impedance decrease in Figure 4. A slow turnoff of potassium permeability upon repolarization explains why the impedance decrease outlasts the action potential. Cole (39) has reviewed impedance measurements.

First Intracellular Recordings from Squid Giant Axons

In 1939 for the first time, Cole, Curtis, Hodgkin, and Huxley (50, 122a) succeeded in recording from inside a nerve fiber. They used the newly rediscovered giant axon of the squid, a cylindrical cell large enough to accommodate glass pipettes or metal wires introduced axially in its cytoplasm. It became possible to make recordings like those of Figure 1. Since the axoplasm of the giant axon could also be squeezed out in quantity sufficient for chemical analysis, the stage was set to develop the ionic hypothesis.

RESTING POTENTIAL. Chemical analysis of squid axoplasm reveals a pattern of ionic concentration differences typical of most cells, whether excitable or not (Table 3). There is more potassium and less sodium inside the cell than in the bathing medium. Ionic gradients are set up by the sodium pump at the expense of metabolic energy, as explained in the chapter on metabolic processes accompanying excitation by Cohen and De Weer in this *Handbook*. In Bernstein's theory the resting potential is set exclusively by potassium ions and therefore should be close to -93 mV, the value for E_K calculated from Table 3 and the Nernst equation at 20°C . However, recorded resting potentials were closer to -60 mV, clearly less than expected (50, 122a).

Curtis & Cole (50) tested the potassium theory more fully by replacing varying amounts of sodium in seawater with potassium (Fig. 5). The circles are the observations, and the straight line labeled E_K is the potassium equilibrium potential calculated from the

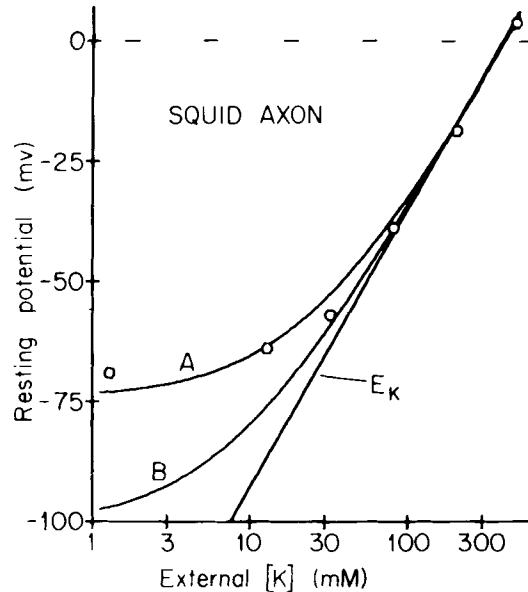


FIG. 5. Potassium dependence of the resting potential in squid giant axon. Sum of external $[K]$ and $[Na]$ kept constant as $[K]_o$, is varied. Standard Woods Hole seawater has 13 mM K. Potentials (\circ) measured with axial micropipette electrode are plotted with the assumption that the resting potential in 13 mM K is -64 mV. Curves are theoretical assuming axoplasmic $[Cl]$ is 90 mM, axoplasmic $[Na]$ and $[K]$ as in Table 3, and $T = 20^\circ\text{C}$. E_K : Nernst potential for potassium. A: solution of the Goldman potential equation with $P_K:P_{Na}:P_{Cl} = 1.0:0.04:0.05$. B: same as in A, but with $P_K:P_{Na}:P_{Cl} = 3.0:0.04:0.05$. [Data from Curtis & Cole (50).]

TABLE 3. Concentrations of Ions and Water in Squid Giant Axons

Substance	Concentration, mmol/kg H ₂ O		
	Axoplasm	Squid blood	Seawater
K ⁺	400	20	10
Na ⁺	50	440	460
Ca ²⁺	0.4	10	10
Mg ²⁺	10	54	53
Cl	40-150	560	540
Organic anions	385		
Water	865*	870*	966*

* Value expressed in g/kg. [From Hodgkin (120).]

Nernst equation on the assumption that internal potassium does not change during the experiment. At high potassium concentrations the resting potential does follow E_K well, and in isotonic potassium, where inside and outside concentrations are almost equal, the potential is close to zero. Under these circumstances there is selective potassium permeability. Under physiological conditions, however, the Nernst equation does not fit, and an extension of the potassium theory is needed.

One testable explanation for the discrepancy between predicted and observed resting potentials is that the activity of axoplasmic potassium ions is not correctly determined by a chemical analysis of total axoplasm. The ratio $[K]_o/[K]_i$ in the Nernst equation is actually the ratio of external and internal thermo-

dynamic activities of K^+ rather than concentrations. Whenever this distinction is ignored, the tacit assumption is made that internal and external factors affecting ionic activities are equal and cancel out when ratios are taken. The activities of ions are generally lower than measured concentrations because some ions are bound or complexed with others, some ions are sequestered in organelles of the axoplasm, and finally the free ions experience electrostatic shielding caused by nearby ions of the opposite charge. The activities of ions are increased when some of the water measured in the analysis is not free to act as solvent water.

If internal potassium ions were only 25% as free as external ones, the predicted resting potential would be -60 mV in agreement with observations. But then the absence of a resting potential with equal internal and external potassium concentrations would no longer be explained. Measurements by Hodgkin & Keynes (131) showed that the mobility of K^+ in *Sepia* axoplasm is the same, within 10%, as the mobility in 500 mM KCl. They injected ^{42}K and measured diffusional spread and the drift of K^+ in an electric field applied along the length of the axon. Hinke (109) made ion-specific glass microelectrodes to measure sodium and potassium activities in squid axons directly. The results may be expressed as the ratio of measured activity to measured concentration, an apparent activity coefficient. For potassium and sodium the ratios in axoplasm were 0.60 and 0.46 (109), compared with 0.64 and 0.70 in seawater (171). Thus for potassium, activity coefficients are almost equal in and out, and binding definitely does not explain the discrepancy between predicted and observed resting potentials.

Much more recently, work has been done to determine the state of ions and water in muscle cells. The diffusion constants of potassium, sodium, sulfate, sorbitol, sucrose, and ATP in myoplasm of frog skeletal muscle are reduced by a factor of two over their dilute solution values (159). A nuclear magnetic resonance study indicates 40% binding of sodium in frog myoplasm (165). Diffusion constants of water, urea, and glycerol in myoplasm of the giant barnacle are like those in dilute solution (32), whereas apparent activity coefficients of sodium and potassium are actually higher than in seawater, despite some binding, because over 30% of the fiber water does not act as solvent water (110, 111). Although these different effects are so large that they should be considered in any precise work, the measurements are not available for most tissues, so no corrections can be made. Some investigators (161) believe that almost all the internal potassium is bound, although most studies do not confirm this view.

The solution to the resting potential problem was given by Goldman (86). He noted that the normal resting membrane might be permeable to several ions and therefore would not be at an equilibrium

potential such as E_K , but rather at some steady-state potential given by a nonequilibrium formula. The formula would weight the contributions of ions to the potential in proportion to their relative concentrations and relative permeabilities. According to the constant field theory given by Goldman the resting potential is

$$E = \frac{RT}{F} \ln \frac{P_K[K]_o + P_{Na}[Na]_o + P_{Cl}[Cl]_i}{P_K[K]_i + P_{Na}[Na]_i + P_{Cl}[Cl]_o} \quad (2)$$

if potassium, sodium, and chloride are the permeant ions and their permeabilities are P_K , P_{Na} , and P_{Cl} . Equation 2 is generally known as the Goldman or the Goldman-Hodgkin-Katz potential equation. Using this approach, Hodgkin & Katz (130) estimated ratios of $P_K:P_{Na}:P_{Cl}$ to be 1.0:0.4:0.45 for squid axons in standard seawater. Evidently potassium is still the most permeant ion in resting axons, but the contribution of other ions is significant because the potassium content of normal extracellular solutions is so low.

The potential measurements of Curtis & Cole (50) are reanalyzed in Figure 5 using the Goldman equation. Several assumptions regarding absolute levels of potential and ionic concentrations are given in the legend. The calculated permeability ratios are quite sensitive to a 1-mV error in potential and also require the assumption that internal concentrations do not change as the external concentrations are varied, so in most such studies the ratios cannot be accurately determined. *Curve A* corresponds to ratios $P_K:P_{Na}:P_{Cl} = 1.0:0.04:0.05$ and *curve B* to ratios 3.0:0.04:0.05. The measured resting potential in Woods Hole seawater with 13 mM K falls near *curve A*. The potential in 1.3 mM K^+ solution fits a smaller relative value of P_K and that in 33 mM K^+ fits a higher value. This increase of P_K with increasing external potassium comes from the effect of voltage on the potassium permeability system, a phenomenon related to the increase of P_K with depolarizing current (40).

The assumptions and derivations of this and other equations relating to ionic movements across membranes are given in the final section of this chapter. An exact definition of permeability (Eq. 43) is given there as well. With several permeant ions there are steady ionic fluxes that would eventually reduce all concentration differences to zero unless some ion pumps continually restore the ions lost or gained. Evidence for such pumps is given in the chapter on metabolic processes accompanying excitation by Cohen and De Weer in this *Handbook*. Even when pumps are not operating, the concentration gradients may last hours, since the fluxes in question are often minute. Typical values of ionic fluxes at rest are measured in picomoles per second per square centimeter of membrane area. Small nerve fibers with large surface-to-volume ratios lose their ionic concentration gradients before large fibers, if pumping is stopped.

A complete description of resting potentials is still missing. The resting state has seemed less interesting than the excited state and has attracted less attention. The situation is complicated because even ions with small permeabilities can make significant contributions, as the separation of the three lines in Figure 5 shows. All permeabilities may be very voltage-dependent, and internal concentrations may change. Careful simultaneous measurements of potential, flux, and resistance are needed if the theory is to be refined much further. The most careful description so far is for frog skeletal muscle in which, unlike axons, chloride permeability is the dominant resting permeability [(121, 122); see the chapter on muscle by Costantin in this *Handbook*].

Recent work shows that resting potential is affected by sources of current not included in the Goldman potential equation. These current sources are ion pumping mechanisms in the membrane, sometimes requiring metabolic energy. Their effect on the resting potential is described in the chapter by Cohen and De Weer in this *Handbook*. In brief the sodium pump is electrogenic because more Na⁺ is pumped out than K⁺ pumped in. The net outward transfer of positive charge hyperpolarizes the cell with respect to the potential predicted from the Goldman equation without a pump. If the net outward electric current from electrogenic pumping is I_{pump} , the potential equation [(170); see also final section of this chapter] takes the implicit form

$$E = \frac{RT}{F} \ln \frac{P_K[K]_o + P_{Na}[Na]_o + P_{Cl}[Cl]_i + (RT I_{pump}/F^2E)}{P_K[K]_i + P_{Na}[Na]_i + P_{Cl}[Cl]_o + (RT I_{pump}/F^2E)} \quad (3)$$

The pump current depends on temperature, concentrations of external potassium and internal sodium, and other factors. As already mentioned the rate of pumping also has a long-term effect on axoplasmic ion concentrations.

In resting axons electrogenic pumping may contribute little to the resting potential. The squid axon depolarizes only 1–2 mV, immediately upon blocking the sodium pump with strophanthidin (54). However, some kinds of axons loaded with sodium by a period of intense activity develop a posttetanic hyperpolarization of tens of millivolts (198, 217). The hyperpolarization can last many minutes until the extra sodium is extruded. Nerve cell bodies also can have a significant pump component of resting potentials, perhaps because their higher specific membrane resistance increases the effect of a given I_{pump} (170).

ACTION POTENTIAL. In its simplest form, Bernstein's theory predicts a near-zero membrane potential at the peak of the action potential. For example, if P_{Na} , P_{Cl} , and P_K all become equal in the spike, Equation 2 and Table 3 predict a potential of -15 mV at the peak. It was a surprise then when Hodgkin & Huxley

(122a) and Curtis and Cole (50) first recorded action potentials overshooting zero by +20 to +50 mV like those in Figure 1. Neither this overshoot nor the delicate impedance change of Cole and Curtis agreed fully with the prevailing concept of extensive membrane breakdown. An improved theory was needed.

The problem was resolved by the sodium hypothesis. Hodgkin & Katz (130) proposed that the permeability to sodium, P_{Na} , rises during the action potential to a value much higher than P_K or P_{Cl} . This would permit a sudden inward movement of positively charged Na⁺, causing the potential to surge from near the potassium potential E_K to near the sodium potential E_{Na} .

$$E_{Na} = \frac{RT}{F} \ln \frac{[Na]_o}{[Na]_i} \quad (1a)$$

By the chemical analysis in Table 3, E_{Na} is around +53 mV, again assuming no complications from internal binding. Hodgkin and Katz tested their hypothesis by replacing some of the external NaCl with sucrose, dextrose, or choline chloride. As shown in Figure 6, the action potential rises more slowly and

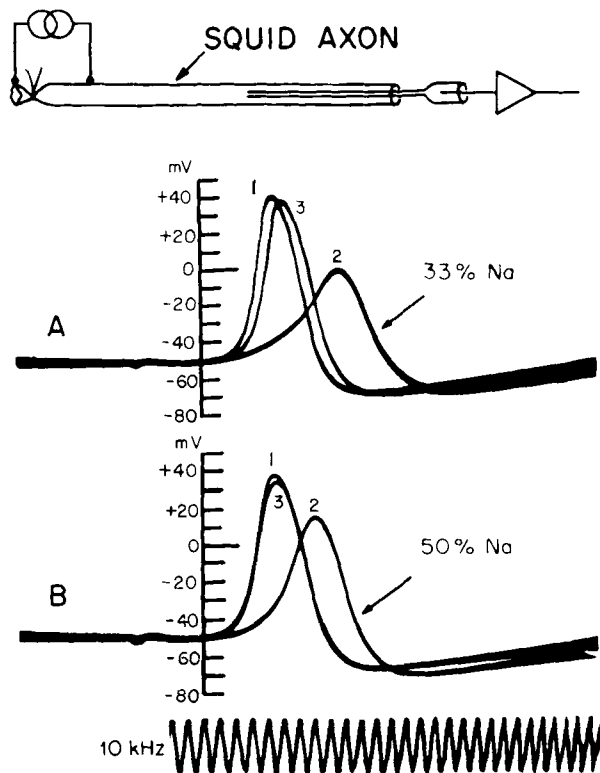


FIG. 6. Experiment showing that the action potential is smaller and rises more slowly in solutions containing less than the normal amount of sodium. Squid giant axon with axial micropipette recording electrode. Bathing solutions: records 1 and 3 in seawater; record 2, part A in low-sodium solution containing 1 part seawater to 2 parts isotonic dextrose; record 2, part B, same as above, but with a 1:1 mixture of seawater and dextrose. Recorded potentials are probably 10–15 mV too positive because of a junction potential between micropipette and axoplasm. [From Hodgkin & Katz (130).]

overshoots less when the external sodium is reduced. Specifically with only 50% of the normal sodium, the peak of the spike is 21 mV less positive. Since the reduction of E_{Na} calculated from the Nernst equation is 17 mV, the observation agrees reasonably well with the sodium theory.

The reduction in rate of rise of the action potential in Figure 6 also fits the sodium theory, but the reasoning requires several electrical arguments from cable theory. The membrane has electrical capacitance, which means that a certain quantity of charge (ions) must be moved up to or away from the surface of the membrane in order to change the membrane potential; the charge q_c in the capacitor per unit area of axon is proportional to the potential

$$q_c = C_m E \quad (4)$$

where C_m is the capacitance per unit area. A change of potential requires a change of stored charge or a current I_c flowing into the membrane capacitor

$$I_c = \frac{\partial q_c}{\partial t} = C_m \frac{\partial E}{\partial t} \quad (5)$$

Since this capacity current flows in parallel with ionic current I_i across the membrane, the net membrane current is given by the sum of ionic and capacitive currents

$$I_m = I_i + I_c \quad (6)$$

By the cable theory the net membrane current I_m per unit area is proportional to the second derivative of voltage with distance

$$I_m = \frac{a}{2R_i} \frac{\partial^2 E}{\partial x^2} \quad (7)$$

where a is the axon radius and R_i the axoplasmic resistivity. Finally for any propagating wave of constant velocity and shape, like the action potential, the shape of E against time at any position is the same as the shape against distance at any time and therefore

$$\frac{\partial^2 E}{\partial x^2} = \frac{1}{\Theta^2} \frac{\partial^2 E}{\partial t^2} \quad (8)$$

where Θ is the conduction velocity. Taken together Equations 5-8 give

$$\frac{a}{2R_i \Theta^2} \frac{\partial^2 E}{\partial t^2} = I_m = I_i + C_m \frac{\partial E}{\partial t} \quad (9)$$

During the rising phase of the action potential $\partial E/\partial t$ passes through a maximum and $\partial^2 E/\partial t^2$ therefore becomes zero. According to Equation 9 the net membrane current I_m vanishes at this moment to give

$$I_i = -C_m \frac{\partial E}{\partial t} \quad (10)$$

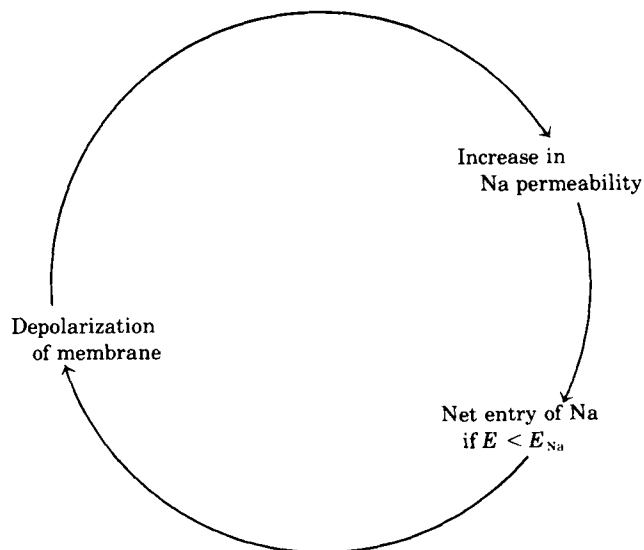
Hodgkin and Katz found that the maximum rate of

rise and hence I_i in the above formula both fall by 50% when 50% of the bathing sodium is removed. If all the ionic current at that time were carried by Na^+ , the Goldman-Hodgkin-Katz flux equation (see Eq. 42) would predict a 58% drop in current, in fair agreement with the observations.

The velocity of conduction also falls as the external sodium concentration is reduced.

The sodium theory of Hodgkin & Katz (130) was soon confirmed in experiments with ^{24}Na by Keynes (148) who measured a net extra sodium entry of 3.5 pmol/cm² per impulse. This sodium gain is more than enough to account for charging the membrane capacitor to E_{Na} . On the other hand, the gain is so small that the internal sodium concentration of a 500- μ m axon is increased by only one part in 80,000 per impulse.

Within a few years of Hodgkin's and Katz's work on squid axons, conduction in other axons and some muscle cells was shown to be sodium dependent as well. There emerged from these studies the important generalization that an inward sodium movement is the genesis of action potentials in all cells, and in a pivotal review Hodgkin (117) offered the following cycle for regenerative responses: depolarization increases sodium permeability, which allows sodium entry, which increases depolarization.



This generalization applies to every axon studied so far but is now known not to apply to all muscle cells or neuron cell bodies where Ca^{2+} often plays the role of inward current carrier.

AFTERPOTENTIAL. The membrane potential often remains a few millivolts above or below the resting level for a period following an action potential. For example, the squid axon may be hyperpolarized for 3-10 ms after the spike (Figs. 1, 3, and 6). This undershoot is called an *afterpotential*. In the traditional nomenclature dating from the era of extracellular

recording, the squid axon is said to have a *positive* afterpotential because an external electrode would record positivity. Likewise a frog skeletal muscle fiber is said to have a *negative* afterpotential. These terms are apt to be confusing and are sometimes more conveniently replaced by *afterhyperpolarization* or *hyperpolarizing afterpotential* and *afterdepolarization* or *depolarizing afterpotential*.

Afterpotentials have several causes. The afterhyperpolarization in squid axons comes from a 15-fold increase of P_K during the action potential that reverses only slowly at rest (126). The afterdepolarization of frog skeletal muscle may come from a lingering permeability increase primarily to potassium but with a low $P_K:P_{Na}$ ratio compared to the resting permeability mechanism (5). Electrogenic sodium pumping, turned on by the sodium gain during an impulse, tends to hyperpolarize. Usually repetitive activity is needed to make an appreciable afterpotential from pumping. High-frequency repetitive activity also tends to bring on a depolarizing effect due to a temporary extracellular accumulation of potassium from each impulse (77). The membrane potential falls in response to the fall of E_K . Permeability changes, electrogenic pumping, and potassium accumulation all occur at the same time. Which is most important depends on factors like the temperature, surface-to-volume ratio of the fiber, number of impulses fired, and presence of diffusion barriers in the extracellular space. Afterpotentials may last from a few milliseconds up to minutes, and they may have several phases. Throughout the afterpotential the excitability of the cell differs from that of a quiescent cell.

DIRECT MEASUREMENT OF IONIC CURRENTS IN AXON MEMBRANES

Studies of the action potential up to 1949 established the important concepts of the ionic hypothesis. The axon membrane separates ionically dissimilar solutions and has selective ionic permeability that varies under applied currents and during the action potential. At rest P_K is the most important permeability, while during excitation P_{Na} increases until it far exceeds P_K . The permeability changes explain the electric excitation of nerve.

These ideas were proven and given a quantitative basis by a new type of experimental procedure developed by Cole (38), Marmont (164), and Hodgkin, Huxley, and Katz (128, 129) in 1947 and 1948. The method is known as the *voltage clamp*. Using this method, Hodgkin & Huxley (126) developed a definitive kinetic description of the voltage and time dependence of ionic permeability changes in squid giant axon membranes. Their model is the cornerstone of the modern theory of excitation. This section describes measurements of ionic current and methods for separating the current into components carried by differ-

ent ions. Modern voltage-clamp studies are the subject of several books (1, 7, 39, 120, 212).

Voltage-clamp Method

To voltage clamp means to control the voltage across the cell membrane. For example, the membrane potential might be forced to step from the resting potential to -10 mV for 3 ms and then back to the resting potential. To maintain a constant potential in the clamp, electric currents must be injected into the cell exactly offsetting the membrane currents. The required current varies rapidly in time as permeability changes occur in the membrane. The object of the method is to use the injected current as a measure of the time dependence and amplitude of ionic permeability changes in the membrane.

In theory the connection of an ideal battery between inside and outside will set the voltage to the desired value, but practical considerations require that the experimenter control the voltage actively by continuously adjusting the applied current as membrane characteristics change. Actually changes of membrane permeability are so rapid that a feedback amplifier with good high-frequency response makes the adjustment instead of the human hand. Some simplified arrangements for voltage clamping axons and cell bodies are shown in Figure 7. Each comprises an intracellular electrode and follower circuit to measure the membrane potential, a feedback amplifier to amplify any difference (error signal) between the recorded voltage and desired value of membrane potential, and a second intracellular electrode for injecting current from the output of the feedback amplifier. The circuits are examples of negative feedback since the injected current has the sign required to reduce the error signal. The method also requires that membrane current be measured in a patch of membrane with no spatial variation of membrane potential. In axons, spatial uniformity of potential, called the *space-clamp* condition, can be achieved by inserting an uninsulated internal axial wire (Fig. 7) or by isolating a very short stretch of axon with a double gap (Fig. 7). Hodgkin, Huxley, and Katz used an internal axial wire in the squid giant axon. Further details of voltage-clamp methods are found in the original literature (5, 8, 35, 45, 51, 57, 129, 185).

As has already been described, the total membrane current is equal to the sum of currents carried by ions crossing the membrane and currents carried by ions moving up to the membrane to charge the membrane capacitor

$$I_m = I_i + I_c = I_i + C_m \frac{\partial E}{\partial t} \quad (9)$$

Equation 9 shows that no capacity current flows while the voltage is held constant, since $\partial E/\partial t$ is zero. At each step of potential, capacity current flows in a very brief surge as the membrane capacitor becomes

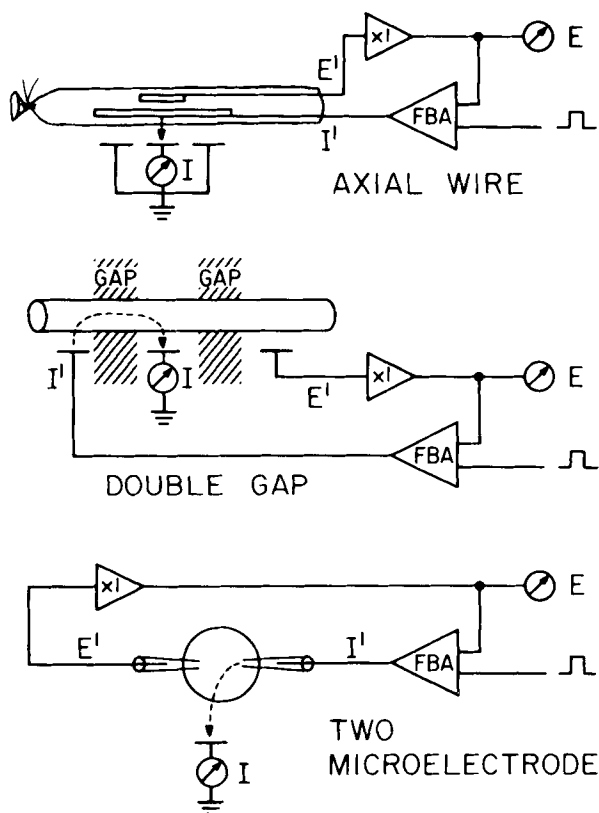


FIG. 7. Simplest form of the 3 common voltage-clamp methods. In each case there is an electrode for voltage recording (E') connected to a high-impedance follower ($\times 1$). The output of the follower is recorded at E and also compared with the voltage-clamp command pulse by a feedback amplifier (FBA). The highly amplified difference of these signals sends a current through the current-passing electrode (I') and across the membrane to a ground electrode, where it is recorded (I). Dashed arrows, path of current flow from current-passing electrode to ground. In the 3 methods the membrane studied is bathed in appropriate saline. In the double-gap method the central saline pool is separated from end pools by insulating gaps of air, sucrose, oil, or petroleum jelly, and the end pools contain isotonic KCl.

charged to a new value. This fact simplifies the interpretation of voltage-clamp records since the total recorded current can be identified with ionic current at most times. The steps in the analysis are to determine which ions carry the current and then to calculate permeabilities from the measured currents and known driving forces.

Much of the following is taken from voltage-clamp studies by Hodgkin, Huxley, and Katz. For technical reasons the electrodes they used were not suited for recording the absolute potential, so all potentials were recorded relative to rest rather than relative to the external potential. In much of the recent voltage-clamp literature, potentials relative to rest are symbolized by V and those relative to outside by E . Throughout this chapter all axons studied under voltage clamp by Hodgkin, Huxley, and Katz are assumed to have resting potentials of -65 mV, and potentials are given on the E scale. All their figures

reproduced here are relabeled using this assumption. Also by the modern convention, current flowing outward across the membrane is considered positive and drawn upward in all figures.

Electrochemical Separation of Ionic Currents

Figure 8 shows current records measured from a squid giant axon under voltage clamp and cooled to 3.8°C . A hyperpolarizing voltage step to -130 mV produces a very small maintained inward ionic current. The 65 -mV hyperpolarization from rest gives an ionic current density of only $30 \mu\text{A}/\text{cm}^2$, corresponding to a low resting conductance of $0.46 \text{ mmho}/\text{cm}^2$. A brief surge of inwardly directed capacity current occurs in the first $10 \mu\text{s}$ of the hyperpolarization but is too fast to be photographed here. When the axon is depolarized to 0 mV, the currents are quite different. A brief outward capacity current is followed by a large transient inward ionic current lasting 1 – 2 ms, giving way finally to a large maintained outward ionic current. The biphasic ionic current seen with this depolarization is qualitatively just what is expected from the results of Hodgkin & Katz (130) on the action potential. The inward and outward current densities of $1 \text{ mA}/\text{cm}^2$ are sufficient to explain the high rates of rise and fall of action potentials in unclamped axons using Equations 9 and 10. The inward current might be an inward movement of Na^+ during an early period of high P_{Na} , and the later outward current could be an outward movement of K^+ . Experiments are now described that confirm these ideas.

ION SUBSTITUTION EXPERIMENTS. As Hodgkin & Huxley (123) first showed, an exact dissection of the total currents into ion-specific components I_{Na} and I_{K} can be achieved by replacing the ions one at a time by inert impermeant ions. Figure 9 shows the results of substituting choline chloride for most of the NaCl in seawater. Curve A is the total ionic current recorded

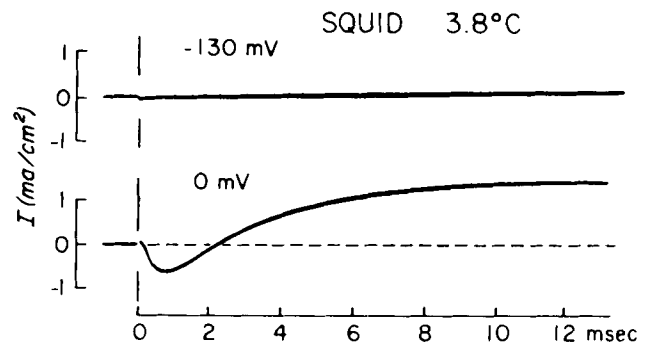


FIG. 8. Different character of voltage-clamp currents with hyperpolarizing and depolarizing pulses. Outward current shown as an upward deflection. *Top*: squid axon hyperpolarized by 65 mV from rest to -130 mV at $t = 0$. Currents are small and inward. *Bottom*: axon depolarized from -65 mV to 0 mV at $t = 0$. Currents are biphasic and much larger than under hyperpolarization. [Adapted from Hodgkin et al. (129).]

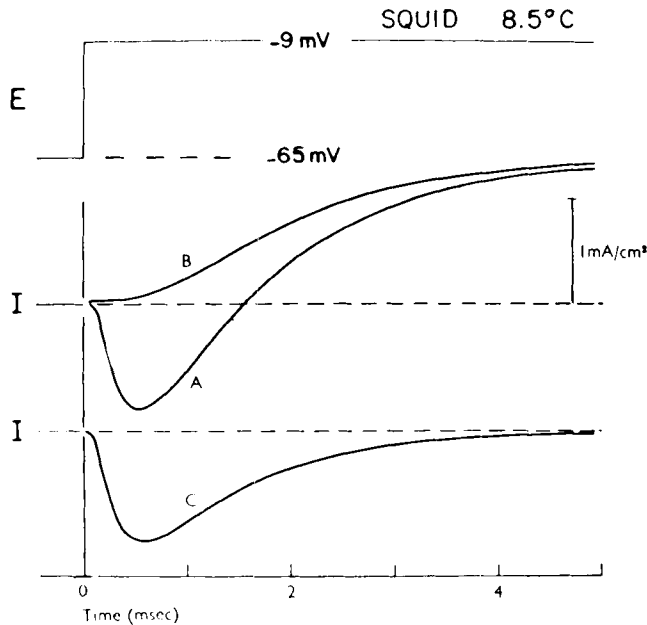


FIG. 9. Separation of ionic currents in squid giant axon by ionic substitution method. Voltage (E) is stepped from rest to -9 mV at $t = 0$. *A*: axon in seawater, showing inward and outward current. *B*: axon in low-sodium seawater with 90% of the NaCl replaced by choline chloride, showing only outward current. *C*: algebraic difference between curves *A* and *B*, showing the transient inward component of current that requires external sodium. [From Hodgkin (119), adapted from Hodgkin & Huxley (123).]

in standard seawater, exactly as in Figure 8, and curve *B* is the current in low-sodium seawater. Removal of sodium eliminates the transient inward current as expected if Na^+ carries that current. Curve *C* is the algebraic difference between curves *B* and *A*. Interpretation of these curves rests on the assumption that the movement of ions is independent of the number and type of other ions present in the bathing medium. This idea is called the *independence principle* (123). If replacement of sodium with choline does not alter other currents, curve *C* is the time course of the transient inward movement of Na^+ in standard seawater, and curve *B* would be the summed time course of all other ionic movements, primarily outward potassium movements. Fortunately other kinds of measurements to be described confirm the identification of curve *C* with sodium current, I_{Na} , and curve *B* with potassium current, I_{K} , so that the assumption of independence is at least roughly correct in this experiment. To be more precise, curve *B* is the sum of potassium current, leakage current, and any residual sodium current, and I_{K} is by far the largest of the three.

REVERSAL OF CURRENT AT NERNST POTENTIAL. An important proof that the observed early transient current is carried by Na^+ comes from application of the Nernst equation. If the external and internal activities of sodium are in the same ratio as the concentration ratio in Table 3, E_{Na} at 3.5°C should be

near $+53$ mV. The degree of internal sodium binding observed by Hinke (109) brings this number up to $+63$ mV. At this potential no net sodium current should be observed, and above this potential sodium should flow out of the axon. The expected reversal of the early current at high voltages is seen in voltage-clamp experiments. Figure 10 shows five traces of ionic current recorded at various voltages in the vicinity of the predicted E_{Na} . The change of current in the initial $300 \mu\text{s}$ of the voltage steps is negligible at $+52$ mV, positive at $+78$ and $+65$, and negative at $+39$ and $+26$. Thus the reversal of current occurs close to $+52$ mV, a somewhat lower potential than expected for a perfectly sodium-selective permeability mechanism.

The most convincing evidence for identifying current carriers comes from combination of the ionic substitution method with measurements of reversal potential. For changes of external sodium from $[\text{Na}]_1$ to $[\text{Na}]_2$ with internal sodium held constant, the theoretical change of equilibrium potential is given by

$$E_{\text{Na},2} - E_{\text{Na},1} = \frac{RT}{F} \ln \frac{[\text{Na}]_2}{[\text{Na}]_1} \quad (11)$$

Note that this equation differs from Equation 4, the Nernst equation, from which it is derived, in that it contains only external sodium concentrations. Hodgkin & Huxley (123) tested Equation 11 on the reversal of early currents in squid giant axons. Reducing the external sodium concentration 10-fold reduced the measured reversal potential by 55 mV at 6.3°C . This is within experimental error of the 55.6-mV theoretical change of E_{Na} , confirming the identification of the early transient current with Na^+ flow. The same kind of experiment with myelinated nerve fibers is shown in Figure 11. Current is recorded at seven voltages spaced nominally 15 mV apart. As external sodium is reduced successively twofold, the reversal potential falls in 15-mV steps. Finally in the absence of sodium

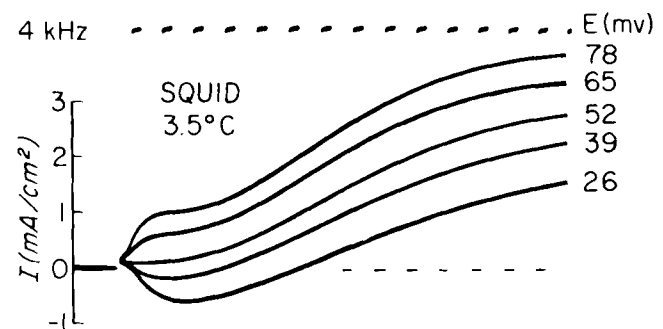


FIG. 10. Ionic currents at large depolarizations showing reversal of early current around sodium equilibrium potential. Squid giant axon under voltage clamp depolarized from rest to the indicated voltages. In the first 0.5 ms the initial current is inward at 26 and 39 mV and outward at 65 and 78 mV. Reversal potential is near 52 mV. As elsewhere in this chapter, potential values are based on the assumption that the resting potential was -65 mV. [From Hodgkin (119), adapted from Hodgkin & Huxley (123).]

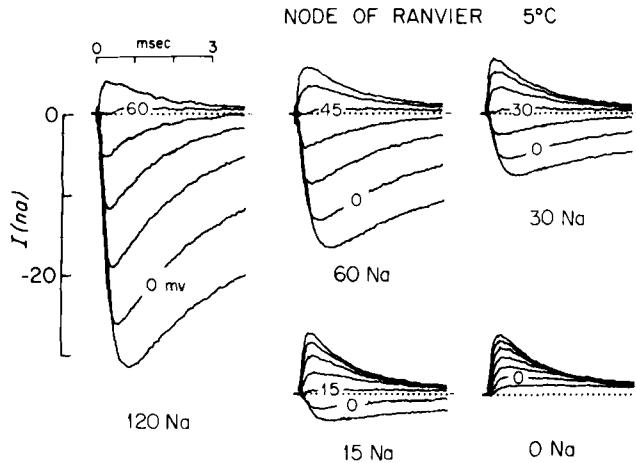


FIG. 11. Sodium ion currents at different voltages, showing that reversal potential falls as external sodium concentration is reduced. Node of Ranvier depolarized under voltage clamp at $t = 0$ to 7 different voltages spaced 15 mV apart and ranging from -15 to $+75$ mV. Capacity and leakage current already subtracted and potassium currents blocked by 6 mM TEA ion in all solutions. Sodium concentration (mM) is given under each family of curves. Tetramethylammonium bromide was substituted for NaCl to make the low-sodium solutions. Labels on current traces are membrane potential in millivolts. The trace at 0 mV and the trace nearest to the reversal potential in each solution are labeled. Dotted line, zero-current level. [Unpublished data, described in Hille (105).]

all currents are outward. The predicted change of E_{Na} at this temperature is 16.6 mV per twofold dilution of sodium. The small difference between theory and experiment here is thought to lie more with difficulties in recording from single myelinated nerve fibers than with imperfections of the theory (58), and again Na^+ seems to carry the early inward current.

Chandler & Meves (35, 36) measured the reversal potential of early current in squid giant axons as a function of internal sodium concentration. The axoplasm was squeezed out of the axon, and the axon was reinflated by perfusing an artificial salt solution through the inside, a procedure that does not damage the excitability mechanism. In this case no arbitrary assumptions concerning internal binding or compartmentalization of Na^+ had to be made since solutions of measured sodium activity were used. As $[Na]_i$ was increased by replacing $[K]_i$, the reversal potential fell almost as predicted by the Nernst equation. There is a small discrepancy between predictions and observations in these experiments which is discussed later as an example of the incomplete selectivity of the early current mechanism.

TRACER FLUX MEASUREMENT. The influx of tracer ^{22}Na has been measured in squid giant axons under voltage-clamp conditions (19, 29). Short depolarizing pulses were applied at 10/s, and the axons were perfused internally with flowing solutions, so the entering radioactivity could be recovered and counted continuously. At the same time the total ionic current

was recorded and separated into sodium and potassium components by conventional voltage-clamp methods. In two series of experiments the measured extra sodium influx was 0.92 ± 0.15 and 1.04 ± 0.07 of the amount estimated by integrating the early transient currents. Measurements of fluxes accompanying depolarizing pulses of different durations confirmed that sodium permeability rises with a small delay and decays to very small values during long depolarization as already seen in the voltage clamp.

POTASSIUM CURRENT. In the first experiments with squid giant axons the evidence that the late outward currents (Fig. 9, B) are carried by K^+ was only indirect. The current remained after all external sodium was replaced, and the reversal potential was near -77 mV as compared with a calculated value of -89 mV for E_K at $6^\circ C$, assuming that no ions are bound. Outward current has to be carried by a cation moving outward or an anion moving in, and Keynes (148, 149) had demonstrated a net potassium efflux of about 4 pmol/cm² per propagated impulse in *Sepia* giant axons. Later experiments used ^{42}K as a tracer in *Sepia* axons depolarized by applied current for many minutes at a time. The measured total potassium efflux agreed precisely with the integrated outward current (127). Newer voltage-clamp evidence shows that outward currents become smaller as the internal potassium concentration is decreased in internally perfused squid giant axons (35) and that the reversal potential for late current becomes more positive as external potassium is elevated, in good quantitative agreement with the Nernst equation (75). Figure 12 shows ionic currents in a myelinated fiber under voltage clamp. First the fiber is bathed in a solution with 120 mM Na. The normal biphasic current appears on depolarization. When potassium is substituted for the external sodium, the early sodium current vanishes and the late current reverses sign to flow inward, as expected if it is carried by K^+ . These results all agree on the identification of late outward currents with I_K .

Pharmacological Separation of Ionic Currents

SELECTIVE BLOCK. Although in many experiments it is desirable to study sodium currents or potassium currents separately, the methods of ionic substitution or tracer flux measurement are often not convenient or compatible with the protocol. Fortunately another practical method is available: the selective block of sodium or potassium permeability mechanisms by drugs. The poisons tetrodotoxin (TTX) and saxitoxin (STX) selectively block the sodium permeability mechanism in most nerve fibers (65, 103, 168). Block develops rapidly when the poisons are applied to the outside of axons at concentrations in the range 5–100 nM. Figure 13 illustrates how TTX is used to separate currents in the voltage clamp. A normal family

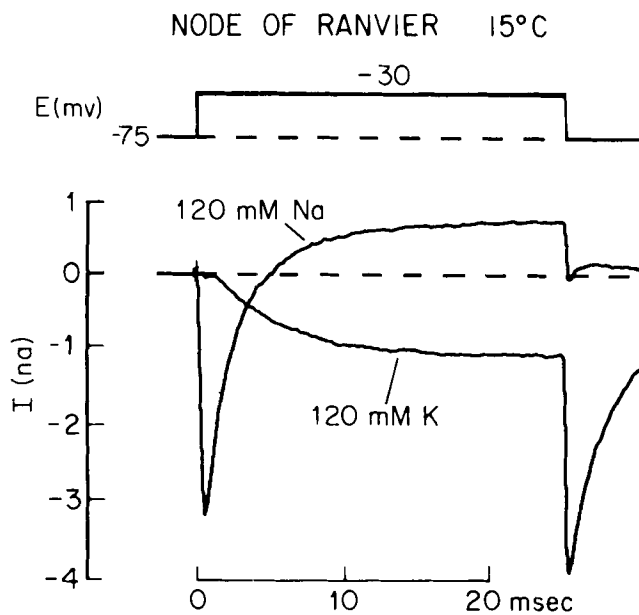


FIG. 12. Reversal of the direction of late current by increasing external K^+ concentration. Ionic currents, after subtracting leakage, of a node of Ranvier depolarized from rest to -30 mV at $t = 0$. In Ringer's solution with 120 mM NaCl there is a transient inward sodium current and a small outward late current. To permit better resolution of late current, sodium current has been reduced 8-fold over normal by inclusion of 30 nM TTX in the medium. When NaCl of Ringer's is replaced by 120 mM KCl, inward sodium current disappears and late current becomes inward as expected for potassium flow with symmetrical potassium concentrations. At the moment the axon is repolarized, the electrical driving force on K^+ is increased and a large tail of potassium current appears.

of ionic currents recorded at many voltages is shown in Figure 13A. After application of 300 nM TTX (Fig. 13B), the sodium component in each trace is gone. The remaining time-dependent current is I_K . The time course of this current is identical to that obtained by the sodium-substitution method of Hodgkin and Huxley.

The effect of TTX on ionic current is shown in a different way in Figure 14. The size of ionic current is plotted against test potential for an experiment with a giant axon of the annelid worm *Myxicola*. Circles are the peak early current, normally carried by Na^+ , and triangles are the plateau of late outward current, carried by K^+ . This type of current-voltage relation is probably the most commonly used graph in voltage-clamp papers. The inward sodium currents are abolished by 10^{-6} M TTX, while potassium currents are unchanged.

Tetraethylammonium (TEA) ion and other quaternary ammonium ions can also be used to separate currents in some cells. These drugs block the potassium permeability mechanism rapidly at 1 - 10 mM concentration (10, 11, 15, 16, 100, 156). In most cases the drug must be applied inside the axon although in myelinated fibers there is also an external site of action. Figure 13, C and D shows the block of I_K with

6 mM TEA ion outside a myelinated fiber. The time-dependent current remaining during TEA treatment (Fig. 13D) is I_{Na} . Tetraethylammonium ion was also used to obtain the sodium currents in Figure 11.

In addition to the voltage- and time-dependent sodium and potassium permeabilities, all axons seem to have a small, relatively constant background permeability called *leakage* or *leak*. The ionic basis of this permeability is not well known. Probably several of the common ions (K, Na, Cl, Ca) are involved. Leakage currents seen in the voltage clamp are not measurably affected by TTX or TEA ion. Most of the current indicated by filled circles in the current-voltage relation of Figure 14 is leakage current.

SEPARATE CHANNELS. The experiments described so far lead to the important conclusion that sodium and potassium permeability mechanisms are separate entities and independent in the membrane. They are kinetically separate since they have quite different voltage and time dependence. They are electrochemically separate with different ionic selectivity; they are pharmacologically separate with different sensitivity to a broad range of applied drugs. Further arguments for this separation are given elsewhere (103). The names *sodium channel* and *potassium channel* are now commonly used for the elementary underlying permeability mechanisms. In some papers the terms *early* or *transient channel* and *late* or *steady-state channel* are used instead. In addition there are *leakage channels*.

The present view of ionic channels, developed in later sections, is that they are discrete macromolecular structures distributed sparsely in the membrane. Their detailed structure allows them to pass ions with some chemical selectivity. The ions are driven through by the electric field, and the field also causes channels to open and close, thus modulating permeability. In the following discussion it is often convenient to assume that each channel has only a fully open and fully closed state, rather than a spectrum of partially open states, although there is no direct evidence on this point.

HODGKIN-HUXLEY MODEL

Quantitative Analysis of I_{Na} and I_K

IONIC CONDUCTANCES. The object of voltage clamping is to determine properties of the ionic permeability mechanisms. After the components of current carried by different ions are sorted out, the next stage is to find a quantitative measure of ionic permeability or the number of open ionic channels. Although several theories give expressions relating permeability to flux, which expression is appropriate is an experimental question. At each potential the time course of ionic current is proportional to the time course of ionic permeability. This proportionality factor also depends on voltage—for example, there is no current

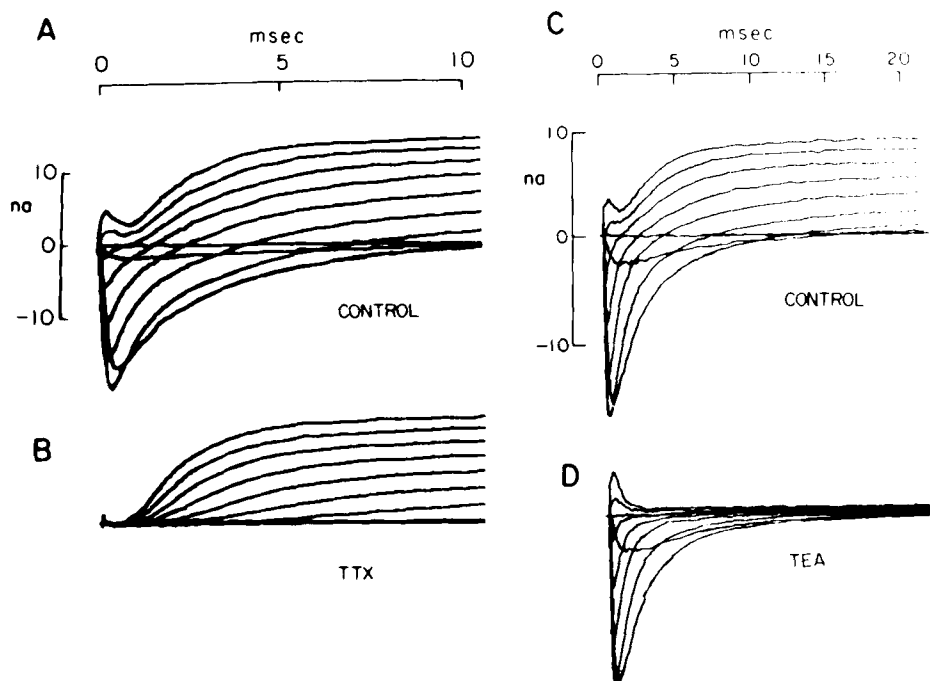


FIG. 13. Pharmacological separation of sodium and potassium currents. Ionic currents with capacity and leakage subtracted of frog myelinated nerve fiber under voltage clamp. Node depolarized at $t = 0$ to 9 or 10 voltage levels spaced at 15-mV intervals from -60 to $+75$ mV. A: normal I_{Na} and I_K recorded in Ringer's solution. B: same node in Ringer's solution with 300 nM TTX. Only I_K remains. Temperature, 13°C . [Adapted from Hille (99).] C: normal I_{Na} and I_K of a different node in Ringer's solution. D: same node in Ringer's solution with 6 mM TEA-ion. Only I_{Na} remains. Temperature 11°C . [Adapted from Hille (100).]

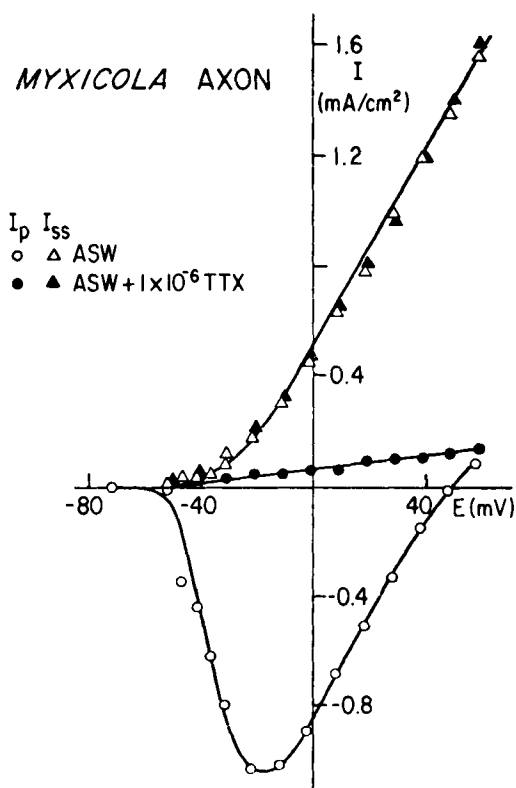


FIG. 14. Current-voltage relations in *Myxicola* showing that $1 \mu\text{M}$ TTX blocks I_{Na} but not I_K . *Myxicola* giant axon under voltage clamp. Points are ionic currents during a voltage step from rest to the indicated voltage, measured on families of currents like those in Figs. 10 and 13. I_p , peak early current, consisting primarily of I_{Na} and leakage current. I_{ss} , steady-state current after about 25 ms, consisting of I_K and leakage current. ASW, artificial seawater. Temperature $1-3^\circ\text{C}$. [From Binstock & Goldman (30).]

at the reversal potential even when permeability is high. An experiment is needed to determine the relation between ionic current and membrane potential at a constant permeability. Hodgkin & Huxley (124) measured this so-called instantaneous current-voltage relation by depolarizing the squid axon for long enough to open some ionic channels, then stepping the voltage to other levels, and measuring current within $10-30 \mu\text{s}$ after the step before further channel opening or closing occurred. One experiment was done at a time when mostly sodium channels are open and another when mostly potassium are open. The instantaneous current-voltage relation was linear in both cases. This means that in normal ionic conditions, the current in open sodium channels and open potassium channels obeys Ohm's law for electric current in resistors, and it follows at once that ionic conductances defined from Ohm's law

$$g_{Na} = I_{Na}/(E - E_{Na}) \quad (12a)$$

$$g_K = I_K/(E - E_K) \quad (12b)$$

are suitable measures of permeability or opening of channels. Leakage channels are also generally assumed to be ohmic. These findings are summarized in Figure 15, which shows one capacitive and three ionic pathways for current across the membrane. The ionic pathways have an ionic electromotive force or battery in series with a conductance. The conductances g_{Na} and g_K are variable.

From a theoretical point of view there is no a priori requirement that open channels obey Ohm's law. Indeed nonlinear current-voltage relations are predicted by most derivations for simple ionic systems,

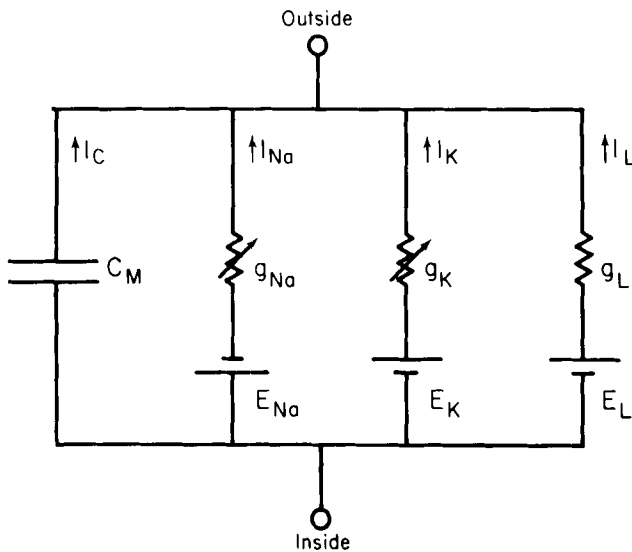


FIG. 15. Electrical equivalent circuit for membrane of squid giant axon showing 4 pathways contributing to membrane current. Two ionic pathways have batteries given by the electromotive force of the appropriate ions and a time variant conductance g . Leakage pathway has a battery and a fixed conductance. Capacitance pathway is a simple capacitor. This circuit gives correct values for membrane current in an isolated patch of membrane and is exactly equivalent to the expressions for current in the Hodgkin-Huxley analysis. Arrows point in the direction of positive outward current. I , current; E , electromotive force; C , capacitance.

including the Goldman-Hodgkin-Katz constant field theory derived in the last section of this chapter (Eq. 42). Furthermore sodium channels are not ohmic in squid giant axons bathed in low-sodium solutions (124) or in myelinated nerve under normal conditions (57, 58). Thus the use of conductance g as a measure of the number of open channels may frequently not be correct. This question is considered again later.

Changes in g_{Na} and g_K during a voltage-clamp step are readily derived from the separated currents using Equations 12a and 12b (Fig. 16). Like the currents, g_{Na} and g_K are voltage- and time-dependent. Both g_K and g_{Na} are low at rest. During a step depolarization g_{Na} rises rapidly with a small delay, reaches a peak, and falls again to a negligible value. The conductance is said to be activated and then inactivated. If the membrane potential is returned to rest during the period of high conductance, g_{Na} falls exponentially and extremely rapidly (*dashed lines*). Potassium conductance rises almost 10 times more slowly than g_{Na} , reaching a steady level without inactivation during the 10-ms depolarization. If the potential is returned to rest, g_K falls exponentially and relatively slowly. The peak values of these conductances in squid giant axons under voltage clamp are in the range 20–40 mmho/cm², like the peak conductance found by Cole & Curtis (41) during the action potential (see Fig. 4). The rise of g_K on depolarization accounts for the delayed rectification found by Cole & Baker (40) with an

externally applied cathode and the increase in P_K when axons are depolarized by added external K⁺.

Observed time courses of g_{Na} and g_K for a variety of depolarizations are shown in Figure 17. Two new features are evident. The larger the depolarization, the larger and the more rapid are the changes in g_{Na} and g_K , and for very large depolarizations the peak value of g_{Na} and the steady-state value of g_K are maximal and independent of voltage. The increase of peak g_{Na} with increasing depolarization corresponds to Hodgkin's (117) cycle for regenerative activity: depolarization increases P_{Na} , increasing sodium entry, increasing depolarization, further increasing P_{Na} , and so on. The saturation of conductance with large depolarization is thought to reflect the limited number of ionic channels in the membrane. Once all channels are open, there is no further increase in conductance.

HODGKIN-HUXLEY EQUATIONS. The final step in the proof of the ionic hypothesis is to show that conductances measured by voltage clamp account quantitatively for all phenomena of excitability. To test this Hodgkin & Huxley (126) formulated a kinetic model approximating the changes of ionic conductance under voltage-clamp conditions and then solved their equations without the restriction of voltage clamp. They obtained threshold phenomena, action potentials, and propagation. In this section, first the rationale and then the mathematical details of their analysis are described.

Rationale. The following considerations served to shape the model. Since sodium and potassium channels behave as separate entities, the equations for g_{Na} and g_K are kept independent. In each case there is an upper limit to the possible conductance, so g_{Na} or g_K

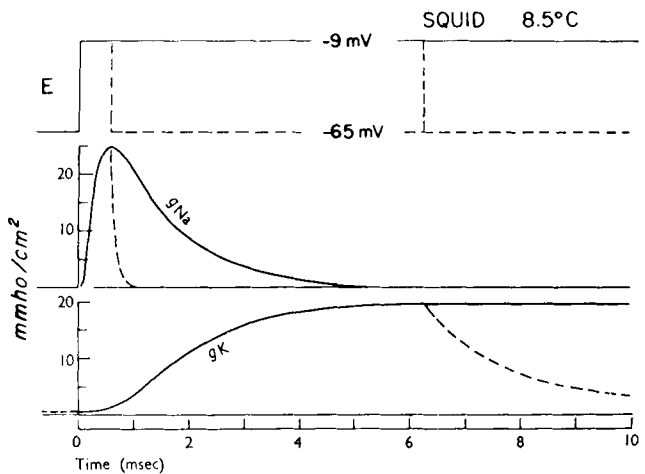


FIG. 16. Time courses of sodium and potassium conductance changes during a depolarizing voltage step. Squid giant axon under voltage clamp. Conductances calculated from currents in Fig. 9 for a step depolarization to -9 mV. *Dashed lines*, effect of repolarizing the membrane at 0.63 ms when g_{Na} is high or at 6.3 ms when g_K is high. [From Hodgkin (119).]

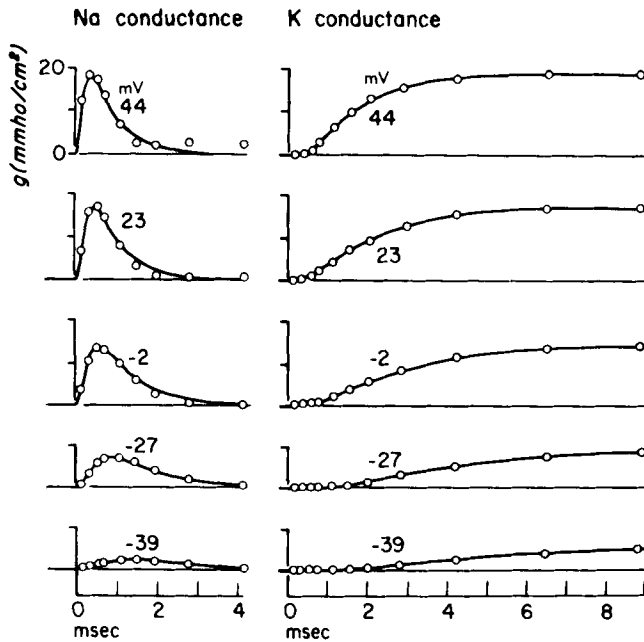


FIG. 17. Time courses of g_{Na} and g_K at 5 potentials. Squid giant axon depolarized to indicated potentials at $t = 0$. (○) ionic conductances calculated from separated currents at 6.3°C using Eq. 12 and 13. Smooth curves, time courses of g_{Na} and g_K calculated from Hodgkin-Huxley model. [From Hodgkin (119), adapted from Hodgkin & Huxley (124).]

are represented as the product of a maximum conductance, \bar{g}_{Na} or \bar{g}_K , and a multiplying coefficient representing the fraction of the maximum conductance actually expressed. The coefficient is a number varying between zero and one. If individual ionic channels open in an all-or-none manner, the coefficient would be the probability that any particular channel is open, and \bar{g} would be the conductance of one open channel times the total number of channels. All the kinetic properties of the model enter as time dependence of the multiplying coefficients. The conductance changes apparently depend only on voltage and not on the concentrations of Na^+ or K^+ or on the direction or magnitude of current flow. All experiments show that g_{Na} and g_K change gradually in time with no sudden jumps, even when the voltage steps to a new level, so the multiplying coefficients must be continuous functions in time.

The time dependence of g_K is easier to describe. The increase on depolarization follows an S-shaped time course, whereas the decrease on repolarization is exponential. As Hodgkin and Huxley noted, this type of kinetics is obtained if the opening of a potassium channel is controlled by several independent membrane-bound particles. Suppose there are four identical particles, each with probability n of being in the correct position to have an open channel. The probability that all four particles are correctly placed is n^4 . Suppose further that each particle moves between its open and closed position with first-order kinetics so

that when the voltage is changed, n relaxes to a new value exponentially. Figure 18 shows that as n rises exponentially, n^4 rises on an S-shaped curve like the increase of g_K on depolarization (Fig. 16), and as n falls exponentially, n^4 also falls exponentially like the decrease of g_K on repolarization (Fig. 16). Thus in the Hodgkin-Huxley model I_K is represented by

$$I_K = n^4 \bar{g}_K (E - E_K) \quad (14)$$

The transient kinetics of g_{Na} are fitted by a similar but more complicated scheme. Hodgkin & Huxley (125) concluded by a variety of voltage-clamp pulse sequences that the fast activation and slower inactivation of sodium channels are mediated by kinetically independent processes. Their model incorporates this separation by using different particles to describe the two processes. Three identical particles with probability m of being in the right place govern activation. The joint probability m^3 for these particles has kinetic properties quite similar to n^4 for potassium channels, a delayed rise on depolarization and an exponential fall on repolarization. A single particle with probability h of being in the open position governs inactivation or more correctly the lack of inactivation. Figure 18 shows that the product $m^3 h$ imitates observed changes in g_{Na} . The Hodgkin-Huxley model represents I_{Na} by

$$I_{Na} = m^3 h \bar{g}_{Na} (E - E_{Na}) \quad (15)$$

It can be noted at once that the concept of particles used in the previous paragraphs need not be taken literally. Similar equations might be derived without this choice of particles, and although the equations

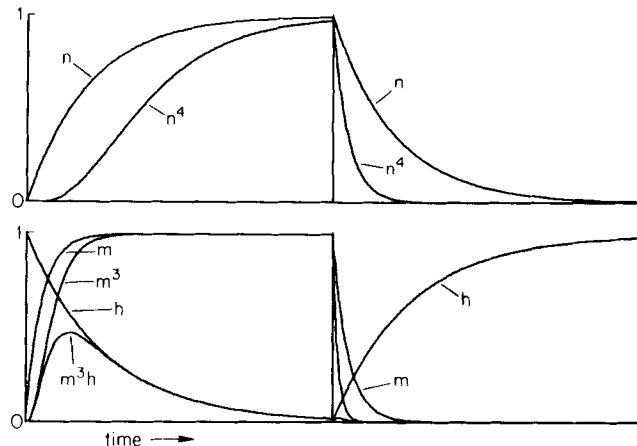


FIG. 18. Relations among the parameters m , h , n and their products during a depolarization (left) and a repolarization (right). Purely hypothetical case with ratios $\tau_m : \tau_h : \tau_n = 1 : 5 : 4$. Curves for n and m on left and h on right are $1 - \exp(-t/\tau)$, i.e., an exponential rise toward a value of 1.0. Curves for n and m on right and h on left are $\exp(-t/\tau)$, i.e., an exponential fall toward a value of 0. Other curves are the indicated powers and products of m , n , and h . Time from origin to repolarization (vertical line) is $4\tau_h$. Unlike a real case, time constants during depolarization and repolarization are assumed to be the same.

adequately describe kinetic changes of g_{Na} and g_K , they do not fit all observations perfectly. For example, powers of n higher than the fourth give still closer fits to the actually observed time courses of g_K (42, 126), and even an infinite number of hypothetical particles has been used (70).

Detailed analysis of sodium inactivation. Sodium inactivation is ordinarily seen as a secondary, exponential fall of g_{Na} during a depolarization. The falling phase can be characterized by a time constant, τ_h , defined as the time to fall to $1/e$ (37%) of the initial value. Both voltage and temperature affect the time constant. In the experiment of Figure 16, τ_h is about 1.1 ms at -9 mV and 8.5°C .

Even depolarizations too small to elicit measurable sodium current produce some sodium inactivation. The effect is illustrated in Figure 19 by a two-pulse voltage-clamp experiment on a myelinated nerve fiber. Initial 50-ms conditioning prepulses modify the amplitude of the sodium current subsequently elicited by a standard 1-ms depolarization to -15 mV. According to the model these changes reflect changes in the parameter h . Hyperpolarizing prepulses increase and depolarizing ones decrease the sodium current elicitable by a subsequent depolarization. In Hodgkin and Huxley's terminology, the value of h reached after the potential has been held constant for some time is called h_∞ . The voltage dependence of h_∞ can be determined approximately by dividing the peak I_{Na} for each prepulse by the peak I_{Na} obtained with the largest hyperpolarizing prepulse. The result is a curve varying from 0 to 1 also shown in Figure 19. At rest h_∞ is near 0.5, that is, sodium channels are about 50% inactivated. Although small voltage steps on either side of the resting potential increase or remove inactivation, they do not do so at once. As for single large depolarizations, h measured in two-pulse experiments approaches its steady-state value h_∞

with an exponential time course characterized by the time constant τ_h . The voltage dependence of τ_h is drawn as a thin line in Figure 19. Changes in inactivation are slowest near the resting potential where h_∞ is near 0.5.

The curves of h_∞ and τ_h complete the description of inactivation. If the initial value of h is known, all future values can be calculated by solving the first-order differential equation

$$\frac{dh}{dt} = \frac{(h_\infty - h)}{\tau_h} \tag{16}$$

using h_∞ and τ_h values from the graphs. This would give the appropriate exponential changes under voltage-clamp conditions and much more complex changes under other conditions. Equation 16 is actually not in the precise form used by Hodgkin and Huxley. They wrote

$$\frac{dh}{dt} = \alpha_h(1 - h) - \beta_h h \tag{17}$$

where α_h and β_h are related to τ_h and h_∞ by

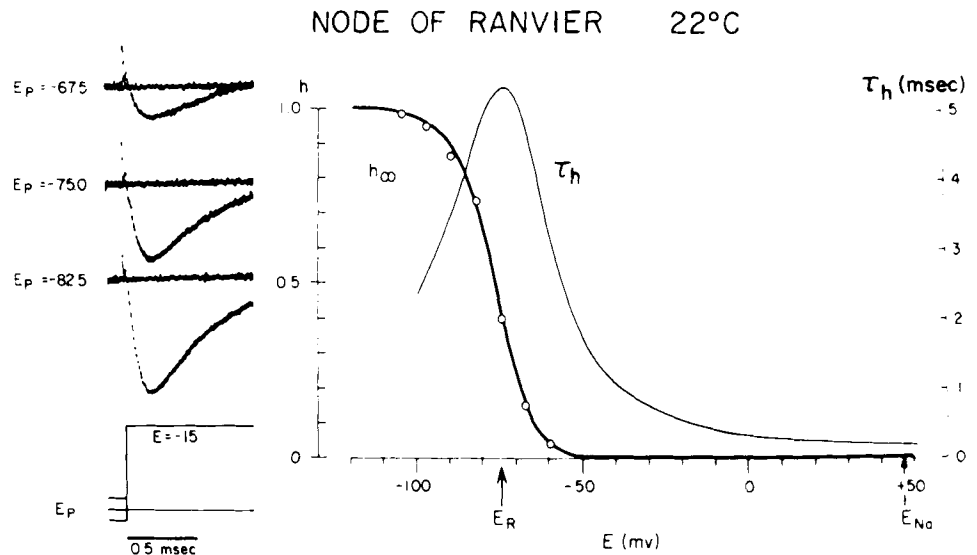
$$\tau_h = \frac{1}{\alpha_h + \beta_h} \tag{18}$$

$$h_\infty = \frac{\alpha_h}{\alpha_h + \beta_h} \tag{19}$$

These approaches are entirely equivalent. In Hodgkin and Huxley's equations α_h and β_h may be considered the rate constants for h particles' taking up and leaving the open position, whereas τ_h and h_∞ are the time constant and equilibrium constant, respectively, for the same reaction.

Full description of m , n , and h . The methods for studying the voltage and time dependence of m and n are similar to those already described for h . Again

FIG. 19. Analysis of sodium inactivation in myelinated nerve under voltage clamp. *Left:* membrane current elicited by depolarization to -15 mV after a 50-ms prepulse to the 3 indicated voltages (E_p). Depolarizing prepulses reduce and hyperpolarizing ones increase the inward sodium current by altering the degree of sodium inactivation. *Right:* voltage dependence of the parameters h_∞ and τ_h describing sodium inactivation from experiments like those of the left. Normal resting potential (E_R) is at -75 mV. [From Dodge (55), copyright 1961 by the American Association for the Advancement of Science.]



steady-state values and time constants are extracted from changes in g_{Na} and g_K . The fourth root of g_K will be proportional to n , and the third root of g_{Na} , after correction for changes in inactivation, is proportional to m . The complete results obtained by Hodgkin and Huxley for squid axons at 6.3°C are given in Figure 20. Although the time constants τ_m , τ_n , and τ_h differ in absolute value, they all peak near the resting potential, falling off sharply on either side. Depolarization increases m_∞ and n_∞ and decreases h_∞ . The curve of the voltage dependence of these functions is steep between -60 and -30 mV, showing that the nerve membrane is a very sensitive detector of potential differences in this range.

Now the kinetic properties of ionic conductances have been cast into mathematical form. To summarize, the equation for current across the membrane becomes

$$\begin{aligned} I_m &= I_l + I_c = I_{Na} + I_K + I_L + I_c \\ &= g_{Na}(E - E_{Na}) + g_K(E - E_K) + g_L(E - E_L) + C_m \frac{\partial E}{\partial t} \\ &= m^3 h \bar{g}_{Na}(E - E_{Na}) + n^4 \bar{g}_K(E - E_K) \\ &\quad + \bar{g}_L(E - E_L) + C_m \frac{\partial E}{\partial t} \quad (20) \end{aligned}$$

where I_L , E_L , and g_L are the current, potential, and conductance of leakage channels. The parameters m , n , and h satisfy the differential equations

$$\frac{dm}{dt} = \frac{m_\infty - m}{\tau_m} = \alpha_m(1 - m) - \beta_m m \quad (21)$$

$$\frac{dn}{dt} = \frac{n_\infty - n}{\tau_n} = \alpha_n(1 - n) - \beta_n n \quad (22)$$

$$\frac{dh}{dt} = \frac{h_\infty - h}{\tau_h} = \alpha_h(1 - h) - \beta_h h \quad (23)$$

The voltage-dependent coefficient pairs, m_∞ , τ_m or α_m , β_m , are determined by the kind of kinetic experiments already described. These equations together

are often called the Hodgkin-Huxley equations and embody the modern view of excitability in axons.

Calculations with Hodgkin-Huxley Model

The ultimate test of the ionic hypothesis is the demonstration that the conductance changes described in the Hodgkin-Huxley model account for the phenomena of excitability. The model has been used to calculate subthreshold responses, threshold, strength-duration curves, action potentials, refractoriness, net fluxes, total impedance change, and other axonal properties both under artificial space-clamp conditions and with the normal axon cable [(49, 71, 126, 140, 166, 182a); see also a review of work before 1966 (182)]. All these calculations agree closely with available experimental observations. This section describes some predictions from the Hodgkin-Huxley model. The last section of this chapter explains further how the equations are solved.

Figure 21 shows the calculation of an action potential propagating away from an intracellular stimulating electrode. The time course of voltage change is calculated entirely from the Hodgkin-Huxley equations applied to a cable with no further adjustments of constants. Recall that the equations were developed from experiments under voltage-clamp and space-clamp conditions. Since the calculations here involve neither a voltage clamp nor a space clamp, they are a sensitive test of the predictive value of the model. For the calculation in Figure 21 an intracellular stimulus current lasting 200 μ s is applied at $x = 0$, and the time course of intracellular voltage change is drawn for this point and three different distances down the axon. At the stimulating electrode the axon is depolarized to -35 mV during the stimulus and then begins to repolarize as soon as the stimulus current is turned off. Sodium channels soon begin to open, developing an inward current that opposes further repolarization, and an action potential is generated by means of the Hodgkin cycle; 0.5 ms later the impulse has traveled 1 cm away from the stimulating electrode, taking on the shape of a propagated im-

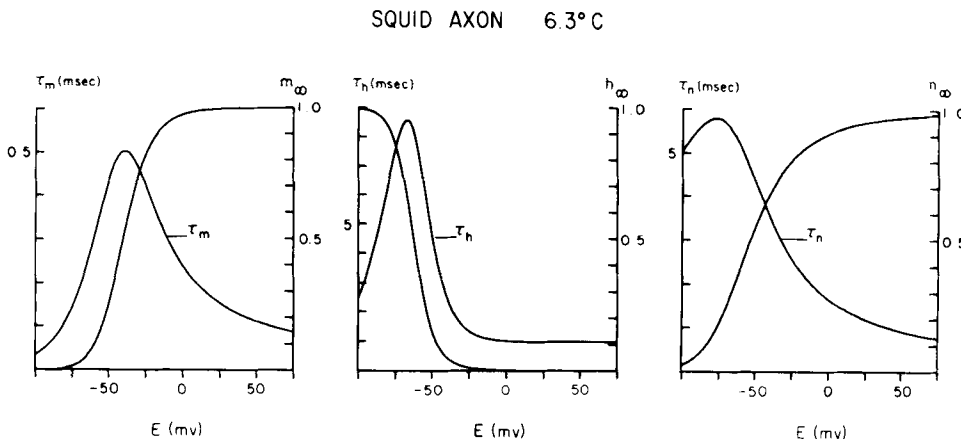


FIG. 20. Time constants τ_m , τ_h , and τ_n and steady-state values m_∞ , h_∞ , and n_∞ from the Hodgkin-Huxley model at 6.3°C. Calculated from Eq. 25-30 of the model using relations of Eqs. 18 and 19. [From Hille (103).]

pulse without local electrode current. After the calculated impulse travels several centimeters, its velocity becomes steady.

The action potential calculated from the model (Fig. 21) compares favorably with experimental recordings like that in Figure 3. Action potential shapes of model and real axons (Fig. 22) are quite similar, although the real axon has a higher overshoot and repolarizes somewhat faster. The experimental fiber of Figure 22 had a conduction velocity of 21.2 m/s at 18.5°C. When scaled to comparable conditions, the theory gives a velocity of 18.7 m/s. The Hodgkin-Huxley theory captures the essential features of impulse propagation.

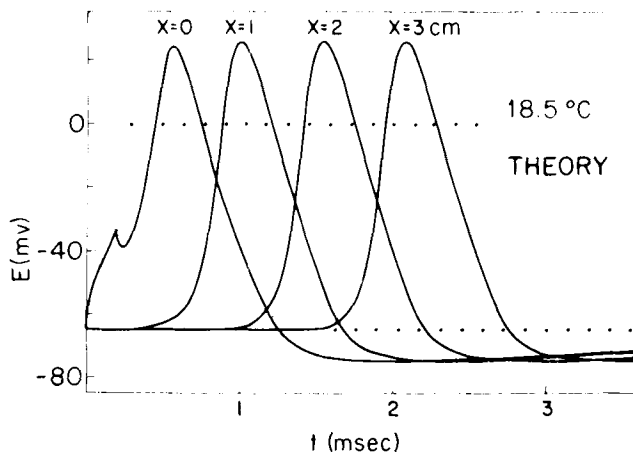


FIG. 21. Time course of the propagated action potential calculated from the Hodgkin-Huxley model. Stimulating current of 10 μ A is applied for 0.2 ms at $x = 0$. Time course of action potential is shown at 4 positions in the axon, up to 3 cm from the stimulus. Compare with Fig. 3. Assumptions: axon diameter, 476 μ m; resistivity of axoplasm, 35.4 Ω -cm; resting potential, -65 mV. [Adapted from Cooley & Dodge (49).]

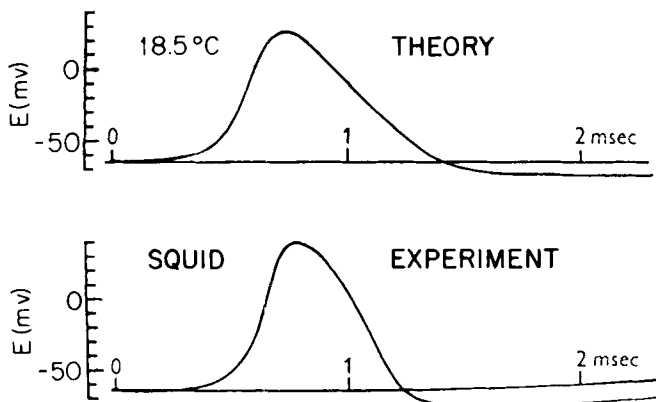


FIG. 22. Comparison of propagated action potentials calculated from the Hodgkin-Huxley model and measured on a real squid giant axon. Real fiber had a diameter of 476 μ m, axoplasmic resistivity of 35.4 Ω -cm, and conduction velocity of 21.2 m/s. The computed spike travels at 18.7 m/s with the same diameter and resistivity. [Adapted from Hodgkin & Huxley (126).]

A particular advantage of a full mathematical model is that time courses of underlying membrane changes are calculated at the same time as the action potential. Time courses of the different components of current, the conductances, and the Hodgkin-Huxley parameters m , n , and h are given in Figures 23 and 24. The action potential may be divided into four phases (Fig. 24, I-IV). During *phase I* local circuit current from preceding excited regions begins to depolarize the axon by discharging the membrane capacitor. Membrane current and capacity current are positive and approximately equal. Ionic conductances are low. During *phase II* the depolarized patch of membrane becomes excited. Sodium conductance, inward sodium current, and the parameter m rise quickly. With the growing sodium influx the membrane potential is pushed toward E_{Na} . Membrane current I_m becomes negative indicating that the excited patch is generating enough extra inward sodium current to send current through local circuits to begin depolarizing the next patch of membrane.

Phase III begins at the peak of the action potential. Two changes bring on repolarization: sodium conductance inactivates (h decreases) and potassium conductance activates (n increases). Net ionic current changes from negative to positive as potassium efflux exceeds sodium influx. When the axon is finally repolarized, it enters *phase IV*, the hyperpolarizing afterpotential. Because sodium conductance is inactivated and potassium conductance remains almost fully turned on, the potential is pulled closer to E_K than in the resting state. During *phase IV* sodium inactivation is gradually reduced, potassium conductance becomes low again, and the axon returns after a few minor oscillations to the resting condition.

Voltage-clamp experiments and the Hodgkin-Huxley model provide answers to very basic questions like: what is the origin of a sharp firing threshold? One view would be that threshold is the voltage at which sodium channels first open. However, this idea is quite incorrect since in voltage-clamp experiments any depolarization opens some sodium channels; the larger the depolarization, the more channels are opened. Instead a threshold depolarization is one that opens a critical number of sodium channels. This is most easily understood in a space-clamped axon that also exhibits a sharp threshold for firing. With a space clamp $\partial E/\partial x$ is zero, so the net membrane current (see Eq. 7) must be zero after the stimulus. Hence from Equation 9 when I_m is zero

$$-I_i = I_c = C_m \frac{\partial E}{\partial t} \quad (13)$$

A simple criterion for firing is that the change of membrane potential ($\partial E/\partial t$) becomes positive some time after the stimulus. Then the axon would enter the regenerative Hodgkin cycle. By Eq. 13 $\partial E/\partial t$

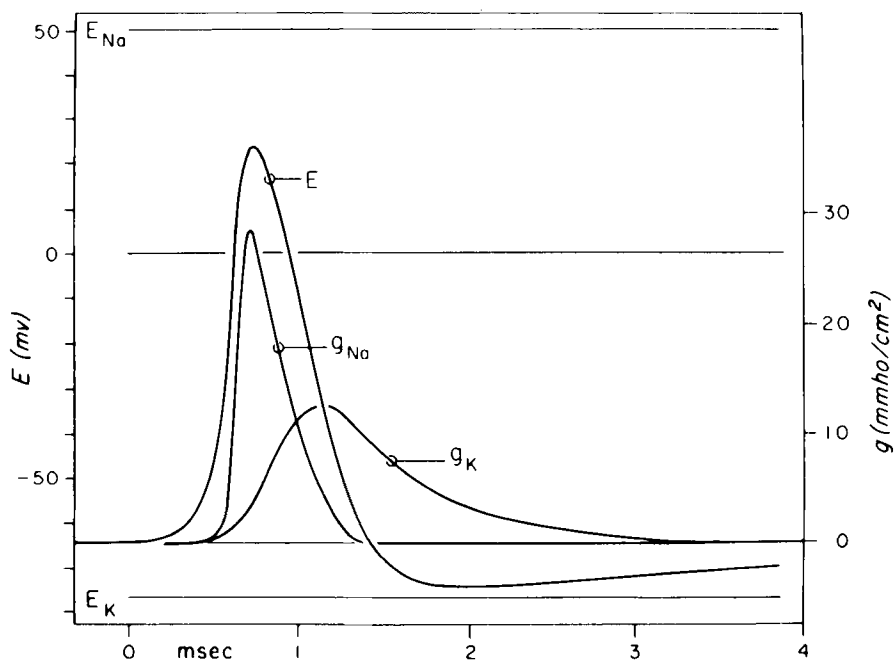


FIG. 23. Calculated time courses of the uniformly propagated action potential and underlying sodium and potassium conductance changes from the Hodgkin-Huxley model. The voltage levels corresponding to the reversal potentials E_{Na} and E_K are also shown. E_L is at -53 mV but is not shown. Assumed temperature 18.5°C . From same calculation as Fig. 22. [Adapted from Hodgkin & Huxley (126).]

is positive if net ionic current becomes inward, that is, if inward sodium current exceeds outward potassium and leak current. This criterion defines the critical number of sodium channels that must be open for an action potential to develop. For stimulation without a space clamp, membrane current I_m after the stimulus is equal to local circuit current given by Equation 7. Then $C_m \partial E / \partial t$ is equal to the difference between I_m and I_i (by Eq. 9), and this difference must become negative for firing to occur [see (182a) for a more careful analysis].

The Hodgkin-Huxley model also explains refractoriness to a second stimulus following too soon after an exciting stimulus. Immediately after activity a depolarizing stimulus will not turn on enough inward current to initiate a propagated response, since sodium channels are still largely inactivated. This is the absolute refractory period. Later after inactivation is partly removed, propagated impulses become possible, but the threshold is high so long as sodium inactivation and potassium conductance are still high. As these two processes return to the resting state, threshold returns to its resting value. Again the role of net ionic current in determining threshold explains the relation between sodium inactivation, potassium conductance, and threshold elevation during the relative refractory period. Threshold elevation in axons slightly depolarized for some time by any mechanism (injury, applied current, raised $[K]_o$) can also be attributed to an excess of sodium inactivation and to a raised potassium conductance.

Calculations from the Hodgkin-Huxley model make quantitative predictions of ion fluxes per impulse that can be tested in chemical experiments. For the model propagated spike of Figures 9 and 10 the

gain of sodium is 4.33 pmol/cm^2 and the loss of potassium about the same. Observed values at 22°C are 3.5 and 3.0 pmol/cm^2 (148, 149). The minimum theoretical amount required in the simplest theory is just the charge required to depolarize the membrane capacity or $C \Delta E$, where ΔE is the spike height. For a 100-mV spike this is 1.0 pmol/cm^2 . The actual fluxes are higher than the ideal because inward and outward currents overlap and cancel each other rather than just charge or discharge the membrane capacitance.

With long applied currents in the right range, the Hodgkin-Huxley model predicts infinite trains of impulses (6, 48, 49, 206b). Like the real axon the longest possible interspike interval in this repetitive firing is quite short, 22 ms at 6.3°C . Thus the squid axon is incapable of firing at very low frequencies with constant current and does not serve as a good model for the slowly firing encoding regions of sensory endings or certain cell bodies. Some modifications of the original model permit steady, low-frequency firing (206).

VARIETY OF EXCITABLE CELLS

By 1952 work on squid giant axons completed the arguments necessary to prove the ionic hypothesis and gave a complete kinetic description of permeability changes in one type of axon membrane. Subsequent work continuing to the present has taken two directions: one is to describe permeability changes in membranes of other axons, cell bodies, and muscle cells, and the second is to determine the molecular and structural basis of permeability changes. This section deals with the comparison of different cell

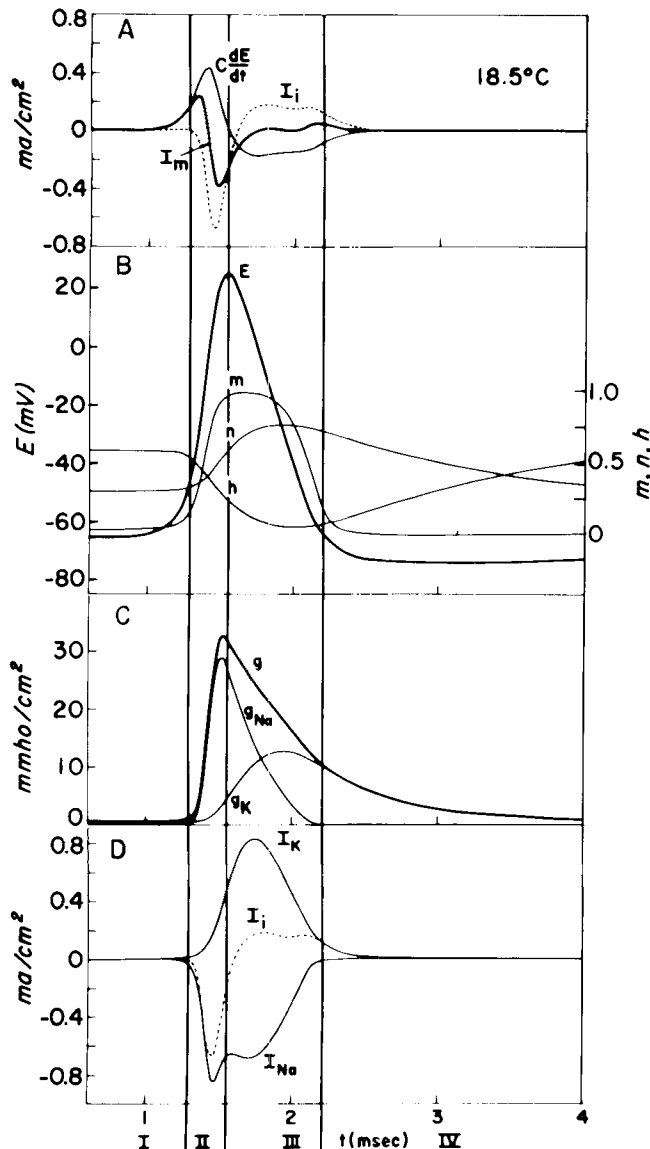


FIG. 24. Summary of the currents and membrane changes during the propagated action potential in the squid giant axon. All curves calculated from the Hodgkin-Huxley equations at 18.5°C. A: membrane current and its ionic and capacitive components. B: membrane potential and the controlling parameters m , h , and n . C: total membrane conductance and its sodium and potassium components. D: ionic current and its sodium and potassium components. [Adapted from Cooley & Dodge (48).]

types. Literally hundreds of excitable cells have been investigated. Only a few of the best known are discussed here. The overall conclusion is that all axons have a similar complement of the three major ionic channels found in squid giant axons, whereas other excitable membranes have a diversity of other types of ionic channels not described so far.

Myelinated Nerve

SALTATORY CONDUCTION. A complete analysis of conduction in myelinated fibers requires the same approach as in the squid giant axon. Cable properties

and ionic permeability changes must be determined in separate experiments and then recombined as a model to see if excitability and impulse propagation are adequately reproduced. Myelinated axons are covered by a concentric laminar myelin sheath over most of their lengths. Myelin is a low-capacity, high-resistance insulator that improves transmitting properties of the axon. The axon membrane is exposed to the bathing solution only at widely spaced nodes of Ranvier where one Schwann or glial cell, forming the myelin sheath, ends and a new one begins. Nodes are about 1.4 mm apart in 16- μ m fibers of cat peroneal nerve (138) and about 2.5 mm apart in fibers of the same size on toad sciatic nerve (210). In smaller fibers the nodes are closer together. The gap between Schwann cells at the node is only 0.5–1.0 μ m.

As Lillie (160) first suggested, the tiny nodes of Ranvier are the seats of excitation in myelinated fibers, and the impulse travels by successive excitation of nodes, a process called saltatory conduction. Experimental evidence for the importance of nodes began to appear in the 1930's. Erlanger & Blair (63) found that progressively increasing hyperpolarization of a nerve twig blocks invading action potentials in a stepwise fashion, as if the impulse fails at successively more distant nodes. In Kato's laboratory (145), M. Kubo, S. Ono, and I. Tasaki found that single myelinated fibers are more easily excited with a cathode at a node than in the internode, and Tasaki showed that anesthetics block impulses within seconds when applied to nodes, but not at all when applied only to internodes. Final proof of the hypothesis of saltatory conduction was developed independently by Tasaki and co-workers (210, 215, 216) and by Huxley & Stämpfli (141) in the period 1939–1949.

Since axon diameters of even the largest myelinated nerve fibers do not reach 30 μ m, intracellular electrodes are not conveniently used. All biophysical studies have been done with extracellular electrodes and nerve chambers that artificially elevate the extracellular resistance at one or several points along the fiber. Figure 25 shows Tasaki's method (215, 216) for measuring membrane current flowing radially out of a short length of fiber. Three pools of Ringer's solution are separated by narrow gaps of air to achieve good electrical isolation. A nerve fiber lying across these pools is stimulated at the left-hand end, and the impulse travels through *pools* 1–3. Current coming out of the fiber into *pool* 2 is led through a resistor R to a wire connecting *pools* 1 and 3 and is measured by determining the voltage drop across the resistor. If the connections between pools did not exist, the impulse would stop at the air gap between *pools* 1 and 2 because no local circuit current could flow.

In Figure 25A a single fiber lies with a node of Ranvier in the middle pool. Just as in the squid giant axon (Fig. 24), there is a biphasic burst of membrane current during the rising phase of the action poten-

tial. The initial outward current is local circuit current from previously excited regions in *pool 1*, and the subsequent inward current is excess sodium current generated locally, being used to depolarize the next region of axon in *pool 3*. When the fiber is moved along so that no node falls in the middle pool (Fig. 25B), the membrane current is very different. There are two outward peaks and no inward phase. Evidently the internode does not produce the inward current needed to depolarize the next patch of membrane. Inward current comes only from nodes of Ranvier.

Huxley & Stämpfli (141) obtained exactly the same records of membrane current by a different method. A single fiber was threaded through a 500- μm length of fine glass capillary to increase the extracellular resistance over a 500- μm region. The recorded voltage between the ends of the capillary is proportional to the opposite but equal longitudinal currents flowing down the axon and in the extracellular medium. Longitudinal currents were measured at different points by sliding the fiber within the capillary. Radial or membrane current was calculated by subtracting longitudinal current records from adjacent points. The shape of the intracellular action potential could also be calculated by integrating the longitudinal current record. Huxley and Stämpfli's method can be applied to undissected fibers still lying within a nerve bundle, if the nerve is uniform and lifted into an insulating medium like oil. Currents recorded this way in rat ventral roots at 37°C have the same features as those from dissected single fibers (196).

The current records of Figure 25B can be used to determine the passive electrical resistance and capacitance of the myelin sheath (141). Suppose that 1 mm of a 16- μm diameter fiber is in *pool 2* and that the action potential amplitude is 110 mV and maximum rate of rise in the internode is 500 V/s. Then the area of myelin sheath in *pool 2* is about $5 \times 10^{-4} \text{ cm}^2$. The two 1-nA peaks of outward current are capacity current, from the rise of membrane potential as the nearest node in *pool 1* and that in *pool 3* fire. According to Equation 6 capacitance equals $I_c / (dE/dt)$, where I_c is 1 nA or, when normalized to the estimated area of myelin, $2.0 \mu\text{A}/\text{cm}^2$. The resulting capacitance is $4 \times 10^{-9} \text{ F}/\text{cm}^2$, or 250 times less than the $1 \mu\text{F}/\text{cm}^2$ capacitance of a single cell membrane. The slowly declining positive current after the peaks is ionic current with a time course like that of the action potential. The maximum of this current is about 0.2 nA or $0.4 \mu\text{A}/\text{cm}^2$ at the peak of the action potential, corresponding to a resistance of $275 \text{ k}\Omega\cdot\text{cm}^2$ or 275 times larger than the $1 \text{ k}\Omega\cdot\text{cm}^2$ resistance of a single resting squid axon membrane. Thus this myelin has the high resistance and low capacitance expected from a stack of 250 passive squid axon membranes in series. Indeed electron microscopy and X-ray diffraction studies show that myelin is a layer of several hundred close-packed Schwann cell mem-

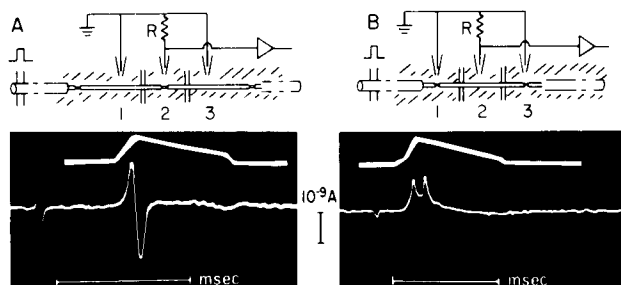


FIG. 25. Different character of membrane current at the node of Ranvier and in the internode. Single myelinated fiber from a frog passes across 2 air gaps. Radial or membrane current during the propagated action potential is recorded as a voltage drop across the resistor R . Current is the lower noisy trace. Upper trace, rough sketch approximating time course of an action potential at 24°C. A: biphasic current from the node and neighboring internode. B: current from 1 mm of internode. 1-3, 3 pools of Ringer's solution. [Adapted from Tasaki (211).]

branes (201). The total capacity of a 2-mm internode is on the order of 2-4 pF, while the node and the incompletely formed paranodal myelin have a capacity of 0.6-1 pF. A complete summary of passive electrical properties of a typical frog myelinated fiber is given in Table 4 of Hodgkin's review (120).

Although conduction in myelinated nerve is called saltatory, its discontinuous nature should not be exaggerated. First, nodes are connected by cablelike internodes so depolarization spreads gradually, even if quickly, down the length of each internode until the next node is depolarized beyond threshold. Second, many nodes are active at once. At 38°C the action potential may last 0.4 ms. In a 16- μm fiber with a 90-m/s conduction velocity and 1.4-mm internodal length, the wavelength of the action potential is 36 mm, meaning that 26 nodes are in various stages of firing at any time. Every 16 μs a new node joins the wave and a refractory one leaves at the other end. To a first approximation the number of nodes in the action potential and the conduction time per node are independent of fiber size (196, 203, 210).

There are two obvious advantages to saltatory conduction: speed and efficiency. A 14- μm myelinated fiber conducts faster than a 500- μm squid giant axon at the same temperature (Table 1). The extra speed comes from the superior electrical quality (high membrane resistance, low membrane capacitance) of the myelin cable for transmitting depolarization rapidly to the distant next node. Frog sciatic nerves at 20°C gain $1.3 \times 10^{-16} \text{ mol}$ of sodium per centimeter length of fiber in each impulse (18, 56). With the simple geometric scaling properties assumed by Rushton (203), this gain is independent of fiber diameter. By contrast a 500- μm squid giant axon at the same temperature gains $5 \times 10^{-13} \text{ mol}/\text{cm}$ in each impulse (120). Thus for a corresponding fast conduction velocity, an unmyelinated fiber occupies 1,300 times the cross-sectional area in a nerve and must consume 4,000 times the metabolic energy per impulse to

pump back the ions compared with a myelinated fiber. Even unmyelinated fibers of the rabbit vagus nerve with a mean diameter of $0.7 \mu\text{m}$ and conduction velocity of only 0.4 m/s at 20°C (136) have larger fluxes, $2 \times 10^{-16} \text{ mol/cm}$ in each impulse, than myelinated fibers (150). However, where speed and energy consumption are not important considerations, unmyelinated fibers may still have some advantages.

IONIC BASIS. The ionic basis of electrical activity at nodes of Ranvier is similar to that in squid giant axons [see (104, 206a)]. Using an ingenious potentiometric method, Huxley & Stämpfli (142, 143) found that the resting potential of larger fibers from *Rana esculenta* is -71 mV and that at rest P_K is much larger than P_{Na} and P_{Cl} . Nodal membrane impedance falls about 10-fold during the spike (214). The overshoot normally reaches $+45 \text{ mV}$ and decreases in accord with the Nernst equation as external sodium is reduced (142, 143). Tetanically stimulated fibers gain sodium and lose potassium during activity (18).

Despite the requirement to use extracellular electrodes, excellent methods are available to record potentials and to voltage clamp myelinated fibers (57, 72, 104, 185). As in squid, ionic currents in the clamp can be separated into ohmic I_L and time- and voltage-dependent I_{Na} and I_K . Examples of these currents have already been given in Figures 11–13 and 19, except that in most figures leakage current is already subtracted. Ionic conductances and current densities are strikingly higher than in squid axon, probably because roughly $30 \mu\text{m}^2$ of nodal membrane has to depolarize $10^5 \mu\text{m}^2$ of myelin in a few hundredths of a millisecond. The resting membrane resistance in frog node is $10\text{--}20 \Omega\text{-cm}^2$ compared with $1,000\text{--}3,000 \Omega\text{-cm}^2$ in squid, and \bar{g}_{Na} and \bar{g}_K are on the order of $2,500$ and 410 mmho/cm^2 compared with 120 and 36 mmho/cm^2 in squid. The resting conductance (mostly \bar{g}_L) is so high that a further activation of g_K is not very important for repolarization of the action potential in the node. Indeed in warm-blooded animals, including pigeon, rat, cat, and man, where internodes are shorter and the capacity per internode probably smaller, the time- and voltage-dependent component of g_K is almost entirely absent (33, 134, 186). Repolarizing outward current is then supplied by fixed leakage channels. In frog node leakage current is carried primarily by K^+ (107), so action potentials still result in a net efflux of K^+ equal to the influx of Na^+ (18).

Complete mathematical descriptions of ionic currents in several different nodes of *Rana pipiens* (55, 56, 104) and of an average node of *Xenopus laevis* (73, 75, 79) have been developed using the approach of Hodgkin and Huxley. The kinetics of permeability change are fitted with coefficients m^3h and n^4 in frog and m^2h and n^2 in toad, and smooth mathematical functions are available for α 's and β 's in machine computations (56, 79, 104). Computed single nodal action potentials, analogous to membrane or space-

clamped action potentials, agree well with recorded ones (55, 56, 76, 79). Even the characteristic differences of the nodal action potentials of the five nodes modeled by Dodge (56) are specifically matched by his equations. Nodal equations combined with cable equations for internodes give reasonable calculated conduction velocities and longitudinal and radial current densities (87, 95, 155). Computer simulations of conduction in partially demyelinated fibers show the same kind of extreme slowing of conduction, notching of action potentials, and temperature sensitivity as is found with experimentally diphtheria toxin-induced demyelination (155, 196). The success of these calculations is definitive proof of the hypothesis of saltatory conduction.

Squid axons and myelinated nerve differ in one detail of their voltage-clamp properties. If a squid axon is stepped to different potentials at a time when g_{Na} is high, the instantaneous steps of current are proportional to the driving voltage (124) giving the linear relation

$$I_{Na} = g_{Na} (E - E_{Na}) \quad (12)$$

Assuming that the steps are so rapid that no sodium channels open or close before the measurement is made, the observation means that open sodium channels obey Ohm's law. In myelinated nerve the same experiment reveals a nonlinear relation between current and voltage (58). The curvature happens to be close to that in the Goldman-Hodgkin-Katz (86, 130) constant field theory (see derivation in last section of this chapter, Eq. 42)

$$I_{Na} = P_{Na} \frac{EF^2}{RT} \frac{[Na]_o - [Na]_i e^{FE/RT}}{1 - e^{FE/RT}} \quad (24)$$

This equation with P_{Na} given by $m^3h\bar{P}_{Na}$ or $m^2h\bar{P}_{Na}$ is used in the mathematical models for nodes of Ranvier. Potassium instantaneous current-voltage relations are slightly less curved than the equivalent expression to Equation 24 for potassium, and either the ohmic or the constant field form is used in models.

Other Axons

Next to squid giant axons and myelinated fibers, the most studied axons are giant fibers from the ventral nerve cord of the marine annelid worm *Myxicola* (Polychaeta). Like squid giant axons this axon can exceed 1 mm in diameter. Studies of voltage-clamp currents with axial wire electrodes (Fig. 7) again reveal sodium, potassium, and leak channels. Current-voltage relations given in Figure 14 show that TTX blocks sodium channels in this axon. A complete kinetic description using three components of current and the coefficients m^3h and n^4 is available (89). Maximum conductances \bar{g}_{Na} and \bar{g}_K in the model are about one-third of their value in squid giant axons, and the open ionic channels are assumed to obey Ohm's law. Predicted action potentials, thresh-

olds, and refractoriness are in fair agreement with experimental observation. Some large arthropod axons from lobster circumesophageal connective (144) and cockroach abdominal nerve cord (190) have also been studied using double-gap voltage-clamp methods (Fig. 7). Sodium and potassium currents are similar to those in squid, but a complete kinetic description was never undertaken; TTX blocks the sodium current (177, 209).

To date there are no direct measurements of permeability changes in vertebrate unmyelinated C fibers because the axons are smaller than $1 \mu\text{m}$ in diameter and are often held together in bundles by enveloping Schwann cells. A requirement for sodium, block by nanomolar concentrations of TTX and STX, depolarization in potassium chloride, and extra tracer effluxes of potassium during activity suggest that unmyelinated C fibers of the rabbit vagus and garfish olfactory nerve have membrane properties close to those of larger axons (43, 44, 150). The extra ionic fluxes per impulse, 0.9 pmol/cm^2 of potassium, are the lowest of any studied unmyelinated cell presumably because of a minimal temporal overlap of I_{Na} and I_{K} and small values of sodium and potassium permeabilities coupled with a low resting potential (150). Electrogenic sodium pumping causes a large posttetanic hyperpolarization in C fibers (195, 198).

Cell Bodies

All axons are outgrowths of a cell body, which has several functions. First, it is a biosynthetic center for manufacture of many macromolecules needed by dendrites and axons, and second, it is often the point where a wide variety of synaptic input signals blend together to drive the spike-generating mechanism. Thus it encodes information that is then sent via axons to new destinations. The excitability mechanisms of cell bodies are still only poorly known because of the difficulty of achieving space clamp, voltage clamp, and solution changes in small cells with many processes buried in masses of other tissue. All studies reveal that cell bodies differ from axons in both their inward and outward current mechanisms.

GASTROPOD GANGLIA. The best studied cell bodies are ganglion cells of gastropod mollusc *Aplysia* (83), *Helix* (84, 167), and *Anisodoris* (45–47). In most of the cells investigated, TTX-sensitive sodium channels contribute only part or even none of the inward current for action potentials. The cells can fire spikes in sodium-free solutions and in the presence of TTX. The amplitude of the spike increases 10–20 mV as calcium concentration is increased 10-fold. Barium and strontium ions, but not magnesium, support action potentials in the absence of calcium, and 15 mM manganous and cobaltous ions block the spike, whereas 15 mM cocaine does not (167). These observations constitute the criteria for inward calcium current in calcium channels (see later section on calcium

channels). Note that the Nernst equation has a factor RT/zF in front of the logarithm (cf. Eq. 1), where z is the valence of the ion, so the predicted change of the calcium equilibrium potential E_{Ca} for a 10-fold change of Ca^{2+} concentration is $58.2/2$ or 29.1 mV at 20°C .

The outward current of molluscan ganglion cells is adapted to give a range of repetitive firing frequencies in response to depolarizing synaptic inputs. Connor & Stevens (45–47) have identified at least two components of voltage- and time-dependent ionic current with reversal potentials near -60 mV in *Anisodoris*. One of these has most of the properties of conventional delayed rectification or potassium current in axons with some additional kinetic complications. This current, called I_{K} in the analysis, is blocked by TEA ion. The other outward current, called I_{A} , activates only transiently during a depolarization. The conductance g_{A} has kinetic properties of activation and inactivation like g_{Na} . Even at the resting potential g_{A} is quite strongly inactivated, so this outward current is considerably enhanced if the cell is briefly hyperpolarized before a depolarization. Tetraethylammonium ions reduce this current, but only weakly.

The *Anisodoris* ganglion cell is the only cell with a physiologically significant spike-initiating function to be completely analyzed by voltage-clamp methods. The kinetic model for I_{K} , I_{A} , inward current I_{I} (probably carried by calcium), and leakage current I_{L} gives repetitive firing of the type seen in experiments (47). Calculated and experimental action potentials with a step-current stimulus are shown in Figure 26A and underlying subthreshold currents at very high amplification in Figure 26B. The initial resting potential is set by the interplay of a small g_{L} with an even smaller g_{A} . Applied current depolarizes to the firing level, and the cell fires. By the end of the spike g_{I} and g_{A} are inactivated. The large g_{K} from the spike hyperpolarizes the cell, despite the applied depolarizing current, and controls the trajectory in the early part of the interspike interval. As g_{K} decreases again, the cell begins to depolarize, but now some A channels have had time to lose their inactivation and g_{A} reactivates with the depolarization. This new outward I_{A} slows the depolarization and stretches out the interspike interval to a much longer period than with I_{K} alone. The interspike interval then depends on how many A channels had a chance to lose their inactivation during the hyperpolarizing early part of the firing trajectory. The presence of the A current permits the firing frequency of the spike encoder to extend down to low frequencies of firing.

VERTEBRATE CELL BODIES. Although action potentials have been recorded from numerous vertebrate nerve cells, little is known about their ionic basis. The action potential in cat spinal motoneurons lasts 2 ms, or 5 times longer than the action potential in the motor axon (see Fig. 1). These cells become inexcita-

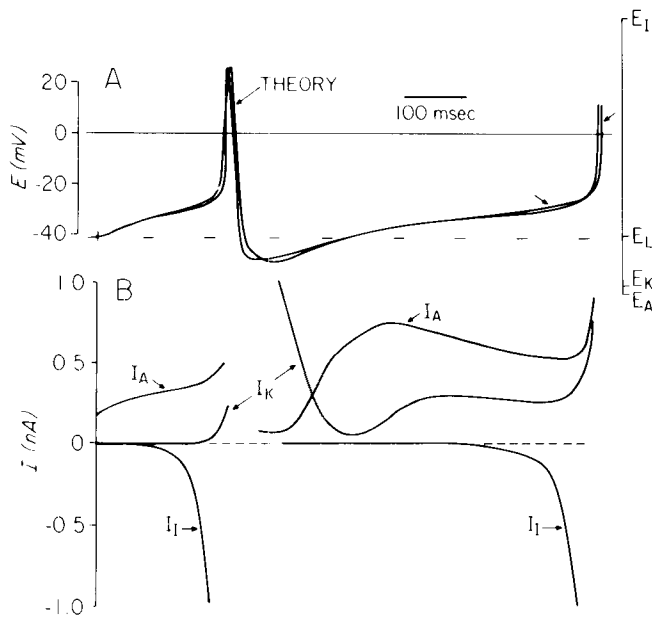


FIG. 26. Action potential and ionic currents in a repetitively firing neuron of *Anisodoris* at 5°C. A: comparison of experimentally recorded time course of firing and the time course predicted from the Connor-Stevens (47) equations (arrows). Steady depolarizing current of 1.6 nA is turned on near the beginning of the trace. Repetitive firing at a frequency of 1.7 spikes/s is initiated. Reversal potentials E_I , E_L , E_K , and E_A of the 4 ionic current components are indicated on right. B: time courses of 3 of the ionic current components, considerably magnified to show better the subthreshold changes that control repetitive firing. Normalizing to the 14-nF capacity of the cell indicates that 1 nA corresponds to a current density of only $0.07 \mu\text{A}/\text{cm}^2$. [Adapted from Connor & Stevens (47).]

ble to intracellular stimulation after a TTX solution is applied to the spinal cord (31). Action potentials in bullfrog lumbar sympathetic ganglion cells and spinal (dorsal root) ganglion cells have both a TTX- and procaine-sensitive Na^+ component and a TTX- and procaine-insensitive Ca^{2+} component (153, 154). Similarly, A-H cells of Auerbach's plexus in guinea pig duodenum have action potentials with both TTX- and manganese-sensitive components (112). Puffer fish supramedullary cells have two components of outward potassium current differing in their sensitivity to TEA ion (174). One component inactivates rapidly after a depolarization and is extensively inactivated even at the resting potential. More work is needed before these features of inward and outward currents may be considered typical of vertebrate cell bodies.

Muscle

Electrical properties of muscle are described in detail in the chapter on muscle by Costantin in this *Handbook*. Voltage-clamp studies have been done on frog fast skeletal muscle (5), various cardiac muscle bundles (24, 51, 52, 183, 184), uterine smooth muscle (8), crayfish skeletal muscle (91), muscle-derived

electric organs (25), and others. The inward current mechanisms in muscle range from all sodium to all calcium with many intermediate examples. The first discovery of calcium channels was in crustacean muscle (68, 69), and barnacle muscle is now the most studied calcium mechanism in any excitable cell (90-94, 151b). The outward current mechanisms in muscles are even more various than described in ganglion cells. There are channels like the potassium channels in squid, channels like A channels of *Anisodoris*, and usually a potassium component that has less conductance in the depolarized state than at rest. This component is called *anomalous rectification* or the *ingoing rectifier* to distinguish it from delayed rectification or the outgoing rectifier of conventional potassium channels.

IONIC CHANNELS

This section deals with efforts to understand the structural or molecular nature of ionic channels. This area of research is changing rapidly because many laboratories are studying ionic channels. Only sodium and potassium channels of axons are described in detail, as little structural information is available on others. Calcium channels are also briefly described.

There is now good evidence that ionic channels are physical pores found at very low density in the membrane. Ions move rapidly through these pores and are selected on the basis of size and hydration energies. It is widely thought that the processes that open and close channels in time, called *gating*, are distinct from those that select which ions can pass. The most information has come from experiments with unphysiological solutions containing either unusual ions or neuroactive drugs, often under voltage-clamp conditions. Other approaches such as measurements of optical (37), thermal, and metabolic (199) concomitants of activity are described in the chapter by Cohen and De Weer in this *Handbook* [for reviews of ionic channels, see (12a, 60, and 103)].

Sodium Channels

NUMBER OF CHANNELS. Pharmacological experiments with TTX and STX have already been described. Moore et al. (169) first used the binding of TTX to nerve bundles to count the number of sodium channels in the bundle. The experiment involves measuring the number of toxin molecules taken up by the nerve, correcting for any unbound and nonspecifically bound molecules, and finally assuming that each specifically bound molecule corresponds to one channel. In refined versions of the experiment with radioactively labeled toxins, the average number of sites per square micrometer of axon membrane is estimated at 27 for rabbit vagus nerve, 16 for lobster walking leg nerve, and 2.5 for garfish olfactory nerve

(43, 97). A density of $16/\mu\text{m}^2$ means that individual sodium channels would be separated by $2,500 \text{ \AA}$ if they are arranged on a regular square grid. There is no information if the arrangement of channels is regular or irregular, but in any case there are not many of them in the membrane. Similar numbers of binding sites are found in cell fractionation experiments on the fractions rich in axon membranes and even on the proteins solubilized by detergents from membrane fractions (97, 98).

The low density of channels establishes some important limits on the properties of single channels (103). Suppose that the lobster giant axon has the same density of sodium channels as the average value measured for all axons in the lobster walking leg nerve ($16 \times 10^8/\text{cm}^2$). In the giant axon, peak g_{Na} averages 260 mmho/cm^2 and peak inward sodium current can be 10 mA/cm^2 under voltage clamp (177). If half the channels are open for this peak activation, then each channel has a conductance of 0.3 nmho and carries a current at -25 mV of 24 pA . Dividing by the unit electronic charge 1.6×10^{-19} , the flux becomes 150 Na^+ per microsecond for a single channel. Even higher currents should pass through open sodium channels at the resting potential. The calculated flux is at least 10^2 times higher than the turnover rate of the fastest known enzyme and 10^5 times higher than the pumping rate of the sodium pump (23), but it is readily accounted for if the sodium channel is a pore or hole through the membrane with a minimum radius of 3 \AA (103). The above calculation rests on the basis of assuming that the density of sodium channels on giant fibers is the same as in small fibers. It is hoped that density of sodium channels will soon be determined in cells with measured sodium conductance so the calculations can be made directly. More recent work gives higher channel densities and lower channel conductances of $1\text{--}10 \text{ pmho}$ (7a).

The high flux in a single channel is the major argument in favor of a pore as opposed to some kind of carrier or shuttle model of the channel. There are several other relevant lines of evidence. The temperature coefficient Q_{10} of g_{Na} and g_{K} is in the range $1.2\text{--}1.3$ like that of aqueous diffusion (80). Thus there are no large energy barriers in the steps of moving Na^+ from one side of the membrane to the other. Further, squid axons internally perfused with a pure K_2SO_4 solution can fire at least 4×10^5 normal-looking impulses, proving that there is no immediate requirement for metabolic energy either in the conductance change or in the translocation steps of excitation (22). Finally the ionic selectivity of the channel is at least consistent with a pore (see below).

IONIC SELECTIVITY. Ionic selectivity of sodium and potassium channels is reviewed in detail elsewhere (108). Sodium channels are not perfectly sodium selective. They are measurably permeant to six metal cations, including Na^+ , and seven organic cations with sizes ranging from ammonium to aminoguanidine

(35, 105, 106). There is virtually no discrimination between Na^+ and Li^+ in sodium channels, and lithium solutions can support action potentials for some time. Since Li^+ is not pumped out of cells as readily as Na^+ , internal accumulation of Li^+ eventually becomes a problem. Even K^+ passes through sodium channels, although quite poorly. The permeability ratio $P_{\text{Na}}:P_{\text{K}}$ is $12:1$. This imperfect selectivity means that the reversal potential for sodium channels should be calculated by the Goldman potential equation (Eq. 2) rather than the Nernst equation (Eq. 4). Using the concentrations in Table 3 for squid giant axons, the calculated reversal potential is 12 mV less positive than with perfect selectivity because the 400 mM internal potassium has the effect of an additional 33 mM ($400/12 = 33$) internal sodium. A complete calculation taking into account the internal activity coefficients reported by Hinke (109) and the imperfect selectivity predicts a reversal potential near $+47 \text{ mV}$ at 8.5°C .

The following hypothesis has been advanced to explain how ions are selected in the sodium channel (105, 106, 108). Sodium channels are pores in which the narrowest region has an oblong cross section about $3 \text{ \AA} \times 5 \text{ \AA}$. The contour of this narrow part is formed by oxygen atoms including one negatively charged, ionized oxygen acid with a $\text{p}K_a$ of 5.2 . Most of the length of the pore may not be as narrow as the narrow part. Selectivity against large impermeant cations is simply geometric. The pore is too narrow. Selectivity for small cations is energetic. Permeant cations briefly associate with the negative group, losing some of their water of hydration in the narrow region on the way through. The ionic attraction to the negative group is greater for sodium with an ionic diameter of 1.90 \AA than for potassium with a diameter of 2.66 \AA . The difference in attraction is large enough to exceed the difference in dehydration energy of the two ions, so sodium ions are selected for, relative to potassium. This idea is the same as Eisenman's explanation (62) for sodium-selective glass electrodes. Tests with molecular models suggest that the postulated channel can also explain the blocking action of TTX and STX. These molecules fit neatly in the channel, a narrow guanidinium moiety within the narrow parts of the pore and the rest making many hydrogen bonds to the oxygen contour. The toxin obstructs the flow of ions.

Although the channel prefers sodium over potassium, the channel is not saturated with Na^+ . Hodgkin & Huxley (123) found that sodium currents change in accordance with the independence principle (Eq. 48) as sodium concentration is changed. This tests whether there is interference from other sodium ions on the movement of any given sodium ion. Since there is little interference, the channel is probably empty much of the time.

GATING. The structural origin of the voltage dependence of permeability remains poorly understood. Two

classes of mechanisms may be distinguished at once. In one, the electric field acts on charged or dipolar controlling groups (particles) attached to or in the membrane, altering the permeability of the channel. In the other, the field moves some controlling ions in the solution to or from the channel to alter the permeability. The second class of models can be tested by varying the ionic composition of the internal and external solutions. Equimolar replacements of sodium, potassium, and chloride with a broad range of monovalent anions and cations have only small effects on the kinetics of permeability change (22, 35, 105, 106, 123). The only normal ion with important effects on gating is calcium. Increases in external calcium decrease excitability by increasing the depolarization required to reach threshold. In a voltage-clamp analysis the voltage-dependent functions in the graphs of Figure 20 become shifted to the right as external calcium is raised and to the left as it is reduced (78, 85, 102). The membrane responds as if calcium adds a voltage bias to the gating mechanism. Lowering the total internal salt concentration or raising the total external monovalent salt has the same type of biasing or shifting effect as raising the external calcium concentration (34, 108a, 172).

Voltage shifts probably arise from neutralization of some of the surface negative charge on the axon membrane by ions in the bathing medium (34, 85, 108a, 172). Surface charges set up a local electric field within the membrane that depends on the total salt and on divalent ion concentrations. This local field adds to the normally discussed field set up by the external voltage difference E , and the total field affects the controlling particles in the membrane. Hence, although there is an effect of external ions on gating, the voltage-sensitive components of the channels still seem to be part of the membrane. There are preliminary reports that movement of controlling particles in the membrane can be detected as a minute electric current flowing for a short period following a voltage step (12a, 13, 13a, 151, 151a). This tiny current, called gating current, yields new clues to the gating process within the membrane.

In the Hodgkin-Huxley model changes of sodium conductance are governed by two independent parameters m^3 and h . Whether this separation is correct or whether instead there is coupling between activation and inactivation is debatable. Some kinetic tests with the voltage clamp indicate that the original description may be inadequate (88, 137), but pharmacological experiments suggest that activation and inactivation are nevertheless separable. Inactivation can be eliminated by treating nodes of Ranvier with venom of the scorpion *Leiurus* (157, 158), by treating squid axons with nematocyst poison of the anemone *Condylactis* (173, 178), by internally perfusing squid axons with pronase enzymes (14), or by strongly illuminating dye-sensitized lobster giant axons (193). In these cases activation described by m^3

remains almost normal, despite the loss of inactivation. Inactivation is also modified after internal perfusion of squid axons with unphysiological salt solutions, including CsF and NaF (3, 36). Many other nerve poisons, including veratridine, DDT, and other insecticides, hold sodium channels open longer than usual, overriding both the closing normally attributed to h on depolarization and that attributed to m on repolarization (101, 173, 176, 219, 220). Depolarization with added external K^+ brings on a long-term inactivation of sodium channels that is not described by the Hodgkin-Huxley equations (2).

It is often supposed that channels open in an all-or-none manner, thus giving small, stepwise increments of conductance. This point remains unresolved. In 1958 Lüttgau (163) reported steps of voltage in the subthreshold response of nodes of Ranvier corresponding, appropriately, to conductance steps of 0.1–0.2 nmho. More work is needed. Perhaps spectral or frequency analysis of current fluctuations (noise) under voltage clamp is the most promising technique (207).

Local anesthetics like cocaine, procaine, and lidocaine block impulses by blocking sodium channels. They are freely soluble in cell membranes as free bases (205) and are thought to exert much of their action from the axoplasmic side of the membrane after becoming protonated to the cationic form (175, 200). Permanently cationic quaternary analogs of lidocaine act only from the inside (81, 208). Their action is profoundly increased by a burst of depolarizing voltage pulses in a way suggesting that the analog only enters the blocking position after sodium channels open and that the m^3h gate is closer to the axoplasmic end of the channel than the narrow selectivity filter (208). The susceptibility of inactivation only to internally applied pronase can be interpreted in the same way (14).

Potassium Channels

LONG PORE. Ussing (221) derived a relation between the two simultaneous one-way tracer fluxes across any membrane or series of membranes that must be obeyed if the ions are moving by simple diffusion. For example, for K^+ the ratio of tracer efflux to influx should be $[K]_i \exp(FE/RT)/[K]_o$ (see Eq. 46). Hodgkin & Keynes (132) found that the ratio of potassium fluxes in *Sepia* axons fits instead the 2.5 power of this predicted ratio (Eq. 47), implying some interaction of K^+ crossing the membrane. The same kind of deviation occurs in frog skeletal muscle (135). The interaction is the kind expected in a system with several ions in a row traversing the membrane in single file, as if constrained in a long narrow tunnel (96, 132). The observed deviation from Ussing's flux ratio is often called the *long pore effect* and is the first evidence that potassium channels are pores.

There is also pharmacological evidence favoring a

pore for potassium channels involving kinetics of block of potassium channels by internal TEA ion and its analogs (9–11, 16). This subject is reviewed by Armstrong (12, 12a). These blocking ions seem to be able to enter the mouth of the long pore from the inside end. One of these arguments suggests that there may be perhaps 5–100 times as many potassium channels as sodium channels on squid axon membranes and that the potassium flux in an open channel is 1 ion per microsecond (10). This rate is again more like that possible in a pore than in a carrier or shuttle mechanism.

IONIC SELECTIVITY. Potassium channels are known to be permeable to only four cations in the sequence $Tl^+ > K^+ > Rb^+ > NH_4^+$ (107). All these cations are small, with diameters in the range 2.6–3.0 Å. Selection against Na^+ is strong with a P_{Na} -to- P_K ratio of less than 0.01. A current hypothesis (28, 107) suggests that the narrowest part of the channel has a diameter of roughly 3 Å, is formed by oxygens, and bears little net negative charge. Because it is narrower, the potassium channel requires more completely dehydrated ions than the sodium channel. The narrow part would not provide enough attraction energy for very small cations like Na^+ and Li^+ to make up for the considerable work required for dehydration; thus K^+ is favored over Na^+ . The inside end of the channel is wide enough for quaternary ammonium ions to enter from the axoplasm, and even axoplasmic Na^+ seems free to go some distance into that end of the channel (28). All these ions that enter the inside of the potassium channel without passing all the way through (including Na^+) reduce the magnitude of outward potassium currents (12).

GATING. As with sodium channels, gating in potassium channels probably is controlled by unidentified field-sensitive components that are part of the channel structure. Two conditions change g_K in a way not described by the original Hodgkin-Huxley model. Strong hyperpolarizations considerably delay the subsequent activation of g_K during a depolarization (42), and prolonged depolarization inactivates g_K (59, 204). Kinetic studies of the block of channels by quaternary ammonium ions provide good evidence that the n^1 -gate is near the inner end of the channel and that the selectivity filter is toward the outer end (11, 16). These drugs alter the measured kinetics of g_K , introducing a fast inactivationlike decay, but further experiments show that the change is a time-dependent entry of the drug rather than an alteration of gating kinetics. No drugs or natural toxins are known that have much effect on the gating processes in potassium channels.

Calcium Channels

Although they are widely distributed, little is known about calcium channels, and voltage-clamp

information is only beginning to be obtained. Calcium action potentials have been reviewed (90, 197). Calcium channels are permeable to Ca^{2+} , Ba^{2+} , and Sr^{2+} but not to Mg^{2+} (68, 84, 90a, 92, 154). They are blocked by millimolar concentrations of Mn^{2+} , Co^{2+} , and other heavy metals (90a, 93, 94, 167) and of verapamil and its methoxy derivative D 600 (20, 152). They are not blocked by concentrations of local anesthetics that block sodium channels (69, 93, 154, 167).

Voltage-clamp measurements on barnacle muscle (90a, 91, 151b) and gastropod ganglion cells (45–47, 179) show kinetic similarities and differences between calcium and sodium channels. Both types of channels activate and inactivate following a depolarization, although in barnacle muscle inactivation may not always be complete (90a, 151b). In *Anisodoris* ganglion cell, inward current is probably carried by Ca^{2+} and the kinetics have been described by parameters A^3B , which, in complete analogy with m^3h , give a sigmoid activation and exponential inactivation (47, 179). The curves of steady-state values A_x and B_x are very similar to those of m_x and h_x in axons except that the cell body or muscle must be more depolarized than the axon to get to equivalent points on the curve. Time constants of activation and inactivation of g_{Ca} are about 10–20 times slower than for g_{Na} at equivalent temperatures. Peak inward calcium current densities are on the order 0.1–0.2 mA/cm² rather than the 1–5 mA/cm² of sodium current in giant axons. Both the slow permeability changes and the low current densities make calcium action potentials characteristically slower than typical sodium action potentials.

Propagation of impulses in squid giant axons is accompanied by a small influx of Ca^{2+} in addition to the larger influx of Na^+ . In seawater with 11 mM calcium, the extra influx per impulse is 0.006 pmol/cm² at 20°C (133). Voltage-clamp studies using the protein aequorin as a fluorescent indicator of internal calcium show two pathways for this extra calcium entry. One is sodium channels, in which $P_{Ca}:P_{Na}$ is calculated to be in the range 0.01–0.1, and the calcium influx is blocked by TTX (21, 167a). The second is calcium channels that open with almost the same time course as the increase of g_K but are blocked by Mn^{2+} and D 600 and not by TTX or TEA (21). Thus even axons have calcium channels, although not enough to affect the normal electrical response. Calcium fluxes in axons are described in a review (20).

The relative adaptive advantages of using sodium channels in one place and calcium channels in another have not been analyzed. Sodium channels have been found in all fast-reacting cells. The cells respond rapidly with a sharp threshold and short spike to incoming stimuli. The resting impedance of the cell can be low. Calcium channels are found in cells with slower, often more graded responses, lower upstroke velocity, longer spikes, and higher resting impedance. In a conducting system calcium spikes travel

more slowly. Combinations of sodium and calcium channels are found in cells with a sharp upstroke yet a long action potential, like some heart cells. In addition to carrying current, the entering Ca^{2+} can serve as an intracellular messenger. In axons and cell bodies intracellular Ca^{2+} may activate metabolic changes in response to stimulation, as it is known to do in muscle fibers. At synaptic terminals entering calcium is probably the stimulus for release of synaptic vesicles (147). In muscles, entering calcium is in part a direct stimulus to the contractile proteins and metabolism and in part a precursor to replenish the internal stores of stimulating calcium.

EQUATIONS OF IONIC HYPOTHESIS

In this section some of the equations and biophysical theories used in the ionic hypothesis are provided. The first part describes in detail empirical equations and constants used in the Hodgkin-Huxley model and explains which equations must be solved to calculate predicted responses of the model. The second part derives from diffusion theory the equations relating ionic currents, permeabilities, and concentrations in simple homogeneous membranes.

Solving Hodgkin-Huxley Model

EMPIRICAL CONSTANTS. All practical calculations from the Hodgkin-Huxley and other nerve models are now done by digital computer, so all coefficients must be in mathematical form. The experimentally observed values of α 's and β 's are represented approximately by smooth mathematical functions. The functions for squid axons (126) at 6.3°C are

$$\alpha_m = \frac{0.1(E + 40)}{1 - \exp[-(E + 40)/10]} \quad (25)$$

$$\beta_m = 0.108 \exp(-E/18) \quad (26)$$

$$\alpha_n = \frac{0.01(E + 55)}{1 - \exp[-(E + 55)/10]} \quad (27)$$

$$\beta_n = 0.0555 \exp(-E/80) \quad (28)$$

$$\alpha_h = 0.0027 \exp(-E/20) \quad (29)$$

$$\beta_h = \frac{1}{1 + \exp[-(E + 35)/10]} \quad (30)$$

where E is in millivolts absolute potential and α 's and β 's are in reciprocal milliseconds. As elsewhere in this chapter, the formulas are derived from those in the original paper assuming that the resting potential is -65 mV. In doing this the coefficients in

front of β_m , β_n , and α_h are rounded off to the third significant figure. Adrian et al. (5) have given a version of Equations 25–30 assuming a resting potential of -62 mV. For calculations at other temperatures, the Q_{10} 's for all rate constants are often assumed to be 3.0. Thus α_m at a temperature T would be $3^{(T-6.3)/10}$ times the value at 6.3°C. It probably would be more accurate to use the specific Q_{10} 's for each rate constant measured in *Xenopus* and *Myxicola* axons (80, 204a). The standard values of the other membrane parameters are $E_{\text{Na}} = 50$ mV; $\bar{g}_{\text{Na}} = 120$ mmho/cm²; $E_{\text{K}} = -77$ mV; $\bar{g}_{\text{K}} = 36$ mmho/cm²; $E_{\text{L}} = -54.387$ mV; $\bar{g}_{\text{L}} = 0.3$ mmho/cm²; $C = 1$ $\mu\text{F/cm}^2$. A small temperature dependence of conductances is usually ignored in calculations, but again values are available in the literature (80, 126, 204a).

SOLUTIONS. The space-clamped condition is the easiest to solve mathematically. There is excitation but no propagation. Since the inside potential is uniform, no currents flow longitudinally in the axon, and there are no external sources of membrane current except the stimulating electrode. The equation to solve is

$$I_s(t) = I_m = C \frac{dE}{dt} + I_{\text{Na}} + I_{\text{K}} + I_{\text{L}} \quad (31)$$

where $I_s(t)$ is the stimulus current density. The simplest approach is with the rearranged form

$$\frac{dE}{dt} = \frac{[I_s(t) - I_{\text{Na}} - I_{\text{K}} - I_{\text{L}}]}{C} \quad (32)$$

An initial value for I_{Na} , I_{K} , and I_{L} is calculated using Equations 14 and 15, and dE/dt is calculated from Equation 32. Then E is incremented the appropriate amount for a small time step like 1 μs . New values of m , n , and h are found by integrating Equations 21–23 over the small time step, and currents are calculated again. The process is repeated several thousand times until the appropriate response is developed. A variety of other more precise or efficient methods can be used instead of the one given here (49, 126). In computer calculations a few seconds usually suffice to obtain the time course of one action potential with space-clamped conditions (often called a membrane action potential to distinguish it from a propagated action potential).

As soon as the space-clamp condition is removed, longitudinal current flow is permitted, and neighboring parts of the axon become sources of membrane current from each patch of membrane. There are two methods for incorporating these local circuits in the calculations. The first (126) is to assume that the cable properties are uniform in space and that an action potential is propagating at constant velocity and shape. These assumptions lead to Equation 9 for I_m derived earlier, which can now be expanded

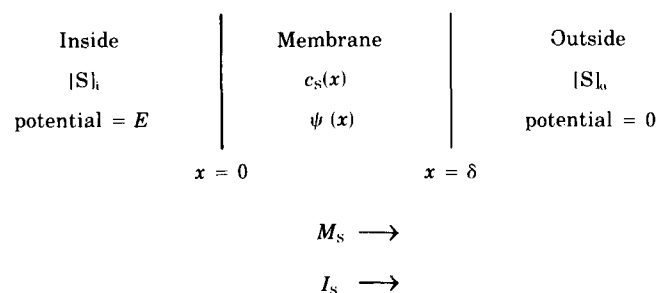
$$I_m = \frac{a}{2R_i\theta^2} \frac{\partial^2 E}{\partial t^2} = C \frac{\partial E}{\partial t} + I_{\text{Na}} + I_{\text{K}} + I_{\text{L}} \quad (33)$$

Equation 33 is solved by using the Hodgkin-Huxley expressions for currents and guessing a value for the conduction velocity. For wrong values of θ the calculated membrane potential quickly diverges beyond the physiological range. New values of θ are tried until a stable solution is found. Figures 22–24 are calculated this way. Again the integration is done in short time steps like $1 \mu\text{s}$. The method is of no use in calculating thresholds or any local responses since it starts at once with the assumption of uniform propagation.

The second method for solving the equations without space clamping is much more general and requires much more storage in the computing machine (48, 49, 182a). The cable is broken into a large number of small sections all represented within the computer. The response of all sections is developed in parallel allowing each to receive local current from its neighbor on each side. This procedure is more like what the axon does and can be used to study nonuniform cables with branching, tapering, locally modified excitability, and so forth. Figure 21 was calculated this way.

Diffusion of Charged Particles in Electric Field

NERNST-PLANCK EQUATIONS. Consider a membrane of thickness δ (cm) bathed on both sides by well-stirred ionic solutions containing, among others, ion S at concentration $[S]$ (mol/cm^3). Note that the unit of concentration is different from conventional molarity. Equations are derived for the flux of S (M_s , $\text{mol}/\text{cm}^2\cdot\text{s}$) and the current carried by S (I_s , A/cm^2) across 1 cm^2 of the membrane.



The dimensions and names of the required variables are c_s (mol/cm^3), concentration in membrane; z_s (dimensionless), charge on ion; u_s ($[\text{cm}/\text{s}]/[\text{V}/\text{cm}] = \text{cm}^2\cdot\text{V}/\text{s}$), mobility in membrane; D_s (cm^2/s), diffusion constant in membrane; ψ (V), electric potential within membrane; E (V), potential drop across membrane. The quantities c_s , u_s , D_s , and ψ may vary from point to point within the membrane.

In the absence of an electric field ($E = 0$), ions and nonelectrolytes diffuse according to Fick's law

$$-M_s = D_s \frac{dc_s}{dx} \quad (34)$$

In a field with no concentration gradient, ions move according to the electrophoresis equation

$$-M_s = z_s u_s c_s \frac{d\psi}{dx} \quad (35)$$

These simple equations embody the linear relations empirically observed between the fluxes and driving forces. The coefficients D_s and u_s express the same quality, namely, the ease of motion of the particles, and are exactly related by Einstein's formula (61)

$$D_s = \frac{RT}{F} u_s \quad (36)$$

where R , T , and F are the usual thermodynamic quantities. The net flux in a concentration gradient and an electric field is the sum of Equations 34 and 35. Using Equation 36 an expression for the sum is

$$-M_s = D_s \left(\frac{dc_s}{dx} + \frac{Fz_s c_s}{RT} \frac{d\psi}{dx} \right) \quad (37)$$

Multiplying both sides by $z_s F$ ($\text{C}\cdot\text{mol}^{-1}$) gives the Nernst-Planck (180, 181, 191, 192) equation for the current carried by S

$$-I_s = z_s F D_s \left(\frac{dc_s}{dx} + \frac{Fz_s c_s}{RT} \frac{d\psi}{dx} \right) \quad (38)$$

Useful practical equations may be derived from this general equation by inserting conditions appropriate to different problems and integrating across the membrane to eliminate derivatives. Different assumptions lead to practical formulas like the Goldman-Hodgkin-Katz current and voltage equations, the independence relation, and the Ussing flux ratio. In particular, assumptions often must be made regarding the variation of c_s , u_s , D_s , and ψ within the membrane.

Multiplying by an integrating factor gives

$$-I_s = z_s F D_s \frac{e^{z_s F \psi / RT}}{e^{z_s F \psi / RT}} \left(\frac{dc_s}{dx} + \frac{Fz_s c_s}{RT} \frac{d\psi}{dx} \right) \quad (39)$$

$$-I_s = \frac{z_s F D_s}{e^{z_s F \psi / RT}} \frac{d}{dx} (c_s e^{z_s F \psi / RT}) \quad (40)$$

Let the concentration just inside the edges of the membrane be related to the bulk concentrations by a simple partition coefficient β (dimensionless), so that c_s at $x = 0$ is $\beta_s [S]_i$ and c_s at $x = \delta$ is $\beta_s [S]_o$. Then integrating Equation 40 across the membrane gives

$$-I_s = \frac{z_s F \beta_s ([S]_o - [S]_i) e^{z_s F \psi / RT}}{\int_{x=0}^{\delta} \frac{e^{z_s F \psi / RT}}{D_s} dx} \quad (41)$$

The integral in the denominator cannot be evaluated without knowing the variation of potential and diffusion constant within the membrane.

GOLDMAN-HODGKIN-KATZ EQUATION. Goldman (86) introduced two assumptions: a constant value of D_s independent of x , equivalent to a homogeneous mem-

brane; and a constant electric field. With these conditions Equation 41 may be integrated to give (86, 130)

$$I_s = P_s E z^2 S \frac{F^2}{RT} \frac{[S]_o - [S]_i e^{zFE/RT}}{1 - e^{zFE/RT}} \quad (42)$$

where

$$P_s = \frac{D_s \beta_s}{\delta} \quad (43)$$

Equation 42 is called the Goldman-Hodgkin-Katz current equation or the constant field equation and is a useful relation among permeability, ionic concentrations, membrane potential, and current for single ions. The equation is used both in electrical studies and in chemical or tracer flux measurements on biological membranes. Equation 43 is the formal definition of permeability in a homogeneous membrane. Permeability has the units centimeters per second.

Note that the predicted current is not a linear function of voltage except when $[S]_o$ and $[S]_i$ are equal, that is, systems fitting this equation do not satisfy Ohm's law if concentrations are asymmetric. Later authors have introduced asymmetry in the membrane properties to derive analogous constant field equations that give linear current-voltage relations under asymmetric ionic conditions like those in axons (74, 222).

When a membrane is permeable to several ions, the resting potential of the system is determined by the simultaneous diffusion of several ions and generally differs from the Nernst potential for any one of those ions. The membrane potential in this nonequilibrium, steady state can be calculated by adding together the formulas for current carried by each ion and solving for the potential corresponding to zero current flow. For example, if the membrane is permeable to Na^+ , K^+ , and Cl^- , the zero-current potential is obtained by solving

$$0 = I_{Na} + I_K + I_{Cl} \quad (44)$$

If each current component obeys the constant field Equation 42, substitution into Equation 44 gives

$$E = \frac{RT}{F} \ln \frac{P_K [K]_o + P_{Na} [Na]_o + P_{Cl} [Cl]_i}{P_K [K]_i + P_{Na} [Na]_i + P_{Cl} [Cl]_o} \quad (2)$$

This is the Goldman-Hodgkin-Katz potential equation. It is used in studies of the resting potential and of the driving or reversal potential of membrane permeability mechanisms to determine the underlying permeabilities, or more accurately, permeability ratios. Again, since not all ions have the same equilibrium potential, there will be steady, net downhill fluxes of several ions at this potential. Similar equations can be derived from some other special assumptions without a constant field (108). For a membrane exclusively permeable to divalent ions, the factor in front of the logarithm is $RT/2F$. Equations for membranes permeable to monovalent and divalent ions

are more complicated. The Goldman-Hodgkin-Katz potential equation reduces to the Nernst equation (Eq. 1) when only one ion is permeant.

Moreton's (170) equation (Eq. 3) for resting potential in the presence of a pump current I_{pump} is obtained by solving

$$0 = I_{Na} + I_K + I_{Cl} + I_{pump} \quad (45)$$

USSING FLUX RATIO. Consider one type of ion S but imagine that those ions on one side are labeled to distinguish them from those on the other side. Then unidirectional fluxes M_{io} and M_{oi} can be measured in addition to the net flux M . For an ion satisfying the constant field equation, M_{io} can be obtained by inserting $[S]_o = 0$ into Equation 42 and similarly with $[S]_i = 0$ for M_{oi} . The ratio of the resulting expressions becomes

$$\frac{M_{io}}{M_{oi}} = \frac{[S]_i}{[S]_o} e^{zFE/RT} \quad (46)$$

Actually neither a constant field nor a constant D_s is necessary (221), and Equation 46 is derivable as described above using Equation 41 because the unknown integral in Equation 41 must be the same for M_{io} as for M_{oi} . The Ussing flux ratio is a useful criterion for distinguishing free diffusion from more complex processes, including active transport, exchange diffusion, and certain couplings of the flow of individual test ions to the flow of other ions or nonelectrolytes. In long pores the flux ratio becomes (96, 132)

$$\frac{M_{io}}{M_{oi}} = \left(\frac{[S]_i}{[S]_o} e^{zFE/RT} \right)^n \quad (47)$$

where n is roughly the number of S particles within the pore at one time.

INDEPENDENCE RELATION. According to the constant field equation, if the external concentration of S is changed to $[S]_o'$ but E is held constant and $[S]_i$ is assumed to stay constant, the new current I_s' is related to the old current I_s by

$$\frac{I_s'}{I_s} = \frac{[S]_o' - [S]_i e^{zFE/RT}}{[S]_o - [S]_i e^{zFE/RT}} \quad (48)$$

This relation can also be derived from Equation 41 provided that the unknown integral in the denominator of Equation 41 stays constant, that is, if changing $[S]_o$ does not alter the profiles of potential and diffusion constant. Hodgkin & Huxley (123) derived Equation 48 from the even simpler assumption that changing $[S]_o$ has no effect on the unidirectional efflux M_{io} and changes the unidirectional influx M_{oi} exactly in proportion to the change in $[S]_o$. This is the same as saying that the chance that an S ion crosses the membrane is independent of the presence of other S ions. Thus Equation 48 is called the independence relation. It is a useful test for free diffusion without

the influence of other ions. Hodgkin's and Huxley's simple assumption is also another route to Ussing's flux ratio, Equation 46.

EYRING RATE THEORY. An alternative method to the Nernst-Planck equations for calculating fluxes and potentials for ionic channels is Eyring rate theory (66), whereby a channel is considered to be a series of microscopic energy barriers that ions must cross. The theory has the capability of incorporating atomic microstructure of a channel in the flux equations and thus will probably see more use in the future. With suitable assumptions all equations derived in this section on diffusion can be obtained by rate theory (67, 96, 222).

PRACTICAL CALCULATIONS. More practical discussion of ionic diffusion and electrophoresis in aqueous media is given by Robinson & Stokes (202). Appendices in their book also give the most useful tables of experimentally measured ionic mobilities, diffusion constants, and activity coefficients needed for many calculations. Finally, in many formulas the expression RT/F appears. Table 4 lists values at different temperatures to facilitate calculation. Also given are values of $2.303 RT/F$ to be used when \log_{10} is used for

TABLE 4. Values of RT/F

Temperature, °C	RT/F , mV	$2.303 RT/F$, mV
0	23.54	54.20
5	23.97	55.19
10	24.40	56.18
15	24.83	57.17
20	25.26	58.17
25	25.69	59.16
30	26.12	60.15
35	26.55	61.14
37	26.73	61.54

calculation of potentials instead of \ln . For example, the Nernst equation may be written

$$E_{\text{Na}} = \frac{RT}{F} \ln \frac{[\text{Na}]_o}{[\text{Na}]_i} = 2.303 \frac{RT}{F} \log_{10} \frac{[\text{Na}]_o}{[\text{Na}]_i} \quad (1b)$$

Then from Table 4 at 20°C an e -fold Na^+ concentration ratio corresponds to $E_{\text{Na}} = 25.3$ mV and a 10-fold ratio corresponds to $E_{\text{Na}} = 58.2$ mV.

I am grateful to my colleagues Drs. L. L. Costantin, C. A. Lewis, H. D. Patton, R. W. Tsien, and J. W. Woodbury for many helpful comments on the manuscript. I thank Susan A. Morton for invaluable secretarial assistance.

REFERENCES

1. ADELMAN, W. J., JR. (Editor). *Biophysics and Physiology of Excitable Membranes*. New York: Van Nostrand Reinhold, 1971.
2. ADELMAN, W. J., JR., AND Y. PALT. The effects of external potassium and long duration voltage conditioning on the amplitude of sodium currents in the giant axon of the squid, *Loligo pealei*. *J. Gen. Physiol.* 54: 589-606, 1969.
3. ADELMAN, W. J., JR., AND J. P. SENFT. Voltage clamp studies on the effect of internal cesium ion on sodium and potassium currents in the squid giant axon. *J. Gen. Physiol.* 50: 279-293, 1966.
4. ADRIAN, E. D., AND K. LUCAS. On the summation of propagated disturbances in nerve and muscle. *J. Physiol. London* 44: 68-124, 1912.
5. ADRIAN, R. H., W. K. CHANDLER, AND A. L. HODGKIN. Voltage clamp experiments in striated muscle fibres. *J. Physiol. London* 208: 607-644, 1970.
6. AGIN, D. Hodgkin-Huxley equations: logarithmic relation between membrane current and frequency of repetitive activity. *Nature* 201: 625-626, 1964.
7. AGIN, D. P. (Editor). *Perspectives in Membrane Biophysics, a Tribute to Kenneth S. Cole*. New York: Gordon and Breach, 1972.
- 7a. ALMERS, W., AND S. R. LEVINSON. Tetrodotoxin binding to normal and depolarized frog muscle and the conductance of a single sodium channel. *J. Physiol. London* 247: 483-509, 1975.
8. ANDERSON, N. C., JR. Voltage-clamp studies on uterine smooth muscle. *J. Gen. Physiol.* 54: 145-165, 1969.
9. ARMSTRONG, C. M. Time course of TEA⁺-induced anomalous rectification in squid giant axons. *J. Gen. Physiol.* 50: 491-503, 1966.
10. ARMSTRONG, C. M. Inactivation of the potassium conductance and related phenomena caused by quaternary ammonium ion injection in squid axons. *J. Gen. Physiol.* 54: 553-575, 1969.
11. ARMSTRONG, C. M. Interaction of tetraethylammonium ion derivatives with the potassium channels of giant axons. *J. Gen. Physiol.* 58: 413-437, 1971.
12. ARMSTRONG, C. M. Channels and voltage dependent gates in nerve. In: *Membranes - a Series of Advances. Artificial and Biological Membranes*, edited by G. Eisenman. New York: Dekker, 1975, vol. 3, 325-358.
- 12a. ARMSTRONG, C. M. Ionic pores, gates, and gating currents. *Quart. Rev. Biophys.* 7: 179-210, 1974.
13. ARMSTRONG, C. M., AND F. BEZANILLA. Currents related to movement of the gating particles of the sodium channels. *Nature* 242: 459-461, 1973.
- 13a. ARMSTRONG, C. M., AND F. BEZANILLA. Charge movement associated with the opening and closing of the activation gates of the Na channels. *J. Gen. Physiol.* 63: 533-552, 1974.
14. ARMSTRONG, C. M., F. BEZANILLA, AND E. ROJAS. Destruction of sodium conductance inactivation in squid axons perfused with pronase. *J. Gen. Physiol.* 62: 375-391, 1973.
15. ARMSTRONG, C. M., AND L. BINSTOCK. Anomalous rectification in the squid giant axon injected with tetraethylammonium chloride. *J. Gen. Physiol.* 48: 859-872, 1965.
16. ARMSTRONG, C. M., AND B. HILLE. The inner quaternary ammonium ion receptor in potassium channels of the node of Ranvier. *J. Gen. Physiol.* 59: 388-400, 1972.
17. ARRHENIUS, S. Über die Dissociation in Wasser gelöster Stoffe. *Z. Physik. Chem. Leipzig* 1: 631-648, 1887.
18. ASANO, T., AND W. P. HURLBUT. Effects of potassium, sodium, and azide on the ionic movements that accompany activity in frog nerves. *J. Gen. Physiol.* 41: 1187-1203, 1958.
19. ATWATER, I., F. BEZANILLA, AND E. ROJAS. Sodium influxes in internally perfused squid giant axons during voltage clamp. *J. Physiol. London* 201: 657-664, 1969.
20. BAKER, P. F. Transport and metabolism of calcium ions in nerve. *Progr. Biophys. Mol. Biol.* 24: 177-223, 1972.
21. BAKER, P. F., A. L. HODGKIN, AND E. B. RIDGWAY. Depolarization and calcium entry in squid giant axons. *J. Physiol. London* 218: 709-755, 1971.
22. BAKER, P. F., A. L. HODGKIN, AND T. I. SHAW. Replacement

- of the axoplasm of giant nerve fibres with artificial solutions. *J. Physiol. London* 164: 330-354, 1962.
23. BAKER, P. F., AND J. S. WILLIS. On the number of sodium pumping sites in cell membranes. *Biochim. Biophys. Acta* 183: 646-649, 1969.
 24. BEELER, G. W., AND H. REUTER. The relation between membrane potential, membrane currents and activation of contraction in ventricular myocardial fibres. *J. Physiol. London* 207: 211-229, 1970.
 - 24a. BEELER, G. W., JR., AND H. REUTER. Membrane calcium current in ventricular myocardial fibres. *J. Physiol. London* 207: 191-209, 1970.
 25. BENNETT, M. V. L. Comparative physiology: electric organs. *Ann. Rev. Physiol.* 32: 471-528, 1970.
 26. BERNSTEIN, J. Untersuchungen zur Thermodynamik der bioelektrischen Ströme. Erster Theil. *Pfluegers Arch. Ges. Physiol.* 92: 521-562, 1902.
 27. BERNSTEIN, J. *Elektrobiologie*. Braunschweig: Vieweg, 1912.
 28. BEZANILLA, F., AND C. M. ARMSTRONG. Negative conductance caused by entry of sodium and cesium ions into the potassium channels of squid axons. *J. Gen. Physiol.* 60: 588-608, 1972.
 29. BEZANILLA, F., E. ROJAS, AND R. E. TAYLOR. Time course of the sodium influx in squid giant axon during a single voltage clamp pulse. *J. Physiol. London* 207: 151-164, 1970.
 30. BINSTOCK, L., AND L. GOLDMAN. Current- and voltage-clamped studies on *Myxicola* giant axons. Effect of tetrodotoxin. *J. Gen. Physiol.* 54: 730-740, 1969.
 31. BLANKENSHIP, J. E. Action of tetrodotoxin on spinal motoneurons of the cat. *J. Neurophysiol.* 31: 186-194, 1968.
 32. BUNCH, W. H., AND G. KALLSEN. Rate of intracellular diffusion as measured in barnacle muscle. *Science* 164: 1178-1179, 1969.
 33. BURG, D. Untersuchungen am Ranvierschen Schnürring einzelner Taubenervenfaseren. *Pfluegers Arch. Ges. Physiol.* 317: 278-286, 1970.
 - 33a. BURROWS, T. M. O., I. A. CAMPBELL, E. J. HOWE, AND J. Z. YOUNG. Conduction velocity and diameter of nerve fibres of cephalopods. *J. Physiol. London* 179: 39P-40P, 1965.
 34. CHANDLER, W. K., A. L. HODGKIN, AND H. MEVES. The effect of changing the internal solution on sodium inactivation and related phenomena in giant axons. *J. Physiol. London* 180: 821-836, 1965.
 35. CHANDLER, W. K., AND H. MEVES. Voltage clamp experiments on internally perfused giant axons. *J. Physiol. London* 180: 788-820, 1965.
 36. CHANDLER, W. K., AND H. MEVES. Sodium and potassium currents in squid axons perfused with fluoride solutions. *J. Physiol. London* 211: 623-652, 1970.
 37. COHEN, L. B. Changes in neuron structure during action potential propagation and synaptic transmission. *Physiol. Rev.* 53: 373-418, 1973.
 38. COLE, K. S. Dynamic electrical characteristics of the squid axon membrane. *Arch. Sci. Physiol.* 3: 253-258, 1949.
 39. COLE, K. S. *Membranes, Ions and Impulses. A Chapter of Classical Biophysics*. Berkeley: Univ. of California Press, 1968.
 40. COLE, K. S., AND R. F. BAKER. Transverse impedance of the squid giant axon during current flow. *J. Gen. Physiol.* 24: 535-549, 1941.
 41. COLE, K. S., AND H. J. CURTIS. Electric impedance of the squid giant axon during activity. *J. Gen. Physiol.* 22: 649-670, 1939.
 42. COLE, K. S., AND J. W. MOORE. Ionic current measurements in the squid giant axon membrane. *J. Gen. Physiol.* 44: 123-167, 1960.
 43. COLQUHOUN, D., R. HENDERSON, AND J. M. RITCHIE. The binding of labelled tetrodotoxin to non-myelinated nerve fibres. *J. Physiol. London* 227: 95-126, 1972.
 44. COLQUHOUN, D., AND J. M. RITCHIE. The interaction at equilibrium between tetrodotoxin and mammalian non-myelinated nerve fibres. *J. Physiol. London* 221: 533-553, 1972.
 45. CONNOR, J. A., AND C. F. STEVENS. Inward and delayed outward membrane currents in isolated neural somata under voltage clamp. *J. Physiol. London* 213: 1-19, 1971.
 46. CONNOR, J. A., AND C. F. STEVENS. Voltage clamp studies of a transient outward membrane current in gastropod neural somata. *J. Physiol. London* 213: 21-30, 1971.
 47. CONNOR, J. A., AND C. F. STEVENS. Prediction of repetitive firing behaviour from voltage clamp data on an isolated neurone soma. *J. Physiol. London* 213: 31-53, 1971.
 48. COOLEY, J. W., AND F. A. DODGE. Digital computer solutions for excitation and propagation of the nerve impulse. *IBM Res. Rept.* 1496, 1965.
 49. COOLEY, J. W., AND F. A. DODGE. Digital computer solutions for excitation and propagation of the nerve impulse. *Biophys. J.* 6: 583-599, 1966.
 - 49a. COPPIN, C. M. L., AND J. B. JACK. Internodal length and conduction velocity of cat muscle afferent nerve fibres. *J. Physiol. London* 222: 91P-93P, 1971.
 50. CURTIS, H. J., AND K. S. COLE. Membrane resting and action potentials from the squid giant axon. *J. Cell. Comp. Physiol.* 19: 135-144, 1942.
 51. DECK, K. A., R. KERN, AND W. TRAUTWEIN. Voltage clamp technique in mammalian cardiac fibres. *Pfluegers Arch. Ges. Physiol.* 280: 50-62, 1964.
 52. DECK, K. A., AND W. TRAUTWEIN. Ionic currents in cardiac excitation. *Pfluegers Arch. Ges. Physiol.* 280: 63-80, 1964.
 53. DEL CASTILLO, J., AND J. W. MOORE. On increasing the velocity of a nerve impulse. *J. Physiol. London* 148: 665-670, 1959.
 54. DE WEER, P., AND D. GEDULDIG. Electrogenic sodium pump in squid giant axon. *Science* 179: 1326-1328, 1973.
 55. DODGE, F. A. Ionic permeability changes underlying nerve excitation. In: *Biophysics of Physiological and Pharmacological Actions*. Washington, D.C.: Am. Assoc. Advan. Sci., 1961, p. 119.
 56. DODGE, F. A. *A Study of Ionic Permeability Changes Underlying Excitation in Myelinated Nerve Fibers of the Frog* (Ph.D. thesis). New York: The Rockefeller University, 1963. [University Microfilms, Inc., Ann Arbor, Mich. (No. 64-7333).]
 57. DODGE, F. A., AND B. FRANKENHAEUSER. Membrane currents in isolated frog nerve fibre under voltage clamp conditions. *J. Physiol. London* 143: 76-90, 1958.
 58. DODGE, F. A., AND B. FRANKENHAEUSER. Sodium currents in the myelinated nerve fibre of *Xenopus laevis* investigated with the voltage clamp technique. *J. Physiol. London* 148: 188-200, 1959.
 59. EHRENSTEIN, G., AND D. L. GILBERT. Slow changes of potassium permeability in the squid giant axon. *Biophys. J.* 6: 553-566, 1966.
 60. EHRENSTEIN, G., AND H. LECAR. The mechanism of signal transmission in nerve axons. *Ann. Rev. Biophys. Bioeng.* 1: 347-368, 1972.
 61. EINSTEIN, A. On the movement of small particles suspended in a stationary liquid demanded by the molecular-kinetic theory on heat. *Ann. Physik Leipzig* 17: 549-560, 1905. [Reprinted in: Einstein, A. *Investigations on the Theory of the Brownian Movement*. New York: Dover, 1956.]
 62. EISENMAN, G. Cation selective glass electrodes and their mode of operation. *Biophys. J.* 2, Suppl. 2: 259-323, 1962.
 63. ERLANGER, J., AND E. A. BLAIR. Manifestation of segmentation in myelinated axons. *Am. J. Physiol.* 110: 287-311, 1934.
 64. ERLANGER, J., AND H. S. GASSER. *Electrical Signs of Nervous Activity*. Philadelphia: Univ. of Pennsylvania Press, 1937.
 65. EVANS, M. H. Tetrodotoxin, saxitoxin, and related substances: their applications in neurobiology. *Intern. Rev. Neurobiol.* 15: 83-166, 1972.
 66. EYRING, H., D. HENDERSON, B. J. STOVER, AND E. M. EYRING. *Statistical Mechanics and Dynamics*. New York: Wiley, 1964.
 67. EYRING, H., R. LUMRY, AND J. W. WOODBURY. Some applications of modern rate theory to physiological systems. *Record*

- Chem. Progr. Kresge-Hooker Sci. Lib.* 10: 100-114, 1949.
68. FATT, P., AND B. L. GINSBERG. The ionic requirements for the production of action potentials in crustacean muscle fibres. *J. Physiol. London* 142: 516-543, 1958.
 69. FATT, P., AND B. KATZ. The electrical properties of crustacean muscle fibres. *J. Physiol. London* 120: 171-204, 1953.
 70. FITZHUGH, R. A kinetic model of the conductance changes in nerve membrane. *J. Cell. Comp. Physiol.* 66, Suppl. 2: 111-117, 1965.
 71. FITZHUGH, R., AND H. A. ANTOSIEWICZ. Automatic computation of nerve excitation—detailed corrections and additions. *J. Soc. Ind. Appl. Math.* 7: 447-458, 1959.
 72. FRANKENHAEUSER, B. A method for recording resting and action potentials in the isolated myelinated nerve fibre of the frog. *J. Physiol. London* 135: 550-559, 1957.
 73. FRANKENHAEUSER, B. Quantitative description of sodium currents in myelinated nerve fibres of *Xenopus laevis*. *J. Physiol. London* 151: 491-501, 1960.
 74. FRANKENHAEUSER, B. Sodium permeability in toad nerve and in squid nerve. *J. Physiol. London* 152: 159-166, 1960.
 75. FRANKENHAEUSER, B. A quantitative description of potassium currents in myelinated nerve fibres of *Xenopus laevis*. *J. Physiol. London* 169: 424-430, 1963.
 76. FRANKENHAEUSER, B. Computed action potential in nerve from *Xenopus laevis*. *J. Physiol. London* 180: 780-787, 1965.
 77. FRANKENHAEUSER, B., AND A. L. HODGKIN. The after-effects of impulses in the giant nerve fibres of *Loligo*. *J. Physiol. London* 131: 341-376, 1956.
 78. FRANKENHAEUSER, B., AND A. L. HODGKIN. The action of calcium on the electrical properties of squid axons. *J. Physiol. London* 137: 218-244, 1957.
 79. FRANKENHAEUSER, B., AND A. F. HUXLEY. The action potential in the myelinated nerve fibre of *Xenopus laevis* as computed on the basis of voltage clamp data. *J. Physiol. London* 171: 302-315, 1964.
 80. FRANKENHAEUSER, B., AND L. E. MOORE. The effect of temperature on the sodium and potassium permeability changes in myelinated nerve fibres of *Xenopus laevis*. *J. Physiol. London* 169: 431-437, 1963.
 81. FRAZIER, D. T., T. NARAHASHI, AND M. YAMADA. The site of action and active form of local anesthetics. II. Experiments with quaternary compounds. *J. Pharmacol. Exptl. Therap.* 171: 45-51, 1970.
 82. GASSER, H. S. Unmyelinated fibers originating in dorsal root ganglia. *J. Gen. Physiol.* 33: 651-690, 1950.
 83. GEDULDIG, D., AND R. GRUENER. Voltage clamp of the *Aplysia* giant neurone: early sodium and calcium currents. *J. Physiol. London* 211: 217-244, 1970.
 84. GERASIMOV, V. D., P. G. KOSTYUK, AND V. A. MAISKII. Effect of bivalent cations on the electrical characteristics of the membrane of giant neurones. *Biofizika* 10: 447-453, 1965.
 85. GILBERT, D. L., AND G. EHRENSTEIN. Effect of divalent cations on potassium conductance of squid axons: determination of surface charge. *Biophys. J.* 9: 447-463, 1969.
 86. GOLDMAN, D. E. Potential, impedance, and rectification in membranes. *J. Gen. Physiol.* 27: 37-60, 1943.
 87. GOLDMAN, L., AND J. S. ALBUS. Computation of impulse conduction in myelinated fibers; theoretical basis of the velocity-diameter relation. *Biophys. J.* 8: 596-607, 1968.
 88. GOLDMAN, L., AND C. L. SCHAUF. Inactivation of the sodium current in *Myxicola* giant axons. Evidence for coupling to the activation process. *J. Gen. Physiol.* 59: 659-675, 1972.
 89. GOLDMAN, L., AND C. L. SCHAUF. Quantitative description of sodium and potassium currents and computed action potentials in *Myxicola* giant axons. *J. Gen. Physiol.* 61: 361-384, 1973.
 90. HAGIWARA, S. Ca^{++} dependent action potentials. In: *Membranes—a Series of Advances. Artificial and Biological Membranes*, edited by G. Eisenman. New York: Dekker, 1975, vol. 3, 359-382.
 - 90a. HAGIWARA, S., J. FUKUDA, AND D. C. EATON. Membrane currents carried by Ca, Sr, and Ba in barnacle muscle fiber during voltage clamp. *J. Gen. Physiol.* 63: 564-578, 1974.
 91. HAGIWARA, S., H. HAYASHI, AND K. TAKAHASHI. Calcium and potassium currents of the membrane of a barnacle muscle fibre in relation to the calcium spike. *J. Physiol. London* 205: 115-129, 1969.
 92. HAGIWARA, S., AND K-I. NAKA. The initiation of spike potential in barnacle muscle fibers under low intracellular Ca^{++} . *J. Gen. Physiol.* 48: 141-162, 1964.
 93. HAGIWARA, S., AND S. NAKAJIMA. Differences in Na and Ca spikes as examined by application of tetrodotoxin, procaine, and manganese ions. *J. Gen. Physiol.* 49: 793-806, 1966.
 94. HAGIWARA, S., AND K. TAKAHASHI. Surface density of calcium ions and calcium spikes in the barnacle muscle fiber membrane. *J. Gen. Physiol.* 50: 583-601, 1967.
 95. HARDY, W. L. Propagation speed in myelinated nerve: theoretical dependence on external Na^+ and on temperature. *Biophys. J.* 13: 1071-1089, 1973.
 96. HECKMANN, K. Single-file diffusion. In: *Passive Permeability of Cell Membranes. Biomembranes*, edited by F. Kreuzer and J. F. G. Slegers. New York: Plenum Press, 1972, vol. 3, 127-153.
 97. HENDERSON, R., J. M. RITCHIE, AND G. R. STRICHARTZ. The binding of labelled saxitoxin to the sodium channels in nerve membranes. *J. Physiol. London* 235: 783-804, 1973.
 98. HENDERSON, R., AND J. H. WANG. Solubilization of a specific tetrodotoxin-binding component from garfish olfactory nerve membrane. *Biochemistry* 11: 4565-4569, 1972.
 99. HILLE, B. The common mode of action of three agents that decrease the transient change in sodium permeability in nerves. *Nature* 210: 1220-1222, 1966.
 100. HILLE, B. The selective inhibition of delayed potassium currents in nerve by tetraethylammonium ion. *J. Gen. Physiol.* 50: 1287-1302, 1967.
 101. HILLE, B. Pharmacological modifications of the sodium channels of frog nerve. *J. Gen. Physiol.* 51: 199-219, 1968.
 102. HILLE, B. Charges and potentials at the nerve surface. Divalent ions and pH. *J. Gen. Physiol.* 51: 221-236, 1968.
 103. HILLE, B. Ionic channels in nerve membranes. *Progr. Biophys. Mol. Biol.* 21: 1-32, 1970.
 104. HILLE, B. Voltage clamp studies on myelinated nerve fibers. In: *Biophysics and Physiology and Excitable Membranes*, edited by W. J. Adelman, Jr. New York: Van Nostrand Reinhold, 1971.
 105. HILLE, B. The permeability of the sodium channel to organic cations in myelinated nerve. *J. Gen. Physiol.* 58: 599-619, 1971.
 106. HILLE, B. The permeability of the sodium channel to metal cations in myelinated nerve. *J. Gen. Physiol.* 59: 637-658, 1972.
 107. HILLE, B. Potassium channels in myelinated nerve. Selective permeability to small cations. *J. Gen. Physiol.* 61: 669-686, 1973.
 108. HILLE, B. Ionic selectivity of Na and K channels of nerve membranes. In: *Membranes—a Series of Advances. Artificial and Biological Membranes*, edited by G. Eisenman. New York: Dekker, 1975, vol. 3, 255-324.
 - 108a. HILLE, B., A. M. WOODHULL, AND B. I. SHAPIRO. Negative surface charge near sodium channels of nerve: divalent ions, monovalent ions, and pH. *Phil. Trans. Roy. Soc.* 270: 301-318, 1975.
 109. HINKE, J. A. M. The measurement of sodium and potassium activities in the squid axon by means of cation-selective glass microelectrodes. *J. Physiol. London* 156: 314-335, 1961.
 110. HINKE, J. A. M. Solvent water for electrolytes in the muscle fiber of the giant barnacle. *J. Gen. Physiol.* 56: 521-541, 1970.
 111. HINKE, J. A. M., J. P. CAILLÉ, AND D. C. GAYTON. Distribution and state of monovalent ions in skeletal muscle based on ion electrode, isotope, and diffusion analyses. *Ann. NY Acad. Sci.* 204: 274-296, 1973.
 112. HIRST, G. D. S., AND I. SPENCE. Calcium action potentials in mammalian peripheral neurones. *Nature New Biol.* 243: 54-56, 1973.

113. HODGKIN, A. L. Evidence for electrical transmission in nerve. Part I. *J. Physiol. London* 90: 183-210, 1937.
114. HODGKIN, A. L. Evidence for electrical transmission in nerve. Part II. *J. Physiol. London* 90: 211-232, 1937.
115. HODGKIN, A. L. The subthreshold potentials in a crustacean nerve fibre. *Proc. Roy. Soc. London Ser. B* 126: 87-121, 1938.
116. HODGKIN, A. L. The local electrical changes associated with repetitive action in a non-medullated axon. *J. Physiol. London* 107: 165-179, 1948.
117. HODGKIN, A. L. The ionic basis of electrical activity in nerve and muscle. *Biol. Rev.* 26: 339-409, 1951.
118. HODGKIN, A. L. A note on conduction velocity. *J. Physiol. London* 125: 221-224, 1954.
119. HODGKIN, A. L. Ionic movements and electrical activity in giant nerve fibres. *Proc. Roy. Soc. London Ser. B* 148: 1-37, 1958.
120. HODGKIN, A. L. *The Conduction of the Nervous Impulse*. Springfield, Ill.: Thomas, 1964.
121. HODGKIN, A. L., AND P. HOROWICZ. The influence of potassium and chloride ions on the membrane potential of single muscle fibres. *J. Physiol. London* 148: 127-160, 1959.
122. HODGKIN, A. L., AND P. HOROWICZ. The effect of sudden changes in ionic concentrations on the membrane potential of single muscle fibres. *J. Physiol. London* 153: 370-385, 1960.
- 122a. HODGKIN, A. L., AND A. F. HUXLEY. Action potentials recorded from inside a nerve fibre. *Nature* 144: 710-711, 1939.
123. HODGKIN, A. L., AND A. F. HUXLEY. Currents carried by sodium and potassium ions through the membrane of the giant axon of *Loligo*. *J. Physiol. London* 116: 449-472, 1952.
124. HODGKIN, A. L., AND A. F. HUXLEY. The components of membrane conductance in the giant axon of *Loligo*. *J. Physiol. London* 116: 473-496, 1952.
125. HODGKIN, A. L., AND A. F. HUXLEY. The dual effect of membrane potential on sodium conductance in the giant axon of *Loligo*. *J. Physiol. London* 116: 497-506, 1952.
126. HODGKIN, A. L., AND A. F. HUXLEY. A quantitative description of membrane current and its application to conduction and excitation in nerve. *J. Physiol. London* 117: 500-544, 1952.
127. HODGKIN, A. L., AND A. F. HUXLEY. Movement of radioactive potassium and membrane current in a giant axon. *J. Physiol. London* 121: 403-414, 1953.
128. HODGKIN, A. L., A. F. HUXLEY, AND B. KATZ. Ionic currents underlying activity in the giant axon of the squid. *Arch. Sci. Physiol.* 3: 129-150, 1949.
129. HODGKIN, A. L., A. F. HUXLEY, AND B. KATZ. Measurement of current-voltage relations in the membrane of the giant axon of *Loligo*. *J. Physiol. London* 116: 424-448, 1952.
130. HODGKIN, A. L., AND B. KATZ. The effect of sodium ions on the electrical activity of the giant axon of the squid. *J. Physiol. London* 108: 37-77, 1949.
131. HODGKIN, A. L., AND R. D. KEYNES. The mobility and diffusion coefficient of potassium in giant axons from *Sepia*. *J. Physiol. London* 119: 513-528, 1953.
132. HODGKIN, A. L., AND R. D. KEYNES. The potassium permeability of a giant nerve fibre. *J. Physiol. London* 128: 61-88, 1955.
133. HODGKIN, A. L., AND R. D. KEYNES. Movements of labelled calcium in squid giant axons. *J. Physiol. London* 138: 253-281, 1957.
- 133a. HODGKIN, A. L., AND W. A. H. RUSHTON. The electrical constants of a crustacean nerve fibre. *Proc. Roy. Soc. London Ser. B* 133: 444-479, 1946.
134. HORÁČKOVÁ, M., W. NONNER, AND R. STÄMPFLI. Action potentials and voltage clamp currents of single rat Ranvier nodes. *Proc. Intern. Union Physiol. Sci.* 7: 198, 1968.
135. HOROWICZ, P., P. W. GAGE, AND R. S. EISENBERG. The role of the electrochemical gradient in determining potassium fluxes in frog striated muscle. *J. Gen. Physiol.* 51: 193S-203S, 1968.
136. HOWARTH, J. V., R. D. KEYNES, AND J. M. RITCHIE. The origin of the initial heat associated with a single impulse in mammalian non-myelinated nerve fibres. *J. Physiol. London* 194: 745-793, 1968.
137. HOYT, R. C., AND W. J. ADELMAN, JR. Sodium inactivation. Experimental test of two models. *Biophys. J.* 10: 610-617, 1970.
138. HURSH, J. B. Conduction velocity and diameter of nerve fibers. *Am. J. Physiol.* 127: 131-139, 1939.
139. HURSH, J. B. The properties of growing nerve fibers. *Am. J. Physiol.* 127: 140-153, 1939.
- 139a. HUTCHINSON, N. A., Z. J. KOLES, AND R. S. SMITH. Conduction velocity in myelinated nerve fibers of *Xenopus laevis*. *J. Physiol. London* 208: 279-289, 1970.
140. HUXLEY, A. F. Ion movements during nerve activity. *Ann. NY Acad. Sci.* 81: 221-246, 1959.
141. HUXLEY, A. F., AND R. STÄMPFLI. Evidence for saltatory conduction in peripheral myelinated nerve fibres. *J. Physiol. London* 108: 315-339, 1949.
142. HUXLEY, A. F., AND R. STÄMPFLI. Direct determination of membrane resting potential and action potential in single myelinated nerve fibres. *J. Physiol. London* 112: 476-495, 1951.
143. HUXLEY, A. F., AND R. STÄMPFLI. Effect of potassium and sodium on resting and action potentials of single myelinated nerve fibres. *J. Physiol. London* 112: 496-508, 1951.
144. JULIAN, F. J., J. W. MOORE, AND D. E. GOLDMAN. Current-voltage relations in the lobster giant axon membrane under voltage clamp conditions. *J. Gen. Physiol.* 45: 1217-1238, 1962.
145. KATO, G. On the excitation, conduction, and narcotisation of single nerve fibres. *Cold Spring Harbor Symp. Quant. Biol.* 4: 209-213, 1936.
146. KATZ, B. Experimental evidence for a non-conducted response of nerve to subthreshold stimulation. *Proc. Roy. Soc. London Ser. B* 124: 244-276, 1937.
147. KATZ, B. *The Release of Neural Transmitter Substances*. Springfield, Ill.: Thomas, 1969.
148. KEYNES, R. D. The ionic movements during nervous activity. *J. Physiol. London* 114: 119-150, 1951.
149. KEYNES, R. D., AND P. R. LEWIS. The sodium and potassium content of cephalopod nerve fibres. *J. Physiol. London* 114: 151-182, 1951.
150. KEYNES, R. D., AND J. M. RITCHIE. The movements of labelled ions in mammalian non-myelinated nerve fibres. *J. Physiol. London* 179: 333-367, 1965.
151. KEYNES, R. D., AND E. ROJAS. Characteristics of the sodium gating current in the squid giant axon. *J. Physiol. London* 233: 28P, 1973.
- 151a. KEYNES, R. D., AND E. ROJAS. Kinetics and steady state properties of the charged system controlling sodium conductance in the squid giant axon. *J. Physiol. London* 239: 393-434, 1974.
- 151b. KEYNES, R. D., E. ROJAS, R. E. TAYLOR, AND J. VERGARA. Calcium and potassium systems of a giant barnacle muscle fibre under membrane potential control. *J. Physiol. London* 229: 409-455, 1973.
- 151c. KHODOROV, B. I. *The Problem of Excitability. Electrical Excitability and Ionic Permeability of the Nerve Membrane*. New York: Plenum Press, 1974.
152. KOHLHARDT, M., B. BAUER, H. KRAUSE, AND A. FLECKENSTEIN. Differentiation of the transmembrane Na and Ca channels in mammalian cardiac fibers by the use of specific inhibitors. *Pflugers Arch. Ges. Physiol.* 335: 309-322, 1972.
153. KOKETSU, K., AND S. NISHI. Effects of tetrodotoxin on the action potential in Na-free media. *Life Sci., Part 2*, 5: 2341-2346, 1966.
154. KOKETSU, K., AND S. NISHI. Calcium and action potentials of bullfrog sympathetic ganglion cells. *J. Gen. Physiol.* 53: 608-623, 1969.
155. KOLES, Z. J., AND M. RASMINSKY. A computer simulation of conduction in demyelinated nerve fibres. *J. Physiol. London* 227: 351-364, 1972.
156. KOPPENHÖFFER, E. Die Wirkung von Tetraäthylammoniumchlorid auf die Membranströme Ranvierscher Schnürringe

- von *Xenopus laevis*. *Pfluegers Arch. Ges. Physiol.* 293: 34-55, 1967.
157. KOPPENHÖFER, E., AND H. SCHMIDT. Die Wirkung von Skorpiongift auf die Ionenströme des Ranvierschen Schnürrings. I. Die permeabilitäten P_{Na} und P_K . *Pfluegers Arch. Ges. Physiol.* 303: 133-149, 1968.
 158. KOPPENHÖFER, E., AND H. SCHMIDT. Die Wirkung von Skorpiongift auf die Ionenströme des Ranvierschen Schnürrings. II. Unvollständige Natrium-Inaktivierung. *Pfluegers Arch. Ges. Physiol.* 303: 150-161, 1968.
 159. KUSHMERICK, M. J., AND R. J. PODOLSKY. Ionic mobility in muscle cells. *Science* 166: 1297-1298, 1969.
 160. LILLIE, R. S. Factors affecting transmission and recovery in the passive iron nerve model. *J. Gen. Physiol.* 7: 473-507, 1925.
 161. LING, G. N. *A Physical Theory of the Living State*. Waltham, Mass.: Blaisdell, 1962.
 162. LUCAS, K. The analysis of complex excitable tissues by their response to electric currents of short duration. *J. Physiol. London* 35: 310-331, 1906.
 163. LÜTTGAU, V. H-C. Sprunghafte Schwankungen unter-schwelliger Potentiale an markhaltigen Nervenfasern. *Z. Naturforsch.* 13B: 692-693, 1958.
 164. MARMONT, G. Studies on the axon membrane. I. A new method. *J. Cellular Comp. Physiol.* 34: 351-382, 1949.
 165. MARTINEZ, D., A. A. SILVIDI, AND R. M. STOKES. Nuclear magnetic resonance studies of sodium ions in isolated frog muscle and liver. *Biophys. J.* 9:1256-1260, 1969.
 166. MAURO, A., F. CONTI, F. DODGE, AND R. SCHOR. Subthreshold behavior and phenomenological impedance of the squid giant axon. *J. Gen. Physiol.* 55: 497-523, 1970.
 167. MEVES, H. The ionic requirements for the production of action potentials in *Helix pomatia* neurones. *Pfluegers Arch. Ges. Physiol.* 304: 215-241, 1968.
 - 167a. MEVES, H., AND W. VOGEL. Calcium inward currents in internally perfused giant axons. *J. Physiol. London* 235: 225-265, 1973.
 168. MOORE, J. W., AND T. NARAHASHI. Tetrodotoxin's highly selective blockage of an ionic channel. *Federation Proc.* 26: 1655-1663, 1967.
 169. MOORE, J. W., T. NARAHASHI, AND T. I. SHAW. An upper limit to the number of sodium channels in nerve membrane? *J. Physiol. London* 188: 99-105, 1967.
 170. MORETON, R. B. An investigation of the electrogenic sodium pump in snail neurones, using the constant-field theory. *J. Exptl. Biol.* 51: 181-201, 1969.
 171. MORTON, S. D., AND G. F. LEE. Calcium carbonate equilibria in the oceans. Ion pair formation. *J. Chem. Educ.* 45: 513-515, 1968.
 172. MOZHAYEVA, G. N., AND A. P. NAUMOV. Effect of surface charge on the steady-state potassium conductance of nodal membrane. *Nature* 228: 164-165, 1970.
 173. MURAYAMA, K., N. J. ABBOTT, T. NARAHASHI, AND B. I. SHAPIRO. Effects of allethrin and condylactis toxin on the kinetics of sodium conductance of crayfish axon membranes. *Comp. Gen. Pharmacol.* 3: 391-400, 1972.
 174. NAKAJIMA, S. Analysis of K inactivation and TEA action in the supramedullary cells of puffer. *J. Gen. Physiol.* 49: 629-640, 1966.
 175. NARAHASHI, T., D. T. FRAZIER, AND M. YAMADA. The site of action and active form of local anesthetics. I. Theory and pH experiments with tertiary compounds. *J. Pharmacol. Exptl. Therap.* 171: 32-44, 1970.
 176. NARAHASHI, T., AND H. G. HAAS. Interaction of DDT with the components of lobster nerve membrane conductance. *J. Gen. Physiol.* 51: 177-198, 1968.
 177. NARAHASHI, T., J. W. MOORE, AND W. R. SCOTT. Tetrodotoxin blockage of sodium conductance increase in lobster giant axons. *J. Gen. Physiol.* 47: 965-974, 1964.
 178. NARAHASHI, T., J. W. MOORE, AND B. I. SHAPIRO. Condylactis toxin: interaction with nerve membrane ionic conductances. *Science* 163: 680-681, 1969.
 179. NEHER, E. Two fast transient current components during voltage clamp in snail neurons. *J. Gen. Physiol.* 58: 36-53, 1971.
 180. NERNST, W. Zur Kinetik der in Lösung befindlichen Körper: Theorie der Diffusion. *Z. Physik. Chem. Leipzig* 2: 613-637, 1888.
 181. NERNST, W. Die elektromotorische Wirksamkeit der Ionen. *Z. Physik. Chem. Leipzig* 4: 129-181, 1889.
 182. NOBLE, D. Applications of Hodgkin-Huxley equations to excitable tissues. *Physiol. Rev.* 46: 1-50, 1966.
 - 182a. NOBLE, D., AND R. B. STEIN. The threshold conditions for initiation of action potentials by excitable cells. *J. Physiol. London* 187: 129-162, 1966.
 183. NOBLE, D., AND R. W. TSIEN. The kinetics and rectifier properties of the slow potassium current in cardiac Purkinje fibres. *J. Physiol. London* 195: 185-214, 1968.
 184. NOBLE, D., AND R. W. TSIEN. Outward membrane currents activated in the plateau range of potentials in cardiac Purkinje fibres. *J. Physiol. London* 200: 205-231, 1969.
 185. NONNER, W. A new voltage clamp method for Ranvier nodes. *Pfluegers Arch. Ges. Physiol.* 309: 176-192, 1969.
 186. NONNER, W., AND R. STÄMPFLI. A new voltage clamp method. In: *Laboratory Techniques in Membrane Biophysics*, edited by H. Passow and R. Stämpfli. Berlin: Springer Verlag, 1969.
 187. PAINTAL, A. S. Effects of temperature on conduction in single vagal and saphenous myelinated nerve fibres of the cat. *J. Physiol. London* 180: 20-49, 1965.
 188. PAINTAL, A. S. The influence of diameter of medullated nerve fibers of cats on the rising and falling phases of the spike and its recovery. *J. Physiol. London* 184: 791-811, 1966.
 189. PEARSON, K. G., R. B. STEIN, AND S. K. MALHOTRA. Properties of action potentials from insect motor nerve fibres. *J. Exptl. Biol.* 53: 299-316, 1970.
 190. PICHON, Y., AND J. BOISTEL. Current-voltage relations in the isolated giant axon of the cockroach under voltage-clamp conditions. *J. Exptl. Biol.* 47: 343-355, 1967.
 191. PLANCK, M. Ueber die Erregung von Elektrizität und Wärme in Elektrolyten. *Ann. Physik Chem.* 39: 161-186, 1890.
 192. PLANCK, M. Ueber die Potentialdifferenz zwischen zwei verdünnten Lösungen binärer Elektrolyte. *Ann. Physik Chem.* 40: 561-576, 1890.
 193. POOLER, J. Photodynamic alteration of sodium currents in lobster axons. *J. Gen. Physiol.* 60: 367-387, 1972.
 194. PUMPHREY, R. J., AND J. Z. YOUNG. The rates of conduction of nerve fibres of various diameters in cephalopods. *J. Exptl. Biol.* 15: 453-466, 1938.
 195. RANG, H. P., AND J. M. RITCHIE. On the electrogenic sodium pump in mammalian non-myelinated nerve fibres and its activation by various external cations. *J. Physiol. London* 196: 183-211, 1968.
 196. RASMINSKY, M., AND T. A. SEARS. Internodal conduction in undissected demyelinated nerve fibres. *J. Physiol. London* 227: 323-350, 1972.
 197. REUTER, H. Divalent cations as charge carriers in excitable membranes. *Progr. Biophys. Mol. Biol.* 26: 1-43, 1973.
 198. RITCHIE, J. M. Electrogenic ion pumping in nervous tissue. In: *Current Topics in Bioenergetics*, edited by D. R. Sanadi. New York: Academic, 1971.
 199. RITCHIE, J. M. Energetic aspects of nerve conduction: the relationships between heat production, electrical activity and metabolism. *Progr. Biophys. Mol. Biol.* 26: 147-187, 1973.
 200. RITCHIE, J. M., AND P. GREENGARD. On the mode of action of local anesthetics. *Ann. Rev. Pharmacol.* 6: 405-430, 1966.
 201. ROBERTSON, J. D. The molecular structure and contact relationship of cell membranes. *Progr. Biophys. Biophys. Chem.* 10: 344-418, 1960.
 202. ROBINSON, R. A., AND R. H. STOKES. *Electrolyte Solutions*. London: Butterworths, 1965.
 203. RUSHTON, W. A. H. A theory of the effects of fibre size in medullated nerve. *J. Physiol. London* 115: 101-122, 1951.
 204. SCHWARZ, J. R., AND W. VOGEL. Potassium inactivation in

- single myelinated nerve fibres of *Xenopus laevis*. *Pfluegers Arch. Ges. Physiol.* 330: 61-73, 1971.
- 204a. SCHAUF, C. L. Temperature dependence of the ionic current kinetics of *Myxicola* giant axons. *J. Physiol. London* 235: 197-205, 1973.
205. SEEMAN, P. The membrane actions of anesthetics and tranquilizers. *Pharmacol Rev.* 24: 583-656, 1972.
206. SHAPIRO, B. I., AND F. K. LENHERR. Hodgkin-Huxley axon: increased modulation and linearity of response to constant current stimulus. *Biophys. J.* 12: 1145-1158, 1972.
- 206a. STÄMPFLI, R., AND B. HILLE. Amphibian peripheral nerves In: *Handbook of Frog Neurobiology*, edited by R. Llinas and W. Precht. Heidelberg: Springer Verlag. In press.
- 206b. STEIN, R. B. The frequency of nerve action potentials generated by applied currents. *Proc. Roy. Soc. London Ser. B* 167: 64-86, 1967.
207. STEVENS, C. F. Inferences about membrane properties from electrical noise measurements. *Biophys. J.* 12: 1028-1047, 1972.
208. STRICHARTZ, G. R. The inhibition of sodium currents in myelinated nerve by quaternary derivatives of lidocaine. *J. Gen. Physiol.* 62: 37-57, 1973.
209. TAKATA, M., J. W. MOORE, C. Y. KAO, AND F. A. FUHRMAN. Blockage of sodium conductance increase in lobster giant axon by tarichatoxin (tetrodotoxin). *J. Gen. Physiol.* 49: 977-988, 1966.
210. TASAKI, I. *Nervous Transmission*. Springfield, Ill.: Thomas, 1953.
211. TASAKI, I. Conduction of the nerve impulse. In: *Handbook of Physiology. Neurophysiology*, edited by H. W. Magoun. Washington, D.C.: Am. Physiol. Soc., 1959, sect. 1, vol. I, p. 75-121.
212. TASAKI, I. *Nerve Excitation. A Macromolecular Approach*. Springfield, Ill.: Thomas, 1968.
213. TASAKI, I., AND M. FUJITA. Action currents of single nerve fibers as modified by temperature changes. *J. Neurophysiol.* 11: 311-315, 1948.
214. TASAKI, I., AND K. MIZUGUCHI. The changes in the electric impedance during activity and the effect of alkaloids and polarization upon the bioelectric processes in the myelinated nerve fibre. *Biochim. Biophys. Acta* 3: 484-493, 1949.
215. TASAKI, I., AND T. TAKEUCHI. Der am Ranvierschen Knoten entstehende Aktionsstrom und seine Bedeutung für die Erregungsleitung. *Pfluegers Arch. Ges. Physiol.* 244: 696-711, 1941.
216. TASAKI, I., AND T. TAKEUCHI. Weitere Studien über den Aktionsstrom der markhaltigen Nervenfasern und über die elektrosaltatorische Übertragung des Nervenimpulses. *Pfluegers Arch. Ges. Physiol.* 245: 764-782, 1942.
217. THOMAS, R. C. Electrogenic sodium pump in nerve and muscle cells. *Physiol. Rev.* 52: 563-594, 1972.
218. TOMITA, T., AND E. B. WRIGHT. A study of the crustacean axon repetitive response. I. The effect of membrane potential and resistance. *J. Cell. Comp. Physiol.* 65: 195-210, 1965.
219. ULBRICHT, W. The effect of veratridine on excitable membranes of nerve and muscle. *Ergeb. Physiol. Biol. Chem. Exptl. Pharmacol.* 61: 18-71, 1969.
220. ULBRICHT, W. Rate of veratridine action on the nodal membrane. I. Fast phase determined during sustained depolarization in the voltage clamp. *Pfluegers Arch. Ges. Physiol.* 336: 187-199, 1972.
221. USSING, H. H. The distinction by means of tracers between active transport and diffusion. The transfer of iodide across the isolated frog skin. *Acta Physiol. Scand.* 19: 43-56, 1949.
222. WOODBURY, J. W. Eyring rate theory model of the current-voltage relationships of ion channels in excitable membranes. In: *Chemical Dynamics: Papers in Honor of Henry Eyring*, edited by J. O. Hirschfelder. New York: Wiley, 1971, p. 601-617.